# Morphogen Gradient Creation and Bio-modified Surfaces for Rebuilding a Stem Cell Microenvironment

Zur Erlangung des akademischen Grades eines

DOKTORS DER NATURWISSENSCHAFTEN

(Dr. rer. nat.)

Fakultät für Chemie und Biowissenschaften

Karlsruher Institut für Technologie (KIT) - Universitätsbereich

genehmigte

DISSERTATION

von

M.Sc. Chorong Kim

aus

Incheon, Südkorea

# Statutory declaration

The work described in this thesis was performed by the author at the Zoological Institute, Cell and Developmental Biology from October 2009 to September 2012. I herewith declare that I have completed the present thesis independently making use only of the specified literature and aids. The thesis in this form or in any other form has not been submitted to an examination body and has not been published.

Karlsruhe, November 1. 2012

Chorong Kim

# Acknowledgements

# Abstract

Recreation of a stem cell microenvironment where they maintain pluripotency or initiate differentiation is crucial especially when they are used for therapeutic needs. Microtechnology has been vigorously combined to this issue, to generate more *in vivo* like environments.

A microfluidic approach was chosen to rebuild morphogen gradients and to study the cellular reaction on distinct morphogen concentrations within a gradient. The two-stacked polycarbonate microfluidic chip was developed in collaboration with the Institute of Microstructure Technology at Karlsruhe Institute of Technology. A zig-zag mixer generates a step-like gradient of soluble molecules in gradient reservoir channels. The soluble molecules reach the cells in the cell observation part only by passing a porous polycarbonate membrane. Simply by opening /closing the flow inlets and outlets, the microfluidic chip allows switching between different modes of how the soluble morphogen reaches the cells, either by diffusion or by convective flow. The cellular reaction on the GSK-3 inhibitor demonstrates that both diffusion mode and convection mode can be applied. The cellular reaction on a Wnt3a gradient and a Dkk-1 counter-gradient indicates that the microfluidic chip is suitable for the simultaneous application of different morphogens.

SNAP-tagged E-Cadherin ectodomains were immobilized on the specific pattern formed by nanografting to rebuild the cellular environment in the niche. Spreading of E-Cadherin expressing cells demonstrates the suitability of this approach.

A future challenge will be the combination of both approaches; the application of morphogen gradients on stem cells adhering to defined micro-patterned surfaces.

# Zusammenfassung

Die Mikroumgebung einer Stammzelle definiert, ob sie ihre Stammzell-Eigenschaften behält oder ob sie beginnt, sich zu differenzieren. Um solche natürlichen Mikroumgebungen künstlich nachzubilden, bietet sich insbesondere an, moderne Mikrotechnologien zu kombinieren.

Um die zelluläre Antwort auf die Exposition distinkter Morphogen-Konzentrationen innerhalb eines Gradienten zu untersuche.n wurde in der vorliegenden Arbeit ein auf Mikrofluidik basierender Ansatz gewählt. Der Zwei-Kammer Mikrufluidik-Chip wurde in Kollaboration mit dem Institut für Mikrostrukturtechnik am Karlsruher Institut für Technologie entwickelt. Dabei wird über einen Zick-Zack-Mixer ein stabiler Gradient in der unteren Kammer aufgebaut. Nur über eine poröse Membran erreichen die löslichen Faktoren die in der oberen Kammer befindlichen Zellen. Durch Öffnen und Schließen der Zu- und Abläufe lässt sich einfach regulieren, ob dieser Transport durch die Membran über Diffusion oder über Konvektion erfolgt. Die zelluläre Reaktion auf den GSK-3 Inhibitor BIO zeigt, dass beides möglich ist. Die zelluläre Reaktion auf einen Wnt3a Gradienten und einen Dkk-1 Gegengradienten macht deutlich, dass der Microfluidik-Chip geeignet ist, gleichzeitig mehrere Morphogen-gradienten zu applizieren.

Um die zelluläre Umgebung in der Stammzell-Nische nachzustellen, wurde in der vorliegenden Arbeit über Nanografting SNAP-getaggte E-Cadherin Ectodomänen auf strukturierten Oberflächen immobilisiert. Die Ausbreitung E-Cadherin explizierender Zellen unterstreicht, dass die in der vorliegenden Arbeit vorgestellten experimentellen Ansätze anwendbar sind.

Als zukünftige Herausforderung verbleibt, die in der vorliegenden Arbeit erfolgreich angewandten Systeme zu kombinieren, und damit das Schicksal der Stammzellen gleichzeitig über die Wahl der lokalen Morphogen-Konzentrationen und der zellulären Umgebung zu regulieren.

# List of abbreviations

| | |
|---|---|
| AFM | Atomic force microscopy |
| AGT | $O^6$-alkylguanine-DNA-alkyltransferase |
| BCA | Bicinchoninic acid |
| BGT | Benzyl guanine thiol |
| BIO | 6-bromoindirubin-3'-oxime |
| BSA | Bovine serum albumin |
| CBB | Coomasie brilliant blue |
| CM | Conditioned medium |
| CPR | Critical perfusion rate |
| Dkk | Dickkopf |
| EB | Embryoid body |
| EC | Extracellular domain / ectodomain |
| ECM | Extracellular matrix |
| EDTA | Ethylenediaminetetraacetic acid |
| ECT | Effective culture time |
| EG | Ethylene glycol |
| FPLC | Fast protein liquid chromatography |
| GFP | Green fluorescent protein |
| GSK | Glycogen synthase kinase |
| GST | Glutatione S-transferase |
| LIF | Leukemia inhibitory factor |
| MEF | Murine embryonic fibroblast |
| mES | Murine embryonic stem cell |
| OEG | Oligo (ethylene glycol) |
| PDMS | Polydimethylsiloxane |
| PEG | Poly (ethylene glycol) |
| *Re* | Reynolds number |
| SAM | Self-assembled monolayer |
| SEM | Scanning electron microscopy |
| SFRP | Soluble Frizzled-Related Protein |
| ToF-SIMS | Time-of-flight secondary ion mass spectrometry |

# List of figures and tables

Figures

Tables

# Contents

# 1. Introduction

The therapeutic needs to use stem cells for tissue replacement or regenerative medicine have been vigorously increased although there are still a lot of ethical controversies in issues all over the world. Naturally stem cells reside in a microenvironment, called stem cell *niche*, where numerous biochemical and biophysical factors affect precisely whether the cells maintain their pluripotency or start differentiating into distinct cell types. To apply stem cells in therapeutic purposes, it is essential to remove them from their natural microenvironment, propagate them in a cell culture system and, most importantly, to recreate an artificial environment (reviewed in Fuchs *et al.*, 2004). More specifically, reliable differentiation towards a distinct phenotype should be confirmed in long-term, cultivations (reviewed in Solanki *et al.*, 2008). The combination of novel microtechnologies, including microarray, microfluidics and soft lithography which have been developed over the past decades, is considered as a suitable approach to recreate stem cell niches and to understand stem cell behavior. In principle, the more the artificial environment is *"in vivo* like", the better the suitability to improve their usage into practical applications (reviewed in Gupta *et al.*, 2010; Toh *et al.*, 2010).

## 1.1 Stem cell niche and its key molecules

A stem cell niche is usually described as a local microenvironment where stem cells are exposed to complex structural, physical elements a defined mixture of signaling elements, including cell adhesion and soluble signaling factors (Fig. 1.1, reviewed in Fuchs *et al.*, 2004; Scadden, 2006; Lutolf & Blau, 2009).

One of the roles of stem cell niche is to regulate symmetric and asymmetric stem cell divisions (Fig. 1.2). Like other cells, stem cells undergo the symmetrical division to generate an identical daughter cell. Additionally, they also possess the ability to divide asymmetrically in order to generate one progenitor daughter cell and one stem cell daughter cell.
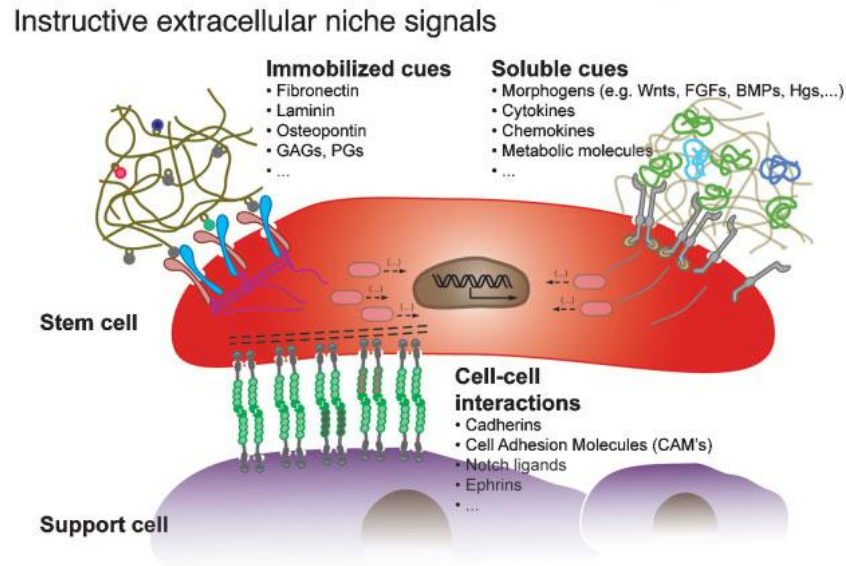
Fig. 1.1 Stem cell niche components categorized into three kinds of signals. (1) Immobilized cues ; extracellular matrices (ECMs). GAGs, glycosaminoglycans; PGs, proteoglycans. (2) Soluble cues including signaling molecules such as Wnts, fibroblast growth factors (FGFs), bone morphogenetic proteins (BMPs), hepatocyte growth factors (Hgs) and calcium ions. (3) Cell-cell interactions by transmembrane adhesion molecules such as cadherins. Adapted from Lutolf & Blau, 2009.

By balancing between symmetrical and asymmetrical division, the proper number of stem cell in niches and differentiated cell is regulated. Asymmetrical decisions are initiated by linking polarity of cells with spindle orientation (Fuchs *et al.*, 2004). As shown in Fig. 1.2, stem cells contact with a basal lamina with stronger or weaker spindle polarizing signal and this determines whether asymmetric differentiation-specific or symmetric mitosis follows. Additionally, the microtubule-associated adenomatpus polyposis coli (APC) protein, dynein-dynactin, PKC, actin and myosins could participate in intrinsic polarity cues and in orienting the spindle poles to asymmetric cell divisions (Perez-Moreno *et al.*, 2003; Petritsch *et al.*, 2003; Etienne-Manneville & Hall, 2003).

For distinct adult stem cell niches these niches might look differently (Fig.1.3). However, they all contain three types of niche components: (1) extracellular matrices (ECMs), (2) signaling soluble cues and (3) cell-cell interactions (Fig. 1.1).
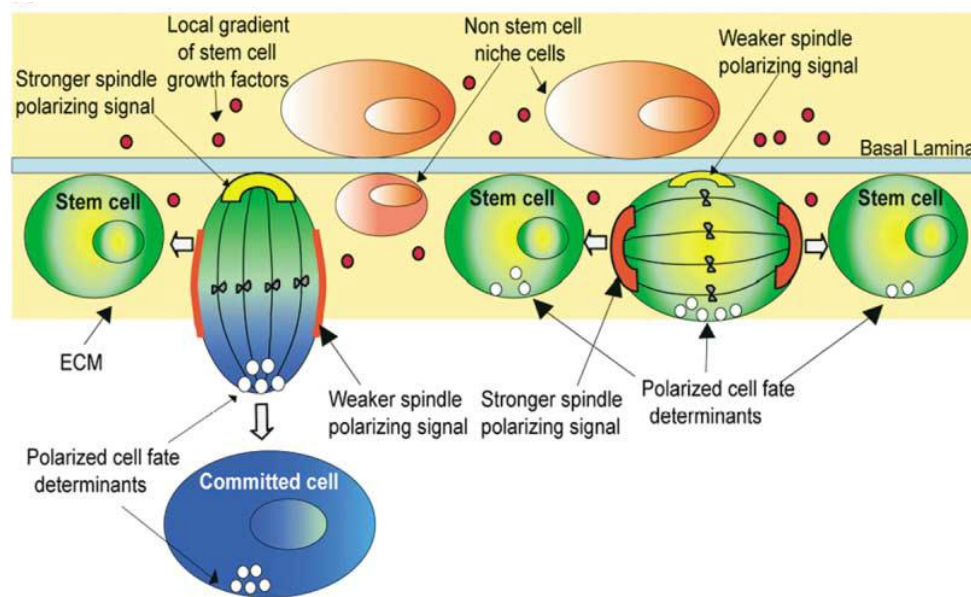
**Fig. 1.2 Schematic drawing of a role of stem cell niche in orientation and determination of stem cell divisions. To define symmetric and asymmetric division of stem cells, cell polarity and spindle orientation are important. Adapted from Fuchs *et al.*, 2004.**

Extracellular matrices (ECMs)

The extracellular matrices (ECMs) are composed of a variety of proteins including fibronectin, collagen, laminin and oligosaccharids bound to proteins. The interaction between ECM molecules and stem cells in the niche was first described in invertebrate model systems (Schofield, 1978; Crittenden *et al.*, 2002) and then extended to mammalian stem cell (Habara-Ohkubo, 1996; Comoglio *et al.*, 2003; Flaim *et al.*, 2008). Meanwhile many cell-substrate adhesion molecules are described in various stem cell niches. Among others, ß-1 integrins are expressed on primitive cells in the skin with matrix glycoprotein as ligands (Jones & Watt, 1993; Jensen *et al.*, 1999), tenascin C was found in the nervous system (Garcion *et al.*, 2004), the Arg-Gly-Asp (RGD)-containing sialoprotein, osteoponin is involved haematopoietic stem cell regulation (Stier *et al.*, 2005; Nilsson *et al.*, 2005).

Signaling soluble cues

Cellular responses mediated by soluble factors, including morphogens, cytokines, chemokine have been defined in several organs and organisms. In morphogen gradients cells are positioned in different concentrations and sense a certain
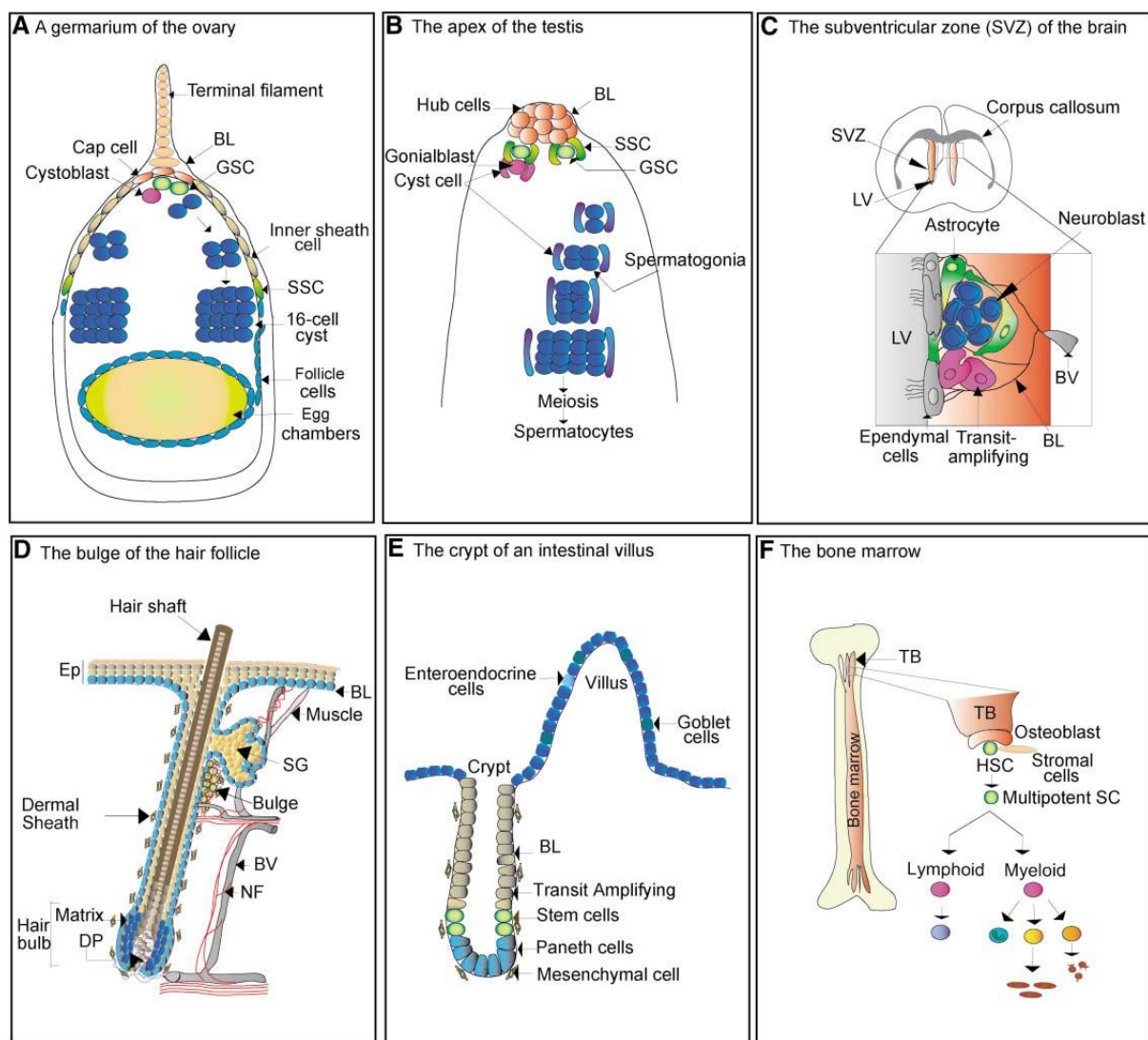
**Fig. 1.3 Illustrated examples of six different adult stem cell niches where stem cells, offspring and non-stem niche cells are present in close proximity. (A) A *Drosophila* germarium (GSCs, germ stem cells; SSCs, somatic stem cells; BL, basal lamina). (B) The apical tip of the *Drosophila* testis showing germline stem cells (GSCs) attached to a cluster of hub cells. (C) The adult mouse brain (SVZ, subventricular zone; LV, lateral ventricle; BV, blood vessel). (D) The skin (SG, sebaceous gland; DP, derma papilla; NF, nerve fibers; Ep, epidermis). (E) The intestine. (F) The bone marrow (HSC, hematopoietic stem cell; TB, trabecular bone). Adapted from Fuchs *et al.*, 2004.**

threshold leading to different target gene expression and therefore distinct developmental fate decision (Wolpert, 1989; Cooke, 1995; Lawrence & Struhl, 1996). These gradient-forming characteristics can be varied from the range of a gradient (short/long range) to the slope of a gradient that can be steeper when antagonistic factors are involved (Gurdon & Bourillot, 2001). Several models of how morphogens are transmitted to receiving cells are discussed. The suggested

ideas include (1) active or facilitated diffusive transport in the extracellular matrix, (2) transcytosis, i.e. internalization and re-emission from cell to cell and (3) cytoneme model (Lander *et al.*, 2002; reviewed in Yan & Lin, 2009; Wartlick *et al.*, 2009).

Mainly eight morphogen-regulated signaling pathways define the fate of stem cells in the niche (Brivanlou & Darnell, 2002): JAK/STAT (Janus-family tyrosine kinase / Signal transducer and activator of transcription), Notch, MAPK/ERK (Mitogen-activated protein kinase/Extracellular signal-regulated kinase), PI3K/AKT (Phosphatidylinositol 3-kinase/ATK), NF-κB (Nuclearfactor-kappa-B), BMP/SMAD (Bone morphogenetic protein / Sma and mothers against decapentaplegic), hedgehogs (HHs), and Wnt signaling pathway. In the ovary of the model organism *Drosophila melanogaster* the BMP homologue Decapentaplegic (DPP) is secreted from cap cells and Glass bottom boat (GBB) is produced by niche cells. This induces SMAD-driven transcription in the germ stem cells followed by suppression of differentiation and thus maintainance of stemness (Xie & Spradling, 1998; Chen & McKearin, 2003; Song *et al.*, 2004). JAK/STAT signaling is also activated when Unpaired (UPD) is secreted by niche cells in *Drosophila* testis, inducing self-renewal (Kiger *et al.*, 2001; Tulina & Matunis, 2001). During hair-follicle formation in mammals, sonic hedgehog (SHH) is necessary to distinguish the follicular niche from the interfollicular epidermis (St-Jacques *et al.*, 1998; Levy *et al.*, 2005). Wnt signaling is required for maintaining self-renewal aspects in adult stem cells including hair follicles (van Genderen *et al.*, 1994; Alonso & Fuchs, 2003; Lowry *et al.*, 2005), intestine (Korinek *et al.*, 1998; Kim *et al.*, 2005; Gregorieff *et al.*, 2005; van Es *et al.*, 2005), and hematopoietic stem cells in bone marrow (Okamura *et al.*, 1998; Reya *et al.*, 2003). This signaling pathway is introduced more in detail in 1.1.1.

In addition to these morphogen-induced signaling pathways, the extracellular calcium ions influence stem cell development as well. High calcium concentration is found at the site near active osteoclasts where osteoblasts and ostelclasts are co-localized (Adams *et al.*, 2006). Cells sense the calcium ions through G-protein-coupled seven membrane-spanning calcium sensing receptor (GaR). In bone-marrow haematopoietic cells, the receptors are found to be expressed in a stem

cell rich region, indicating high calcium ion concentration is crucial for haematopoietic stemness (Adams *et al.*, 2006).

<u>Cell-cell interaction</u>

Physical engagement *via* cell membrane molecules on the cell surface is provided by supporting neighboring cells. Cell-cell interaction is mediated by the family of cadherin proteins, Delta/Notch, Eph/Ephrin receptors and cell adhesion molecules (CAMs) with immunoglobulin domains (Fig. 1.1). Notch as a receptor and its ligand Delta provide a local signaling that requires cell-cell contact. In *Drosophila*, Notch is required to control the cell fate of the sensory organ precursor cell during cell division within the sensory organ lineage (Jan & Jan, 1998; Lu *et al.*, 1998; Lin, 1998; Xie & Spradling, 1998). Also in embryonic and adult tissues of vertebrates, Notch signaling is important in retinal neuroepithelium, skeletal muscle and blood (Lewis, 1998; Artavanis-Tsakonas *et al.*, 1999). Furthermore, the Ephs and Ephrins are known as resoponsible for guiding stem cells in the brain and intestine to their niches (Holmberg *et al.*, 2006; Chumley *et al.*, 2007). The Ig superfamily CAMs are calcium-independent transmembrane glycoproteins. Typically, CAMs bind integrins or other CAMs. These cadherin-like or immunoglobulin-like molecules partially participate in functions for anchoring *Drosophila* GSCs in the niche (Xi, 2009). Cadherins are introduced more in detail in 1.1.2.

### 1.1.1 Wnt gradients

For more than 20 years, the mechanisms of the signal transduction by secreted Wnt proteins have been in the focus of intense research (see also http://www.stanford.edu/group/nusselab/cgi-bin/wnt/). Meanwhile, several distinct pathways triggered by Wnt signaling molecules have been identified (reviewed in Reya & Clevers, 2005; Montcouquiol *et al.*, 2006; Grumolato *et al.*, 2010; Nusse & Varmus, 2012). Among them, the canonical or Wnt/ß-catenin pathway is the best understood. In brief, binding of the Wnt ligand to its frizzled receptor activates a signaling cascade, which results in an inactivation of the glycogen synthase kinase 3ß (GSK3ß) and thus to an accumulation of the transcriptional co-activator ß-catenin in the nucleus. Blocking and/or inhibition of

Wnt signaling can induce sebaceous gland differentiation (Merrill *et al.*, 2001), epidermal differentiation (Huelsken *et al.*, 2001; Niemann *et al.*, 2002) or villus differentiation in the intestine (van de Wetering *et al.*, 2002).

Wnt proteins as morphogens are expected to create a concentration gradient from a secreting source in a long rage. In the *Drosophila* wing, it was found that Wnt-1 homologue Wg (wingless) gradient forms by rapid movement of ligand through the extracellular matrix (Strigini & Cohen, 2000). Bartscherer and Boutros (2008) proposed a model, that short range and long-range gradients of wg are formed simultanousely, with short range signaling at the apical side of an epithelial sheet and long range signaling at the basal side. For vertebrates, Kieker & Niehrs (2001) described that an endogenous anteroposterior (AP) gradient of Wnt/ß-catnin signaling in the presumptive neural plate of the *Xenopus* gastrula (Fig. 1.4) is important for posteriorization of the central nervous system. More recently, Luis *et al.* (2011) confirmed that different lineage-specific Wnt-dosages regulate the development of the hematopoietic stem cell, the myeloid precursors and T lymphoid precursors. Similar to most of the morphogen gradients, the Wnt gradients are also sharpened by antagonist gradients of the opposite direction such as secreted Dickkopf (Dkk) protein (Glinka *et al.*, 1998; Mao *et al.*, 2002), or soluble Frizzled-Related Proteins (SFRPs) (Hoang *et al.*, 1996; Wang *et al.*, 1997; reviewed in Logan & Nusse, 2004).

Further complexity to the cellular reaction on a Wnt concentration is given by the fact that also the competence of a Wnt receiving cell to respond on extracellular Wnt proteins can vary over time (Aulehla *et al.*, 2003; Jensen *et al.*, 2010).
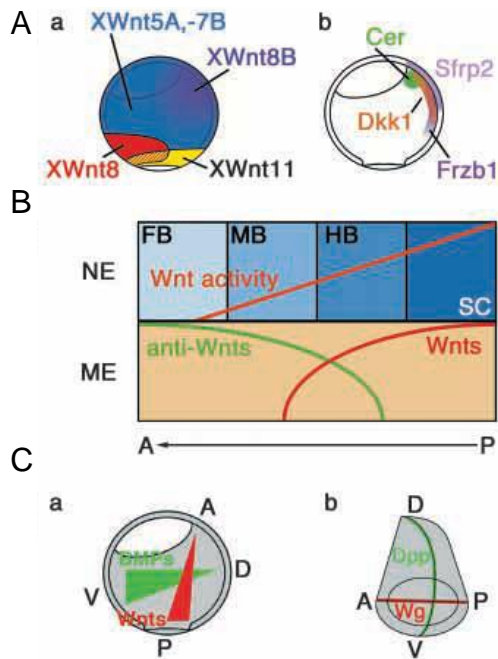
**Fig. 1.4 An established Wnt gradient in the gastrulating *Xenopus* embryo. (A) Schematic domain of expression of Wnt (a) and Wnt antagonists (b). (B) Wnt gradient of neuroectoderm (NE) along anteroposterior (AP) axis. Different expression of Wnt and Wnt antagonists in the mesendoderm (ME) underlies the neuroectoderm (NE). (C) Wnt gradient forms along AP axis and BMPs gradients do along dorsoventral (DV) axis in *Xenopus* embryo (a). In *Drosophila* wing Wingless (Wg) and Decapentaplegic (Dpp) are secreted along AP and DV axis, respectively. Adapted from Kieker & Niehrs, 2001.**

### 1.1.2 Cadherins

Cadherins are transmembrane glycoproteins that act on calcium-dependent cell-cell contacts. By regulating cell-cell interaction, cadherins play a vital role in tissue morphogenesis, the epithelial-mesenchymal transition (EMT) (Hay & Zuk, 1995; Cano *et al.*, 2000), tissue elongation by convergence extension (Keller, 2002), formation of developmental compartments for example rhombomeres in the developing vertebrate hindbrain (Wizenmann & Lumsden, 1997; Lumsden, 1999) and neural growth cone motility (Matsunaga *et al.*, 1988; Bixby & Zhang, 1990). Also, when induced to form teratomas in mice, cadherins control some processes of early differentiation to subtype of tissues, for instance, epithelial or neuroepithelial by E-Cadherin or N-Cadherin, respectively (Larue *et al.*, 1996). E-Cadherin (epithelial cadherin) is one of the classical cadherins and is expressed primarily in epithelial cells associating in the epithelial junction (Johnson *et al.*, 1993; Ko *et al.*, 2000). Its structure contains an extracellular domains (EC) at extracellular region that bind $Ca^{2+}$ to form rod-like proteins as *cis*-dimers (Fig. 1.5). At the intracellular region, cadherins form a complex with p120, β-catenin and α-catenin. This complex is known to interact with other signaling proteins indicating that cadherins have important roles in signaling pathways (reviewed

in Wheelock & Johnson 2003; Suyama *et al.*, 2002; Yap & Kovacs, 2003; Schambony *et al.*, 2004; Soncin *et al.*, 2009). Various signaling pathways are connected to E-Cadherin mediated cell-cell adhesion to cascade information to the cytoplasms and the nuclei (Stepniak *et al.*, 2009). Here, the dual role of ß-catenin is of particular interst since it is an essential component of both cadherin-mediated cell adhesion complexes and Wnt signaling.

Of particular interest, E-Cadherins participate in maintaining pluripotency in stem cell niches. In *Drosophila* germ stem cells (GSCs), a direct physical interaction between GSCs and cap cells by E-Cadherin is critical to maintain stemness in the germarium of adult *Drosophila* (Song *et al.*, 2002). In early mammalian development, the cell-cell contacts *via* cadherins are necessary for the integrity of the embryonic blastocyst. Cell compaction at this stage is lost when E-Cadherin is genetically deleted (Larue *et al.*, 1994). In murine embryonic stem cells, E-Cadherin has a vital role in maintaining pluripotency (Chou *et al.*, 2008; Soncin *et al.*, 2009). Depletion of ß-catenin affects pluripotency maintenance most likely because the cell-adhesive function of E-Cadherin is impaired (Soncin *et al.*, 2009). Recently, Redmer *et al.* (2011) reported E-Cadherin production is associated with the reprogramming of MEFs to induced pluripotent stem cells (iPSCs) process, showing the exogenous expression of E-Cadhrign can replace the Oct4 that is required with other essential transcription factors Sox2, Klf4 and c-Myc for reprogramming to iPSCs (Takahashi & Yamanaka, 2006).

## 1.2 Microfluidic system for Wnt gradients

### 1.2.1 Re-creation of biological gradients *in vitro*

To analyze the impact of stable and changing morphogen gradients on stem cell maintenance and/or cell differentiation an experimental device is required that guarantees the formation of controlled, reproducible, and stable defined morphogen gradients. The set-up of such a device should also ensure sufficient nutrient deposition to cultivate cells for more than one week. Such a system would also allow the analysis of antagonistic effects and cross-talks between signaling cascades (Itasaki & Hoppler, 2010), reflecting the *in vivo* situation.

Classically, the options to generate biomolecular gradients *in vitro* include the usage of biological hydrogels (Chen, *et al.*, 1998; Foxman *et al.*, 1997), micropipettes (Ming *et al.*, 2002), Boyden/Zigmond/Dunn chambers (Boyden, 1962; Zigmond, 1988; Zicha *et al.*, 1997) or transwell assays. Many of them were used to study chemotaxis (reviewed in Keenan & Folch, 2008). To generate morphogen gradients, soaked beads have been used (Gurdon *et al.*, 1994; Papin & Smith, 2000, Kiecker & Niehrs, 2001). Since these methods have limitation in spatiotemporal controls, maintenance for long time and to hardly allow the application of complex multi-factor gradients, microfluidic system was thought to be a suitable approach (Fig. 1.6).
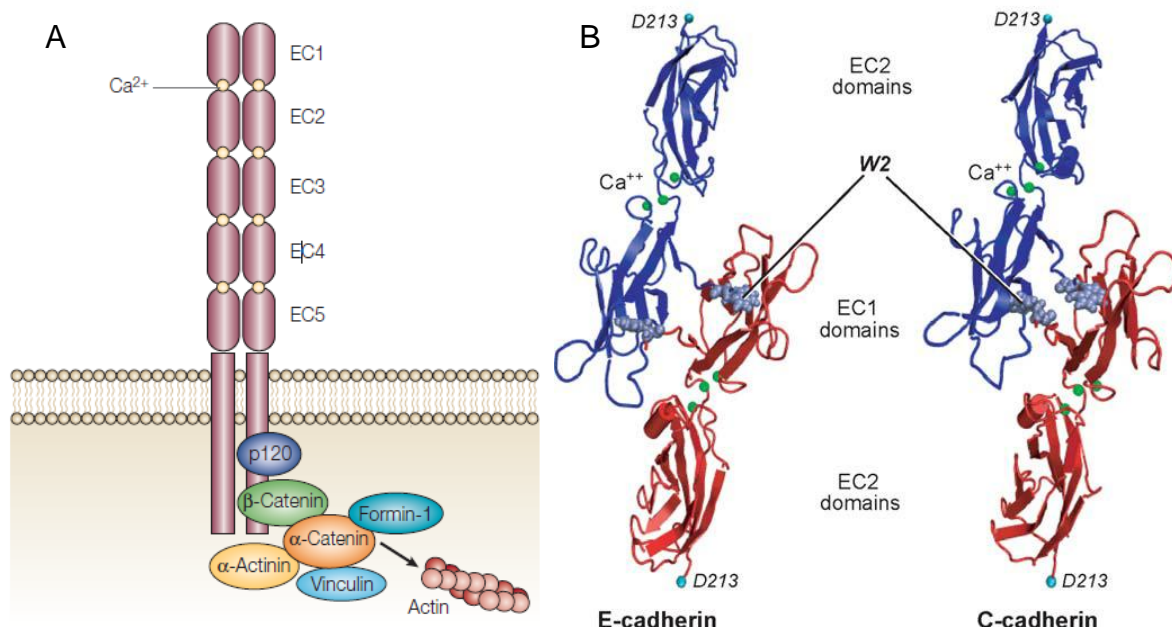


**Fig. 1.5 The cadherin structure. (A) Classical cadherins associated with catenin complex in the adherens junction. Adapted from Gumbiner, 2005. (B) Structures of strand dimers of E-Cadherin and C-Cadherin. Trp2 (W) mediates strand dimerization. EC, extracellular domain. Adapted from Leckband & Prakasam, 2006.**

1.2.2 Microfluidic approach to generate gradients

Microfluidics has the potential to regenerate dimensions of tens to hundreds of micrometers in small volumes from $10^{-9}$ to $10^{-18}$ liters (Whitesides, 2006). The advantage of such small dimension is that it allows mimicking *in vivo* environments for cell biological analyses even with limited reagents. However, with down-scaling from macro-scale to micro-scale physical factors including laminar flow, diffusion and fluidic resistance have to be considered to assure minimal shear stress for the cells but also homogenous distribution of molecules and homogenous gradient formation.
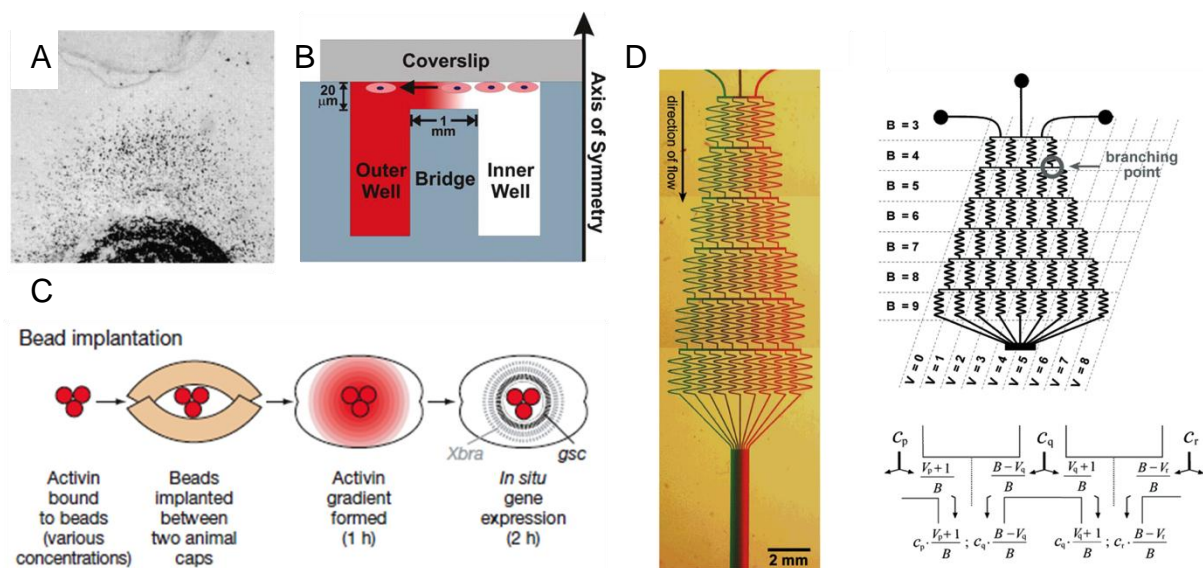


**Fig. 1.6 Various approaches for generating biological gradients. (A) Hydrogel assay for neutrophils chemotaxis towards Il-8 and leukotriene B4. Adapted from Foxman *et al.*, 1997. (B) Dunn chamber based on transwell assay. Gradient is formed in the 20 µm - gap from a source (outer well) to a sink (inner well). Adapted from Keenan & Folch, 2008. (C) Bead implantation. Activin was soaked in beads and implanted into amphibian animal cap cells to analyze gradient interpretation of gene expressions. Adapted from Gurdon & Bourillot, 2001. (D) A zig-zag micro-mixer (left) and splitting definition at each branching point (right). Adapted from Dertinger *et al.*, 2001.**

The Reynolds number of a fluid flow determines its flow regime – laminar or turbulent. It represents the ration between the inertial and viscous forces (Nguyen & Wereley, 2006). Turbulent flow, chaotic and unpredictable regime, is defined as having Re >2300, and Re < 2300 indicates a laminar flow regime. The Reynolds number is dimensionless and is defined as,

$$\mathrm{Re} = \frac{\rho \upsilon D_h}{\mu}$$

where $\rho$ is the fluid density [kg/m²], $\upsilon$ is the flow speed [m/s], $\mu$ is the fluid viscosity [kg/(m · s)], $D_h$ is hydraulic diameter [m], for rectangular channel $L_c = 4\omega h/(2(\omega+h))$, $\omega$ is channel width and $h$ channel height [m].

Diffusion is the process that concentrated particles in a volume spread out over time by Brownian motion as such the concentration reaches a constant level (Beebe *et al.*, 2002). One dimensional diffusion is indicated as *d²=2Dt*, where *d* is the distance particles move [m] in a time *t* [s], and *D* is the diffusivity of the particle [m²/s]. Regarding to two laminar fluid streams, the mixing occurs only by molecular diffusion which is a very slow process. Therefore, to increase mixing in micro-channels, several modifications of micro-channels are introduced, including changes of structure, splitting streams etc (reviewed in Capretto *et al.*, 2011).

Fluidic resistance in a micro-channel is related to pressure drop and is affected by channel geometry (Beebe *et al.*, 2002). The pressure drop [bar] is defined as $\Delta$P=R · Q, where R is the channel resistance [bar/m], Q is the flow rate [mm³/s].

## 1.3  Biological functionalization of surfaces for cadherin adhesion

The well-characterized E-Cadherin is genetically modified to have only extracellular domains EC 1-5 fused with Histidine-SNAP-tag (Fichtner, 2012). Then it is purified and used to generate cadherin mimic surfaces by nanografting method in this work. By re-generating cadherin-functionalized substrates one can expect to find a hint for manipulating cell behaviors.

### 1.3.1  Immobilization of SNAP-tag protein to self-assembled monlayer (SAM)

In the last few years many methods for specific binding of proteins of interest to engineered surfaces have been developed. The interaction can be based on covalent immobilization, non-covalent binding using affinity tags and enzymatic covalent binding. In this work, an affinity tag with the protein of interest was introduced to immobilize selective protein binding on self-assembled monolayer (SAM). The affinity tag derived from the DNA repair enzyme *O⁶*-alkylguanine-

DNA-alkyltransferase (AGT), which was mutated to achieve higher specificity for the benzyl guanine substrate and termed SNAP tag (Fig. 1.7, Pegg, 2000; Keppler *et al.*, 2003; Juillerat *et al.*, 2005; Iversen *et al.*, 2008). Selective protein immobilization is expected by using SNAP tag protein onto benzyl guanine containing SAM. As for the background i.e. non-specific area, oligo(ethylene glycol) (OEG) terminated SAM has been widely introduced since it resembles properties of poly(ethylene glycol) (PEG) that is well known for its protein and cell resistance (Lee *et al.*, 1989; Desai & Hubbell 1991; Chapman *et al.*, 2000; Smith *et al.*, 2003; Montague *et al.*, 2007). The mixture of benzyl guanine thiols and ethylene glycol (EG) containing thiols are used for direct surface immobilization of SNAP-tag fusion protein by nanografting method in this work.
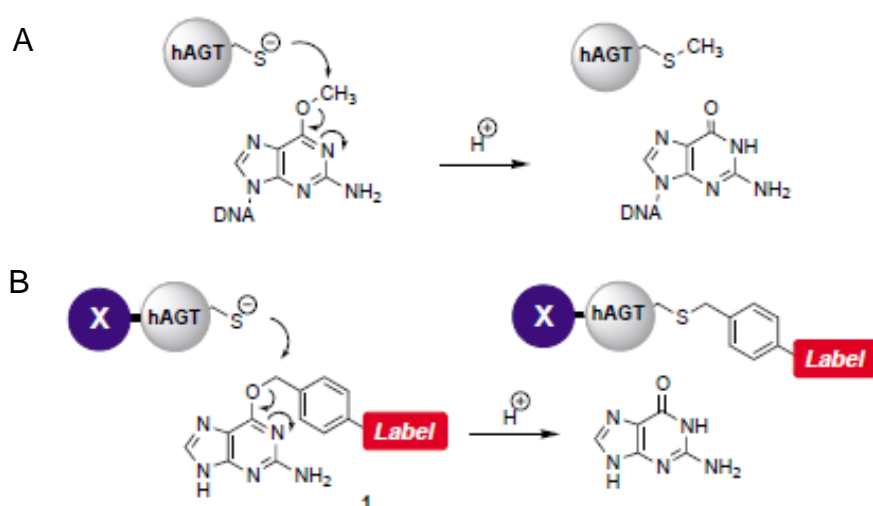


**Fig. 1.7 Mechanism of human DNA repair protein *O⁶*-alkylguanine-DNA-alkyltransferase (hAGT). (A) Basically, alkyl group from its substrate *O⁶*-alkylguanine-DNA is irreversibly transferred to one of its cysteine residues. (B) Out of some derivatives of the subrates, *O⁶*-benzyllguanine is used to bind covalently with hAGT fusion protein X. Adapted from Keppler *et al.* 2003.**

1.3.2 Nanografting

Nanografting was introduced in 1997 as atomic force microscopy (AFM) assisted lithography using thiol adsorption on gold surface (Xu & Liu, 1997). The principle is divided into three steps (Fig. 1.8), starting with scanning (or imaging) an alkanethiol SAM immersed in a solution of different kinds of thiol molecules. At this step, the surface is scanned in intermittent contact mode. In intermittent contact mode the cantilever/tip assembly is vibrated by a piezo element mounted

above and the oscillating tip taps the surface at the resonant frequency of the cantilever (70-400 kHz) with constant 20-100 nm amplitude of vertical oscillation keeping the force constant (Bhushan, 2007). The change in amplitude during scanning the surface is caused by the changing interaction between the tip and the surface due to the sample topography. As the amplitude which is detected optically by a four-quadrant photodiode has to be keep constant the sample has to be moved up or down by a piezo, according to the topography. The piezo potential necessary to move the sample up or down to keep the amplitude constant gives, therefore, an indirect value for the height on each point of the sample. This mode is appropriate to measure topography of soft surfaces since friction and other lateral forces are minimized (Bhushan, 2007).

Then, in contact mode a higher force is applied to shave away the pre-formed SAM. On the exposed gold surface, the rapid specific binding of the other thiol molecules solved in the liquid is enabled *via* strong sulfur-gold bond, therefore a pattern is formed simultaneously. In contact mode, a sharp tip makes contact with the surface. The height of the cantilever is controlled by the Z piezo, keeping the deflection constant which is set by set point. Thus, during scanning the force between tip and sample is constant that enables "shaving" the surface of interest. The applied force is calculated after calibration as,

Force [nN] = Spring constant [nN/nm] * Set point [V] * Deflection InvOLS [nm/V]

The spring constant of the cantilever is determined by thermal tuning method, the set point is given by user (higher set point gives higher force) and the deflection inverse optical lever sensitivity (InvOLS) is obtained from optical lever sensitivity (OLS), OLS = (cantilever deflection [V])/(Z displacement [nm]) that is the slope of the contact region of a force curve. When $\approx$ 400 nN is applied in contact mode, the surface is found shaved.

Lastly, the newly formed area is examined in intermittent contact mode again analyzing topography and phase simultaneously.
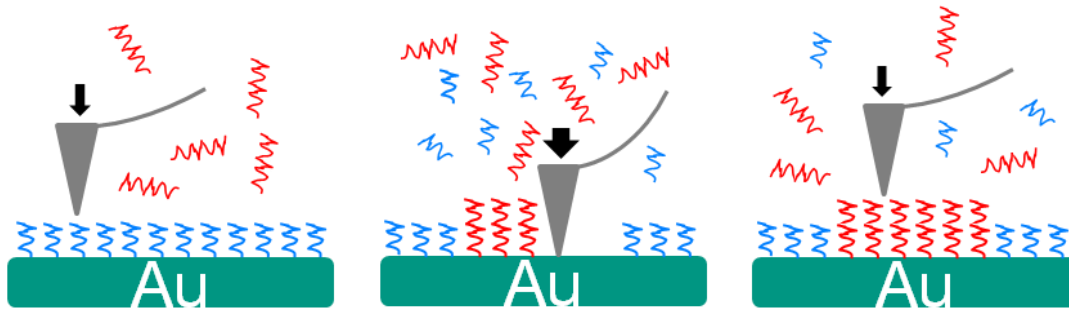
**Fig. 1.8 Schematic processes of nanografting.**

For protein applications the functionalization of surfaces by nanografting gives many advantages as follows. Extremely high spatial resolution can be assured, thus a characterization into sub-100-nm becomes applicable (Ngunjiri *et al.*, 2008). Various functional structures can be generated in one sample without changing tips (Hacker *et al.*, 2004; Yu *et al.*, 2006; Riet *et al.*, 2010) and creation of structured biological molecules such as DNA (Liu *et al.*, 2002; Schwartz, 2001), ligands (Yu *et al.*, 2006) and proteins (Wadu-Mesthrige *et al.*, 2001; Kenseth *et al.*, 2001; Liu *et al.*, 2002) has been successful. Moreover *in situ* observation of reaction mechanisms and kinetics are possible as well (Xu *et al.*, 1998).

# 2. Aim of work

Stem cells maintain the stemness in a complex microenvironment, called *niche*. In here, apart from physiological properties of the microenvironment, the soluble factors and also cellular contacts to the environment define the fate of a stem cell. Rebuilding such a stem cell microenvironment would allow controlling its differentiation and self-renewal.

The aim of this work is to come closer to recreate a stem cell microenvironment. For the application of soluble factors, a microfluidic cell-chip should be designed, produced and evaluated. This chip should allow the application of stable morphogen gradients and counter-gradients. At least, the response of cells on a Wnt3a gradient and a Dkk-1 counter-gradient should be tested.

For the cellular contact to the microenvironment, immobilized cadherin ectodomains should mimic the presence of E-cadherin expressing cells in the niche. Therefore, cadherin-anchored artificial substrates shall be generated by atomic force microscope assisted lithography and the reaction of cells on these surfaces should be analyzed.

# 3. Materials

## Chemicals

| Product | Manufacturer |
| --- | --- |
| Acrylamide, Bis-acrylamide | Carl Roth GmbH & Co., Karlsruhe |
| Acrylglas Polier&Repair Paste | Burnus, Darmstadt |
| Ammoniumpersulfate | BioRad Laboratories GmbH, München |
| BSA (bovine serum albumin) | PAA Laboratories GmbH, Cölbe |
| BSA-FITC | Invitrogen GmbH, Karlsruhe |
| BSA-tetramethylrhodamine | Invitrogen GmbH, Karlsruhe |
| Complete@ EDTA-free Protease inhibitor Cocktail Tablets | Roche Diagnostics GmbH, Mannheim |
| Crystal violet (C.I. 42555) | AppliChem GmbH, Darmstadt |
| DAPI (4',6-diamidino-2-phenylindole) | AppliChem GmbH, Darmstadt |
| DABCO (1,4-diazabicyclo[2.2.2]ocatane) | Carl Roth GmbH & Co., Karlsruhe |
| Dextran, Fluorescein | Invitrogen GmbH, Karlsruhe |
| Dextran, tetramethylrhodamine | Invitrogen GmbH, Karlsruhe |
| Dkk-1, recombinant mouse | R&D Systems GmbH, Wiesbaden |
| DMEM High Glucose (4.5 g/l) | Invitrogen GmbH, Karlsruhe |
| DMEM High Glucose (4.5 g/l) | PAA Laboratories GmbH, Cölbe |
| DMSO (dimethyl sulfoxide) | AppliChem GmbH, Darmstadt |
| DTT (dithiothreitol) | AppliChem GmbH, Darmstadt |
| Dulbecco's PBS (1x) | PAA Laboratories GmbH, Cölbe |
| Ethanol | Carl Roth GmbH, Karlsruhe |
| FCS (fetal calf serum) | Biochrom AG, Berlin |
| FCS for mES | PAN-Biotech GmbH, Aidenbach |
| FuGENE® HD Transfection Reagent | Roche Diagnostics GmbH, Mannheim |
| G418 | Carl Roth GmbH & Co., Karlsruhe |
| Gelatine | Sigma-Aldrich Chemie GmbH, Taufkirchen |
| Glutathione Sepharose™ 4FF | GE Healthcare Europe GmbH, München |
| GSK-3 Inhibitor IX, BIO | Calbiochem-Merck KGaA, Darmstadt |
| GSK-3 Inhibitor IX Control, MeBIO | Calbiochem-Merck KGaA, Darmstadt |
| HEPES | AppliChem GmbH, Darmstadt |
| Horse serum | Invitrogen GmbH, Karlsruhe |
| Imidazol | Carl Roth GmbH, Karlsruhe |
| JetPei™ | Polyplus-transfection SA, France |
| L-Glutamin (200 mM) | Gibco Invitrogen, Darmstadt |
| 2-Mercaptoethanol | Sigma-Aldrich Chemie GmbH, Taufkirchen |
| Methanol | Carl Roth GmbH, Karlsruhe |

| | |
|---|---|
| Methyl green (C.I. 42590) | Sigma-Aldrich Chemie GmbH, Taufkirchen |
| Mitomycin C | Sigma-Aldrich Chemie GmbH, Taufkirchen |
| Mowiol 4-88 | Carl Roth GmbH & Co., Karlsruhe |
| $N_2$ | Gase-Schweisstechnik Fuchs, Karlsruhe |
| NEAA (Non-essential amino acid) | Invitrogen GmbH, Karlsruhe |
| PageRuler™ Plus Prestain Protein Ladder | Fermentas, St. Leon-Rot |
| PBS without Ca/Ma | PAA Laboratories GmbH, Pasching |
| Penicillin/Streptomcin (100x) | PAA Laboratories GmbH, Cölbe |
| Phalloidin-Oregon Green 488 | Invitrogen GmbH, Karlsruhe |
| Pluronic® | Sigma-Aldrich Chemie GmbH, Taufkirchen |
| Poly-l-lysine 0.01% | Sigma-Aldrich Chemie GmbH, Steinheim |
| Profinity™ IMAC Ni-Charged Resin | BioRad Laboratories GmbH, München |
| RPMI1640 | PAA Laboratories GmbH, Cölbe |
| Silver nitrate | Carl Roth GmbH, Karlsruhe |
| Skimmed milk powder | TSI GmbH & Co. KG, Zeven |
| Sodium Chloride | AppliChem GmbH, Darmstadt |
| Sodium Dodecyl Sulfate | Serva Electrophoresis GmbH, Heidelberg |
| Sodium Pyruvate (100 mM) | Biochrom AG, Berlin |
| TEMED | AppliChem GmbH, Darmstadt |
| 1-Thioglycerol | Sigma-Aldrich Chemie GmbH, Taufkirchen |
| TransPass™ COS/HEK293 Reagent | New England Biolabs, Frankfurt am Main |
| Tris | Carl Roth GmbH & Co., Karlsruhe |
| Triton X-200 | AppliChem GmbH, Darmstadt |
| Trypsin/EDTA (1x) | PAA Laboratories GmbH, Cölbe |
| Tween®20 | AppliChem GmbH, Darmstadt |
| UV-light curable adhesive, 1187-M Ultra Light-Weld® | Dymax Europe GmbH, Wiesbaden |
| Wnt-3a, recombinant mouse | R&D Systems GmbH, Wiesbaden |

**Thiol/disulfide**

BGT : Benzylguanin (BG)-Thiol ($C_{48}H_{82}N_6O_9S_2$)
(Senso Path Technologies, Inc., Bozeman, USA)
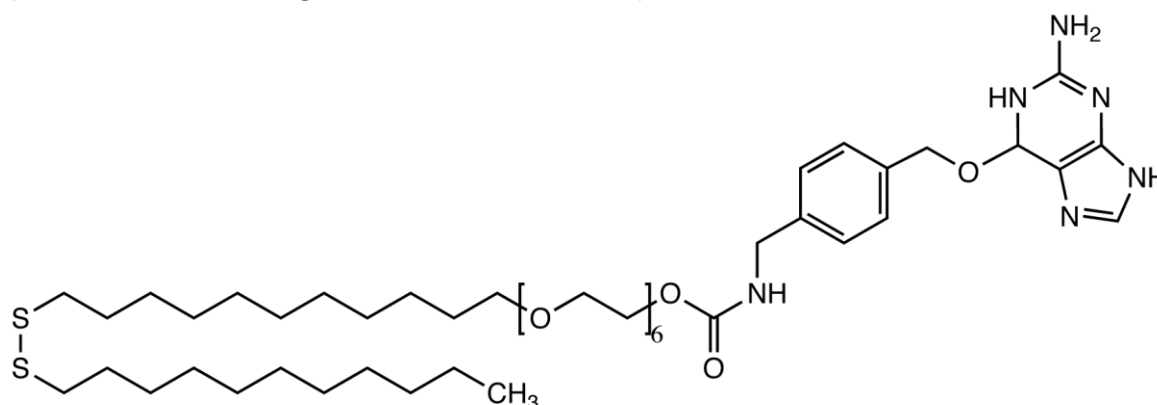
EG$_6$OH : EG6-disulfide (C$_{23}$H$_{48}$O$_7$S)$_2$ (ProChimia, Poland)
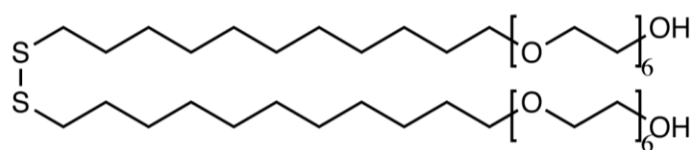


EG$_3$OMe : Methoxy-terminated (MeO)-EG3-Thiol (C$_{18}$H$_{38}$O$_4$S)  (Fraunhofer Institut für Fertigungstechnik und Angewandte Material Forschung, Dr. K. Rischka, Bremen)
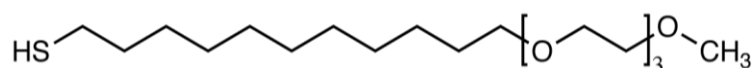


## Disposables

| Product | Manufacturer |
| --- | --- |
| Cell culture flasks/multi-well plate | Greiner Bio-One GmbH, Frickenhausen |
| Cryovials, CRYO.S™ | Greiner Bio-One GmbH, Frickenhausen |
| Falcon tube 15/50 ml sterile | Greiner Bio-One GmbH, Frickenhausen |
| **Membrane,** Isopore™ membrane filter Cyclopore Membrane Pieper Polycarbonate, pvp-free It4ip, partly perforated PC membrane | Millipore GmbH, Schwalbach Whatmann International Ltd, England Pieper Filter GmbH, Bad Zwischenahn it4ip s.a. Activalis, Belgium |
| Millicell® cell culture inserts | Millipore Ireland Ltd, Ireland |
| µ-Slide 8 well ibiTreat microscopy chamber | Ibidi, Martinsried |
| Nitrocellulose Protran Transfer membrane | Whatman GmbH, Dassel |
| **Petri Dish,** CellSTAR® BD Falcon™ | Greiner Bio-One GmbH, Frickenhausen BD Biosciences, USA |
| Polycarbonate sheet, Makrofol® DE 1-1 | Bayer Material Science AG, Leverkusen |
| Silicone Rubber, Elastosil® E41 | Wacker Chemie GmbH, Munich |
| Syringe sterile, 20/10/1ml Omnifix® | B.Braun Melsungen AG, Melsungen |
| Syringe filter, Rotilabo® 0.22 µm | Carl Roth GmbH & Co., Karlsruhe |
| Syringe needle, 0.4 mm | B.Braun Melsungen AG, Melsungen |
| **Tubing,** Polysulfone tube | Laborgeräte Handelsgesellschaft GmbH, Karlsruhe |
| Tygon® tube | Saint-Gobain Performance Plastics, France |
| Valves 2way/3way | Smiths medical Deutschland GmbH, Grasbrunn |
| VivaCell 250/15 Filter insert | Sartorius Stedim Biotech, Göttingen |

## Buffers and solutions

| Buffer | Composition |
|---|---|
| Alcian blue solution | 1 % (w/v) Alcian blue, 1 % (v/v) Acetic acid |
| AP buffer | 100 mM Tris/HCl (pH 9.5), 100 mM NaCl |
| Blocking buffer for WB | 5 % Skimmed milk powder in TBST |
| Blocking buffer for IS | 10 % horse serum in TBST 2.5 % BSA in 1xPBS |
| Coomasie Brilliant Blue Destaining solution | 45% MeOH, 10% Acetic acid in $dH_2O$ |
| Coomasie Brilliant Blue Staining solution | 4 g CBB R250, 100 ml Acetic acid, 450 ml MeOH up to 1 l $dH_2O$ |
| DAPI stock solution | 1 mg/ml in DMF (end dilution 1:1000) |
| Electrophoresis buffer (SDS-running buffer) | 25 mM Tris, 192 mM Glycin, 0.1 % (w/v) SDS, pH 8.3 |
| Elution buffer (GST-tag purification) | 50 mM Tris, 10 mM glutathione, pH 8.0 |
| Elution buffer (His-tag purification) | 500 mM Imidazol in HBS, pH 7.5 |
| Freezing medium | 40 % medium, 40 % FCS, 20 % DMSO |
| Freezing medium for mES/ MEF | 90 % FCS, 10 % DMSO |
| G418 | 1 g in 10 ml DMEM |
| 0.1 % Gelatin | 0.1 % Gelatin in 1x PBS, autoclaved |
| HBS buffer | 10 mM HEPES, 150 mM NaCl, pH 7.5 |
| LB Medium | 10 g Bacto-tryptone, 5 g Yeast Extract, 10 g NaCl up to 1 l $dH_2O$, pH 7.5 |
| Lysis buffer (GST-tag purification) | 400 mM NaCl, 50 mM Na-$PO_4$, 10 mM imidazol, pH 8.0 |
| Mitomycin C stock | 2 mg in 10 ml 1x PBS, 4 ºC |
| Mowiol /DABCO | 6 g Glycerin, 2.4 g Mowiol 4-88, 12 ml 0.2 M Tris/HCl (pH 8.5), 25 mg DABCO per ml |
| Na-$PO_4$ buffer (GST-tag purification) | 500 mM $NaH_2PO_4$, 500 mM $Na_2HPO_4$, pH 8.0 |
| NBT/BCIP | 1.75 ml/ml NBT, 3.5 ml/ml BCIP in AP buffer |
| NP40 lysis buffer | 25 mM HEPES/KOH pH 7.9, 1.5 mM EDTA, 50 mM NaCl, 0.5% NP40 |
| PBS buffer (1x) | 137 mM NaCl, 2.7 mM KCl, 6.5 mM $Na_2HPO_4$, 1.5 mM $KH_2PO_4$, pH 7.5 |
| PBST | 0.1 % (v/v) Tween 20 in PBS |
| Permealizing solution | 0.5 % Triton® X-100 in 1x PBS |

| | |
|---|---|
| PFA fixing solution | 4 % Paraformaldehyde in 1xPBS |
| SDS-loading buffer | 50 mM Tris/HCl (pH 6.8), 10 % (w/v) SDS, 20 % (v/v) Glycerin, 5 % (v/v) ß-Mercaptoethanol, 0.1% (w/v) Bromophenol blue |
| Separation medium | 2 % Chicken serum, 2 mM EDTA in PBS |
| **Silver staining solution,** | |
| Fixation | 40 % EtOH, 7 % acetic acid |
| Staining | 0.1 % $AgNO_3$ |
| Developing | 2-3 % $Na_2CO_3$, 0.02 % Formaldehyde |
| Start buffer | 10 mM Imidazol in HBS, pH 7.5 |
| TBS buffer (10x) | 0.5 M Tris/HCl, 1.5 M NaCl, pH 7.4 |
| TBST | 0.05 % Tween 20 in 1x TBS |

## Bacteria and cell lines

| Bacteria |
|---|
| *E.coli*-BL21-Al™ (Invitrogen, Darmstadt) |
| Genotype : *$F^-$ ompT $hsdS_B(r_B^- m_B^-)$ gal dcm araB::T7RNAP-tetA* |

| Cell lines | Description | Medium | Reference |
|---|---|---|---|
| HEK/ECad_EC1-5_SNAP_12His | Stably transfected with ECad-EC1-5-SNAP-12His | Complete DMEM + 2 mg/ml G418 | Engin, 2010, Karlsruhe |
| HeLa | Human cervical cancer cell | Complete RPMI1640 | ATCC: CCL-2 |
| L-Cell | Murine fibroblast | Complete DMEM | ATCC : CCL-1.3 |
| L-Cell/ ECad_EC1_5_EGFP | Stably transfected with hECadEGFP | Complete DMEM + 2 mg/ml G418 | Fichtner, 2012, Karlsruhe |
| LIF cα-5 | LIF expressing HEK293 | Complete MEMα | Erwin Wagner, Madrid, Spain |
| MCF-7 | Human breast cancer cell | Complete RPMI1640 | ATCC: HTB-22 |
| MEF | Primary murine embryonic fibroblast | Complete DMEM for mES | Prepared with A. Rolletschek, Karlsruhe |
| Oct4-EGFP mES | Murine embryonic stem cell with reporter construct | Complete DMEM for mES, + LIF | Kirchhof *et al.* 2000 |
| W4 mES | Murine embryonic stem cell | Complete DMEM for mES, + LIF | Auerbach *et al.* 2000 |

## Cell culture media

| Type | Composition with supplements |
|---|---|
| Complete DMEM | DMEM High Glucose (PAA), 1% Penicilin/Streptomycin ,10% FCS |
| Complete DMEM for mES | DMEM High Glucose, 1% Penicilin/Streptomycin, 15% FCS, 1mM Sodiumpyruvate, 2mM L-Glutamine, 1x NEAA (100x) , 0.1 mM β-Mercaptoethanol |
| Complete HD-medium | IMDM, 1% Penicilin/Streptomycin, 20% FCS, 2mM L-Glutamine, 1x NEAA (100x), 1.5ml 1-Thioglycerol mixture (13 µl 1-Thioglycerol in 1ml IMDM, sterile filtered) |
| Complete MEMα | MEMα (w/o nucleotides), 1% Penicilin/Streptomycin , 10% FCS |
| Complete RPMI1640 | RPMI1640, 1% Penicilin/Streptomycin, 10% FCS |
| Conditioned RPMI1640 (CM) | 50 % of 2-3 days cultured medium on confluent HeLa, centrifuged and sterile filtered, 50% complete RPMI |
| Leibovitz's medium | Leibovitz's medium (w/o L-Glutamine, phenol red ), 15mM HEPES, 290 mg/ml L-Glutamine, 1% Penicilin/Streptomycin, 5% FCS |

## Antibodies

| Primary antibody | Dilution (IF) | Dilution (WB) | Supplier | Host | Etc. |
|---|---|---|---|---|---|
| α -active β-catenin | - | 1 : 1000 | Millipore | M | 05-665 |
| α -β-actin | - | 1 : 1000 | Sigma-Aldrich | M | A-5441 |
| α -β-catenin | 1 : 100 | 1 : 1000 | BD Transduction Laboratories | M | 610153 |
| α -β III Tubulin | 1 : 140 | - | Millipore/ Chemicon | M | MAB1637 |
| α -Connexin 43 | 1 : 400 | 1 : 500 | Abcam | Rb | Ab11370 |
| α -ECad (DECMA) | 1 : 500 | 1 : 2000 | Sigma-Aldrich | R | U3254 |
| α -ECad | 1 : 250 | 1 : 500 | Santa Cruz Biotechnology | Rb | H-108 |
| α -GFP | - | 1 : 1000 | Abcam | Ch | Ab13970 |
| α -NCad | 1 : 200 | 1 : 2000 | Santa Cruz Biotechnology | Rb | H-63 |
| α -Nestin | 1 : 35 | - | Millipore/Chemicon | M | MAB353 |
| α -Oct 3/4 | 1 : 100 | 1 : 500 | Santa Cruz Biotechnology | M | C-10 |
| α -SNAP | 1 : 100 | 1 : 500 | Thermo | Rb | CAB4255 |
| α -Sox 2 | 1 : 250 | - | Abcam | Rb | AB5603 |
| α-Troponin | 1 : 200 | - | Abcam | M | Ab33589 |

IF : Immuno fluorescence
WB : Western Blot
M : Mouse, Rb: Rabbit, R: Rat, Ch: Chicken

| Secondary antibody | Conjugates | Dilution | Supplier |
|---|---|---|---|
| Goat-anti-Chicken | Allkaline phosphatase | 1: 2000 | |
| Goat-anti-Mouse | Allkaline phosphatase | 1: 2000 | |
| Goat-anti-Mouse | Cy2 or Cy3 | 1 : 400 | |
| Goat-anti-Mouse | Peroxidase | 1 : 20000 | Dianova GmbH |
| Goat-anti-Rabbit | Allkaline phosphatase | 1 : 2000 | |
| Goat-anti-Rabbit | Cy2 or Cy3 | 1 : 400 | |
| Goat-anti-Rabbit | Peroxidase | 1 : 20000 | |
| Goat-anti-Rat | Cy3 | 1 : 400 | |

## Equipments

| Equipment | Manufacturer |
|---|---|
| **AFM,** | |
| MFP-3D-BIO™ | Asylum Reserach, USA |
| Software, IGOR Pro 6.2.2.2 | WaveMetrics, Inc., USA |
| Cantilever, NSC-35/NSC-36 | MicroMasch, Estonia |
| **Balance,** BP221S/PT310 | Sartorius AG, Göttingen |
| **Blot-Apparatur,** Trans-Blot® SD Semi-Dry Electrophoretic Transfer Cell | BioRad Laboratories GmbH, München |
| **Centrifuge,** | |
| Heraeus Multifuge 3 S-R | M&S Laborgeräte GmbH, Wlesloch |
| Hettich Universal 32 R | Andreas Hettich GmbH & Co. KG, Tuttlingen |
| Heraeus® FrescoTM | Thermo Fisher Scientific Inc., Waltham, USA |
| Ultracentrifuge HITACHI SORVALL Discovery M120SE | Thermo Fisher Scientific Inc., Waltham, USA |
| **Chemiluminescence Imaging system,** DIANA II | Raytest, Straubenhardt |
| **Chromatography glass Columns**, TAC15/125PE0-AB-1 | KronLab Chromatography Technology, Dinslaken |
| **Concentrator**, Vivacell 250 | Sartorius AG, Göttingen |
| **Cryo-storage system,** Biorack 5400 | Thermo Fisher Scientific Inc., Waltham, USA |
| **Electrophoresis Apparatus**, Mini Protean® | BioRad Laboratories GmbH, München |
| **FPLC apparatus,** BioLogic HR Chromatography System BioLogic Workstation Fraction Collector Model 2128 BioLogic HR System Software | BioRad Laboratories GmbH, München |

| | |
|---|---|
| **Freezing container**, <br> Nalgene® Mr. Frosty | Sigma-Aldrich Chemie GmbH, <br> Taufkirchen |
| **Incubator,** <br> APT LineSerie BD/ED/FD <br> Steri-Cycle $CO_2$ incubator <br> Series II Water-Jacketed $CO_2$ incubator | <br> Binder, Tuttlingen <br> Thermo Forma, USA |
| **Laminar flow bench**, Microflow2 | NUNC, Roskilde, Denmark |
| **Micromachining** | i-sys Mikro- und Feinwerktechnik GmbH |
| **Microscope,** <br> Inverse Light microscope Olympus CK2 <br> Spinning Disc Microscope Observer Z1 <br>    Cell Observer SD <br>    CCD Camera AxioCam MRm <br>    AxioVision 4.8.2 (Software) <br> MZ FLIII <br>    CCD camera <br>    OpenLab 5.5.0 (Software) <br> DMIRE 2 <br>    Digital Camera C4742-95-12 ERG <br>    OpenLab 5.5.0 (Software) <br> Scanning electron microscope, SmartSEM™ <br>    ELPHY Plus ver. 5.0 (Software) | Olympus Optical Co. GmbH, Hamburg <br> Zeiss MicroImaging GmbH, Jena <br> Yokogawa Electric Coorporation, Ratingen <br> Zeiss MicroImaging GmbH, Jena <br> Zeiss MicroImaging GmbH, Jena <br> Leica Microsystem, Bensheim <br> QIMAGING <br> Improvision, Heidelberg <br> Leica Microsystem, Bensheim <br> Hamamatsu, Herrsching <br> Improvision, Heidelberg <br> Carl Zeiss SMT Ltd, Oberkochen. <br> Raith GmbH, Dortmund |
| **Neubauer-counting chamber** | Marienfeld, Lauda-Königshofen |
| **Pump,** <br> Digital syringe pump PHD 22/2000 <br><br> Peristaltic pump 205/CA8 | <br> Harvard apparatus GmbH, March-Hugstetten <br> Watson-Marlow GmbH, Rommerskirchen |
| **Shaking incubator**, Forma Incubated **Tabletop Orbital Shaker**, Model 420 | Thermo Fisher Scientific Inc., Waltham, USA |
| **Spectrophotometer**, <br> Ultrospec 2100 pro | Amersham Biosciences, Freiburg |
| **Sputtering system**, <br> Leybold-Heraeus Z400 | Leybold-Heraeus GmbH, Hürth |
| **ToF-SIMS,** <br> Bi cluster liquid metal ion source <br> Reflectron type TOF analyzer | ION-TOF GmbH, Münster |
| **Ultra-low Temperature Freezer** | New Brunswick Scientific, New Jersey, USA |
| **Ultrasonic system**, Sonorex | Bandlin, Mörfelden-Walldorf |
| **UV-lamp**, MHL 570 | UV Technik Meyer GmbH, Ortenberg |
| **Vaccum pump**, Laboport N81KT.18 | KNF Neuberger GmbH, Freiburg |
| **Waterbath,** <br> Modell WNB 7 <br> WB12 | <br> Memmert GmbH Co. KG, Schwabach <br> PD industriegesellschaft GmbH, Dresden |

## Other materials

| Plasmids | | Reference |
|---|---|---|
| Xwnt2bEGFP in pCS2 | | Holzer *et al.*, 2012 |
| Super-Top-Flash-dsRed | | Waaler *et al.*, 2011 |
| pCMVLifeAct-TagGFP2 | | Ibidi GmbH, Martinsried |
| GAB43 GFP + H2B mCherry | | Carmona-Fontaine *et al.*, 2008 |

| Kits | Manufacturer |
|---|---|
| BCA Protein Assay Kit | Merck KGaA, Darmstadt |
| ECL Plus™ Western Blotting Detection system | Amersham GmbH, Freiburg |
| Pure Yield™ Plasmid Midiprep | Promega GmbH, Mannheim |

# 4. Methods

## 4.1 Cell biological methods

### 4.1.1 Mammalian cell lines

#### 4.1.1.1 Cultivation, passaging and freezing of cell lines

Cell lines are cultivated in culture medium at 37 ºC, 7% $CO_2$ incubator and divided in an appropriate dilution ratio (1:5 – 1:20) into new flasks. To detach cells from the surface, they are incubated in Trypsin/EDTA for 2 min at 37 ºC. The enzymatic activity stops after adding complete medium. For freezing, detached cells are collected by centrifugation 900 rpm for 5 min at 4 ºC, resuspended in freezing medium and transferred into cryo-vials. To minimize the damage during freezing process, Mr. Frosty is used for gradual pre-freezing at -80 ºC for 2 weeks before transfer into liquid $N_2$ tank.

#### 4.1.1.2 Transfection

Transfection is the introduction of a foreign DNA into eukaryotic cells. Following the manufacturer's guidelines, jetPEI™, FuGENE® HD, TransPass™ are used for each purpose.

For calcium phosphate precipitation, semi-confluent cells are supplied with fresh medium and incubated at 37 ºC for 4 hours. The transfection complex consisting of 1 ml 1xHBS pH 7.12, 4 µg of DNA and 50 µl of 2.5 M $CaCl_2$ is incubated for 20 min at room temperature and added on the cells. The medium is replaced 4 hours later. Stably transfected cells (HEK/ECad_EC1-5_SNAP_12His and L-Cell/ Ecad_EC1-5_EGFP) are maintained by adding 0.02 v/v % of G418 in culture every two-three days.

#### 4.1.1.3 Cell counting

When the exact cell number is needed, the Neubauer haemocytometer is used for counting. Collected cells are resuspended in culture medium. 10 µl of this cell suspension is added into the divided grid by capillarity. The haemocytometer consists of 4 groups of 16 squares and the volume of cell suspension that will

occupy one square is 1.0 x $10^{-4}$ ml. The number of all 4 groups is averaged. Total cell concentration is calculated as follows;

Final cell number / ml = average number of 4 groups x $10^4$ x dilution factor*

*Dilution factor = [(volume of sample + volume of diluent)/volume of sample]

### 4.1.2  Murine embryonic stem cells (mES)

### 4.1.2.1  Cultivation and passaging of W4 and Oct4-EGFP mES

Murine embryonic stem cells (mES) are routinely cultured on a layer of murine embryonic fibroblasts (MEFs). The condition of co-culture with inactive MEFs makes mES maintaining an undifferentiated pluripotent state. Two mES lines, W4 and Oct4-GFP are used in co-culture condition to cultivate supplemented with 1.6 v/v % LIF, passaged every 2 days. If necessary, mES are separated from the MEF layer at maximum after 30 passages.

### 4.1.2.2  Separation of mES from MEFs – "preplating"

To remove MEFs out of the co-cultured condition, cells are collected by Trypsin/EDTA or separation media and plated on bacteriological dishes for 30 min. The non-adherent mES are collected and replated on gelatin-coated dishes. Afterwards, they are grown in mES medium supplemented with 2 v/v % LIF. To obtain MEFs-free mES, the preplating is repeated.

### 4.1.2.3  Extraction of primary mouse embryonic fibroblasts (MEFs) and their preparation as feeder layers

Murine embryonic fibroblasts are obtained from 15.5-16 days-old embryos. Nerve, spleen, liver and gut excluded tissue is dissociated by Trypsin/EDTA. After further mechanical dissociation, blood cells are removed by centrifugation at 1300 rpm for 5 min at 4 °C, incubated in tissue culture dishes and cryo-preserved until use. To avoid contamination by other cells they are used only for 2-5 passages. To use these cells as feeder layers, cell division is inhibited by treatment with 0.01 mg/ml Mitomycin C. Incubation time of Mitomycin C varies from 2 hours for fresh Mitomycin solution over 2.5 hours for 2-5 day-old and 3 hours for 5-30 day-old Mitomycin. The inactive MEFs are prepared in gelatin-

coated dish and used from the next day of Mitomycin treatment.

### 4.1.2.4  Production of leukemia inhibitory factor (LIF)

LIF is routinely used for mES as supplement, which promotes long-term maintenance of pluripotency of mES by suppressing spontaneous differentiation. (Nichols *et al.* 2001; Sato *et al.*, 2004; Noggle *et al.*, 2005). In this thesis work, LIF is obtained from the supernatant of LIF cα-5 stably transfected cells. Cells are seeded in a concentration of $1x10^6$ /ml and cultured in in complete MEMα medium. Supernatant is collected after 48 hours cultivation and sterile filtered before use.

### 4.1.2.5  Formation of embryoid bodies (EBs) for inducing differentiation by hanging drop method

The formation of EBs is one of the mostly used protocols for *in vitro* differentiation of mES into derivatives of all three germ layers. MEFs-free mES are collected in complete HD/EB medium and diluted to 600 cells / drop with a drop size of 20 µl (Day1). The drops are incubated for 48 hours on the lid of a bacteriological dish filled up with PBS. The formed EBs are rinsed in complete HD/EB medium and transferred into a new bacteriological dish (Day3). After 2 days, single EBs are plated in one well of a gelatin-coated 24 well plate (Day5). Differentiated cells are analyzed after certain days by morphological changes, immunostaining and western blotting.

## 4.2  Molecular biological and biochemical methods

### 4.2.1  Transformation of chemo-competent *E.coli*

The introduction of circular foreign plasmid DNA into chemo competent bacterial BL21 is done by heat-shock. DNA is transferred in 50 µl of bacterial cells and incubated for 30 min on ice. The bacterial cells are exposed to 42 °C heat-shock for 45 seconds. After 2 min on ice 900 µl soaking media are added and cells are incubated for 1 hour at 37 °C in a shaking incubator. Bacterial cells are sedimented for 5 min at 2000 rpm and 700 µl is discarded. The rest 200 µl is resuspended and is spread on a pre-warmed agar plate containing appropriate

antibiotics. After 16-20 hours distinguishable colonies are seen.

Plasmid preparation

A single colony of transformed bacteria is incubated in 100 ml LB media with appropriate antibiotics (1:1000) at 37 °C overnight in a tabletop orbital shaker. Plasmid DNA is extracted by the Pure Yield™ Plasmid Midiprep kit following the manufacturer's protocol. The concentration of the pure plasmid solution is determined by measuring the absorbance at 260 ($A_{260}$), with $A_{260} = 1$ for 50 μg/ml of a pure solution of double stranded DNA. The identity of the purified constructs is verified by enzymatic digestion and/or by sequencing.

4.2.2  Production of recombinant proteins in BL21 bacterial cells

10 ml antibiotic containing LB-medium is inoculated with one colony or 50 μl freshly transformed bacterial cells and incubated overnight. On the next day, 1 ml of the incubated culture is added in 100 ml of fresh medium and incubated until $OD_{600}$ reaches 0.6-0.8. For protein induction 1 ml of 100 mM Isopropyl ß-D-1-thiogalactopyranoside (IPTG) is added and the temperature is set to 30 °C. Samples are taken after 1, 2, 3 and 4 hours. At the end of incubation, the cells are sedimented at 5700 rpm for 10 min at 4 °C and stored at -80 °C until use.

Purification

Cell pellets are lysed by ultrasonication in 1 ml lysis buffer including protease inhibitor and centrifuged at 32000 rpm for 30 min at 4 °C. 500 μl of Glutathione sepharose™ is washed with PBS and lysis buffer. The supernatant of the cell lysate is transferred to glutathione sepharose. Binding is conducted by rotating for 2 hours at 4 °C with 20 U/min. The protein-bound sepharose is centrifuged at 3000 rpm for 5 min at 4 °C and washed three times with lysis buffer. Elution buffer is filled as same volume of sepharose and rotated for 5/10/20 min at 4 °C. The purified protein with protease inhibitor is stored at 4 °C up to 2 weeks until use.

4.2.3  Production of recombinant proteins in eukaryotic cells

Stably transfected HEK cells are used for production of E-Cadherin-EC1-5-SNAP-12His in G418 selection condition. After two or three days of culture in 175

cm$^2$ flask the supernatant is collected and centrifuged at 2000 rpm for 10 min at 4 ºC to remove cell debris. Protease inhibitor is added to avoid degradation and the supernatant is filtered through 0.22 μm membrane filter. It is concentrated by pressure filter which is with Vivacell insert, so larger proteins than 30 kDa can be collected from 400-500 ml of cell supernatant to about 10 ml of concentrated volume.

Purification

The high affinity between Histidine and Ni$^{2+}$ allows purification of His-SNAP-GFP and E-Cadherin-EC1-5-SNAP-12His proteins. Crude extracts are prepared either from bacterial cells for His-SNAP-GFP or from eukaryotic cells for E-Cadherin. Low affinity bound proteins or unspecifically bound proteins are washed by low concentrations of phosphate and imidazol (10 mM). Then, the concentration of imidazol is increased in a linear gradient up to 500 mM to elute the Histidine tagged proteins from the NTA-beads. Table.4.1 describes the selected major steps on a Ni$^{2+}$-NTA column of FPLC apparatus.

**Table. 4.1 Selected steps of FPLC protocol for His-tagged proteins.**

| | Step | Buffer | Volume/Flow rate |
|---|---|---|---|
| 1 | Loading column | Crude extract + Start buffer | Crude extract vol. 5 ml Flow rate: 0.5 ml/min |
| 2 | Isocractic flow | Start buffer | Volume: 15 ml Flow rate: 0.5 ml/min |
| 3 | Linear gradient elution | Start buffer 100 % → 0 % Elution buffer 0 % → 100 % | Volume: 30 ml Flow rate: 0.5 ml/min |
| 4 | Isocractic flow | Elution buffer | Volume: 15 ml Flow rate: 0.5 ml/min |
| 5 | Isocractic flow | Start buffer | Volume: 15 ml Flow rate: 0.5 ml/min |

The purification is confirmed by SDS-PAGE and western blot analysis. The fractions containing the desired proteins are pooled and concentrated by VivaSpin15 filter. After the concentration is determined, DTT is added to a final concentration of 1 mM.

4.2.4 Bicinchoninic acid (BCA) assay

Purified protein concentrations are quantified by BCA assay according to a standard curve. Standard samples of each BSA concentration (0-2 µg/µl) are prepared as follows (Table. 4.2). Under alkaline conditions, $Cu^{2+}$-protein complex is formed followed by reduction of the $Cu^{2+}$ to $Cu^{1+}$. BCA forms purple-colored products with $Cu^{1+}$ in alkaline condition. The reduction is directly proportional to the amount of proteins. Working solution (BCA solution:4 % $CuSO_4$ = 50:1) is mixed into samples and standards according to manufacturer's instruction and they are incubated for 25 min at 37 ºC. The absorbance at 562 nm of purple-colored reaction products is determined and used for standard curve calculation and calculation of samples' protein concentration.

**Table. 4.2 BSA samples for a standard curve.**

| Standard | Std 1 | Std 2 | Std 3 | Std 4 | Std 5 | Std 6 |
|---|---|---|---|---|---|---|
| Concentration. (µg/µl) | 0 | 0.125 | 0.25 | 0.5 | 1.0 | 2.0 |
| Dilution | 100 % $H_2O$ | 50% of Std 3 in $H_2O$ | 50% of Std 4 in $H_2O$ | 50% of Std 5 in $H_2O$ | 50% of Std 6 in $H_2O$ | 100 % BSA stock |

4.2.5 Sodium dodecyl sulfate polyacrylamide gel electrophoresis (SDS-PAGE)

Cells are collected in ice-cold PBS by a scraper and transferred into a tube. After centrifugation, the obtained cell pellet is resuspended with NP40 lysis buffer including protease inhibitor and broken by passing through 0.4 mm needle. The lysate is rotated for 1 hour at 4 ºC followed by centrifugation. Final protein mixture is obtained from the supernatant and stored at -20 ºC if needed.

Proteins are denaturized in SDS loading buffer by heating for 5 min at 95 ºC. Equal amounts of protein are loaded into the wells of freshly prepared gels (Table. 4.3) together with marker and separated at 60-80 V until proteins leave the stacking gel followed by 100-120 V for resolving gel. Before the marker bands approach at the end of gels, electrophoresis is stopped and gels are separated and transferred into Transfer buffer. Coomassie brilliant blue or silver are used for staining the separated protein bands.

**Table. 4.3 Composition of SDS PAGE gels**

| Components (ml) | Resolving gel (5 ml) | | | | Stacking gel (2 ml) |
|---|---|---|---|---|---|
| % Gel | 6 % | 8 % | 10 % | 12 % | 5 % |
| $H_2O$ | 2.6 | 2.3 | 1.9 | 1.6 | 1.4 |
| 30 % acryl-bisacrylamide mix | 1.0 | 1.3 | 1.7 | 2.0 | 0.33 |
| 1.5 M Tris (pH 8.8) | 1.3 | 1.3 | 1.3 | 1.3 | - |
| 0.5 M Tris (pH 6.8) | - | - | - | - | 0.25 |
| 10 % SDS | 0.05 | 0.05 | 0.05 | 0.05 | 0.02 |
| 10 % ammonium persulfate | 0.05 | 0.05 | 0.05 | 0.05 | 0.02 |
| TEMED | 0.004 | 0.003 | 0.002 | 0.002 | 0.002 |

### 4.2.6 Coomasie brilliant blue (CBB) staining

The separated gel is incubated in CBB staining solution for 30 min-1 hour (or overnight) on a shaking plate. The Coomasie dye binds to proteins by Van der Waals interaction and ionic interaction between dye sulfonic acid groups and positive amine groups. The gels are cleared with CBB destaining solution for 1-4 hours until the bands are clearly visible and the background is minimized.

### 4.2.7 Silver staining

Silver staining is much more sensitive than CBB staining and used to detect trace amounts of proteins in gels. It can be done on freshly separated gels and CBB stained gels. Gels are incubated in fixation solution for 3 hours or overnight at 4 ºC followed by three times washing steps in 10 % ethanol. Before staining for 30-60 min, they are briefly rinsed in distilled $H_2O$. The silver ions in the staining solution bind to proteins in the gel. In developing solution silver ions are reduced to silver metal granules as such dark brown or black protein bands are visible (10-30 min). Incubation is continued until the signal to noise ratio appears to be optimal. After 10 seconds washing with distilled $H_2O$ the reaction is stopped in 1 % acetic acid for 10-20 min.

### 4.2.8 Western-blot analysis

The transfer of proteins from an SDS-PAGE to a nitrocellulose membrane allows

the detection of specific proteins with antibodies.

Filter papers and nitrocellulose membrane are soaked into Transfer buffer. The separated gel is transferred on a nitrocellulose membrane and sandwiched by filter papers in the following order; (anode) 3 filter papers – gel – nitrocellulose membrane – 3 filter papers (cathode). A constant current of 0.05 A per membrane is applied for 90-120 min. After protein bands are transferred to the membrane, the nitrocellulose membrane is blocked to reduce unspecific binding by soaking in 5 % of skimmed milk powder in TBST for 30 min. After washed with TBST, the membrane is incubated with the primary antibody in TBST overnight at 4 ºC. The antibody can be re-used up to five times. After washing with TBST the membrane is incubated with the secondary antibody in TBST for 2 hours. Depending on the secondary antibody, the specific bands are detected either by chemiluminescence or by a colored precipitation. The enhanced chemi-luminescence reagent mixture is prepared according to manufacturers´ description and added on the membrane. The peroxidase catalyzed reaction leads to an emission of photons which are detected by the DIANA imaging system.

In the case of alkaline phosphatase conjugated secondary antibodies, the substrate solution 5-bromo-4-chloro-3indolyl phosphate (BCIP)/nitro blue tetrazolium (NBT) is applied on membrane which is briefly washed by AP buffer. Development of the band is followed by eye (30 min-5 hours) until the signal to noise ratio appears to be optimal. The reaction is stopped by rinsing the membrane with distilled water.

### 4.2.9  Indirect immunofluorescence staining

Cells which are grown on cover glasses or chamber slides are washed with 1xPBS three times. PBS contains 0.5 mM $CaCl_2$ in case of cadherin-producing cells. Cells are fixed in 4 % formaldehyde in PBS for 10 min at room temperature and permealized in 0.5% Triton X-100 in PBS for 8 min. After three washes with PBST (0.1% Triton X-100 in PBS) unspecific antibody binding is blocked by 10% horse serum in PBST for one hour at room temperature. Primary and secondary antibodies are diluted in blocking buffer. Cells are incubated with the primary antibody for 2 hour at room temperature or 4 ºC over night. Again, cells are washed with blocking buffer, followed by secondary antibody incubation for 1

hour at room temperature in the dark. If necessary, cells are incubated with phalloidin (1:50 in PBS) for 20 min at room temperature to visualize actin filaments. To stain nuclei cells are incubated in DAPI solution (1 μM in PBS) for 4 min. Then samples are mounted with Mowiol 4-88 containing DABCO as anti-bleaching reagent for microscopic analysis.

As for cells on SAM, horse serum is replaced by 2.5 % BSA solution for blocking and dilution of antibodies. Incubation time differs to 30 min at room temperature for blocking, 1 hour at 37 ºC for primary antibody and 30 min at 37 ºC for secondary antibody.

## 4.3  Microfluidic chip

### 4.3.1  Fabrication of microfluidic chip

The micro-processing of the microfluidic chip is conducted at the Institute of Microstructure Technology, Karlsruhe Institute of Technology (Jubert, 2008; Kreppenhofer, 2012). In brief, polycarbonate films (Makrofol® DE1-1, 1mm thick) are used to be replicated on a brass molding insert using hot embossing technique (Fig. 4.1A, Worgull, 2009). The two parts of polycarbonate films which have the upper and lower structure and ion track-etched polycarbonate membrane (Isopore™ Membrane Filter) are sealed together liquid-tightly by thermal boding process (Fig. 4.1B, Tsao & DeVoe, 2009; Becker & Gaertner, 2008). The collaborated work varies the applied temperature, force and time and optimizes to have the range of 134-138 °C, 10-13 kN and 800 sec, respectively. The temperature is set to have under glass transition temperature of the membrane (150 °C) to avoid damage of the pores. The fluidic connection is through polycarbonate adaptors with polysulfone tubes attached.

### 4.3.2  Flow operation and mass transport in microfluidic chip

The two different transport models are characterized by measuring the concentration ratio from the initial concentrations. In both cases, the output solution from the upper chamber is collected at sequential intervals (20 min) and measured with a spectrophotometer in absorption mode at 280 nm for BSA, 616 nm for methylene green and 590 nm for crystal violet.
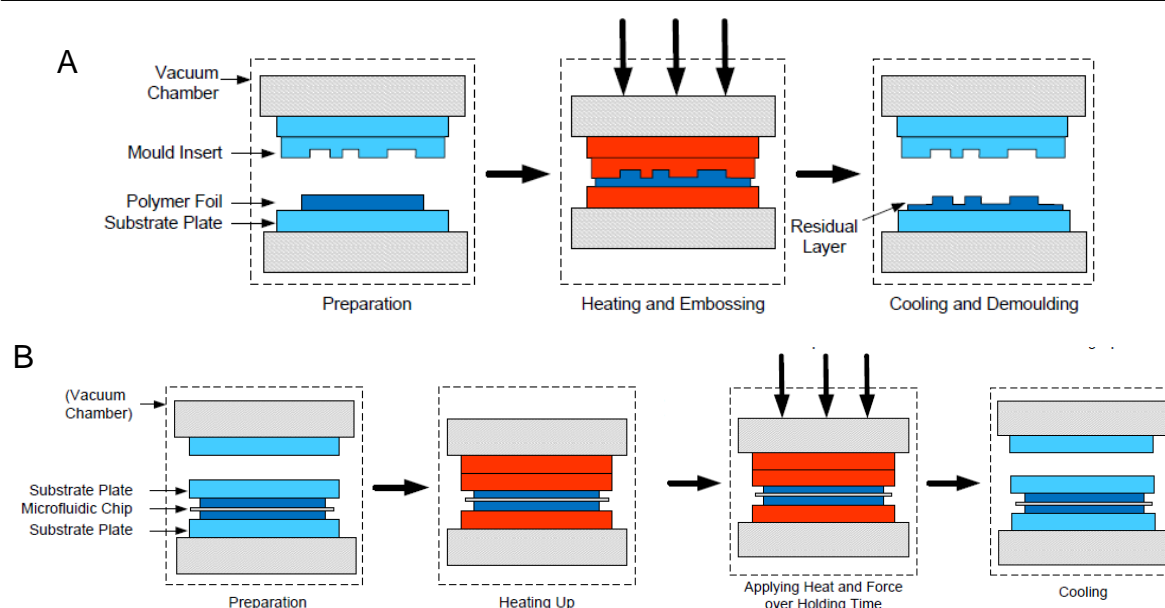
**Fig. 4.1 (A) Scheme of micro hot embossing technique and (B) two-steps thermal bonding. Adapted from Kreppenhofer, 2012.**

Diffusion-based transport

The upper and the lower part are filled with distilled water and replaced to 0.5% BSA solution for the upper and methylene green or crystal violet for the lower. The diffusive dye molecule is delivered by having minimized the hydrodynamic pressure difference between the upper and lower part, with parallel flows of 6.8 µl/min in the upper chamber and 5 µl/min in the lower channels. All inlets/outlets are open in the diffusion mode.

Convection-based transport

The upper chamber is filled with 0.5% BSA solution and the lower gradient reservoir channels are replaced to distilled water before starting pumping. When dye solution is added from the lower inlets, the inlet of the upper chamber and the outlet of the lower channels are closed. The solution passes through the membrane.

4.3.3 Generation of a step gradient by zig-zag mixer

The microfluidic chip is connected to valves and syringes. Prior to applying gradient solutions, 96% ethanol is filled in the whole apparatus to remove air bubbles. Ethanol is replaced with distilled water. To visualize a gradient, purified GST-GFP (1:10 dilution) or 12.5 µg/ml fluorophore labeled BSA-conjugates BSA-

fluorescein and BSA-tetramethylrhodamine are injected to inlets. Flow rates are controlled by digital syringe pumps. Images are captured by fluorescence stereomicroscope equipped with a CCD camera and analyzed by ImageJ. The movie is processed by Openlab 5.5 software. Similarly, BIO, recombinant Wnt3a and Dkk-1 are diluted in culture medium and added to activate the Wnt/ß-Catenin pathway.

### 4.3.4  In-chip cell culture

HeLa cells are cultured in a routine tissue culture condition before seeding into microfluidic chips. Prior to seeding cells, the microfluidic chip including tubing and valves is sterilized with 96 % ethanol filled in under UV light for 30 min for sterile inlets and outlets. PBS is flushed into the apparatus to remove the remaining ethanol and the polycarbonate membrane in the upper chamber is coated with poly-L-lysine for 1 hour at room temperature, followed by incubation of culture medium for two hours at 37°C. Cell suspension ($1.0\text{-}2.0 \times 10^6$ per ml) is seeded into the chip through Tygon tubing and the cells in chip are incubated overnight before starting perfusion. After that, inlets and outlets are connected to digitally controllable syringe pumps. RPMI conditioned medium (CM) is perfused in the upper chamber with 5.0 to 6.8 µl/ml. Comparable in-well culture is performed on glass cover slips in a 24-well plate using 0.5 ml of medium per well (2.5 mm height of medium).

## 4.4  Direct surface modification by nanografting

### 4.4.1  Preparation of Au-sputtered glass surface

Au-coating on glass coverslips is conducted by cathode sputtering at the Institute for Materials Research II, Karlsruhe Institute of Technology. Cathode sputtering means the removal of atoms from a negatively charged target or cathode by positive gas ions of plasma. Glass coverslips ($d$ = 12 mm) are boiled twice in cleaning solution ($H_2O$:$H_2O_2$:$NH_3$ = 5:1:1 volume ratio) for 20 min and washed with Millipore water 5 times. Washing is increased to 10 times after the last boiling. All glass containers for storing thiols are treated in the same manner to remove organic contamination. The "cleaned" glass coverslips are coated with Cr

about 15 nm and with Au another 120 nm thickness. The Au-coated samples are used within 3 weeks.

### 4.4.2 Patterning of self-assembled monolayers (SAM)

<u>Microcontact printing</u>

The PDMS stamp (Engin, 2010) is incubated for 10 min in a drop of absolute EtOH and dried by $N_2$ before use. Before changing the thiols, stamps are washed to prevent cross contamination in the following manner; 10 min ultrasonication in absolute EtOH, 15 min ultrasonication in 10 w/v % SDS in Millipore water, 15 min ultrasonication in Millipore water and blow dried by $N_2$. Ink molecules are dropped on the stamp and incubated for 5 min. After stamping on Au surface for 2 min the surface is filled with filling molecules for 45 min. Then the surface is washed with isopropanol and dried by $N_2$.

<u>Nanografting</u>

Au-coated glass coverslips are prepared as described previously. For SAM preparation a 1 mM thiol/disulfide stock solution is prepared and used in a desired dilution in isopropanol. Gold substrates are immersed in this thiol solution for 18-48 hours. Longer assembly time results in denser monolayer packing. The assembled layers are rinsed with isopropanol and dried by $N_2$. For the grafting experiments the samples are fixed in the middle of a petri dish by nail polish. 3 mL of a 100 µM ink solution, consisting of BGT and $EG_6$ solved in isopropanol is filled in the petri dish and finally the AFM tip is immersed into the ink solution. A laser beam is focused on the reflecting back side of a $Si_3N_4$ NSC35 3-lever cantilever (nominal spring constant A: 7.5 N/m, B: 14 N/m and C: 4.5 N/m) to have highest sum value. The cantilever is washed with isopropanol and dried before grafting. Nanografting is performed in contact mode under 5-9 V deflection set point at 1 Hz resulting in a tip velocity of 37.56 µm/s for 15x15 µm$^2$ and 25.04 µm/s for 10x10 µm$^2$ or at 2 Hz with a tip velocity of 25.04 µm/s for 5x5 µm$^2$.

### 4.4.3 SNAP-tag protein immobilization on patterns

Once SAM patterns are prepared, SNAP-GFP or SNAP-ECad_EC1-5 is coupled on BGT of pattern. Before incubating SNAP proteins, surfaces are washed with

isopropanol, dried and incubated with HBS buffer. The 2 µM protein solution in HBS is centrifuged at 13000 rpm 4 ºC for 10 min to reduce precipitants. Reaction between BG and SNAP occurs in 2 hours at room temperature on a shaking plate.

### 4.4.4 Cell culture on SAM

The specificity of SNAP-E-Cadherin_EC1-5 coated surfaces is tested by the attachment of different cell lines including L-Cell/ ECad_EC1_5_EGFP or Oct4-EGFP mES. Cells are detached by separation medium and resuspended in serum-free culture medium. Before seeding the cell suspension (1.1 x $10^5$ and 5 x $10^5$ per ml for L-Cell/ ECad_EC1_5_EGFP and Oct4-EGFP mES, respectively), surfaces are washed with culture medium without FCS. After 2 hours incubation the cells are analyzed by immune fluorescence staining..

### 4.4.5 Characterization of SAM

### 4.4.5.1 Atomic force microscopy (AFM)

After grafting, simultaneous analysis of topography, phase and amplitude is done in intermittent contact mode. Imaging is performed by scanning 90x90 µm² under <1 V deflection set point at 1 Hz (tip velocity: 225.36 µm/s) or 0.5 Hz (tip velocity: 112.68 µm/s). In both modes - intermittent and contact mode- tips scan back and forth perpendicular to the longitudinal axis of the cantilever. The topographical information is evaluated with the software IGOR.

### 4.4.5.2 Time-of-flight secondary ion mass spectrometry (ToF-SIMS)

Time-of-flight secondary ion mass spectrometry is performed by Dr. Welle at the Institute for Biological Interfaces, Karlsruhe Institute of Technology. Applying a liquid metal ion source, the specimen is bombarded with a pulsed and rastered beam of $Bi^+$ or $Bi_3^+$ primary ions with 25 keV kinetic energy. From the collision cascade of these impingent ions neutral and secondary ions are emitted from the surface of the sample. Secondary ions, being mono-atomic or larger molecular fragments, are extracted, accelerated, mass separated by a reflectron Time-of-Flight analyzer and counted. With a short primary ion pulse (< 1 ns) in "bunched mode" high spectral resolution (5000 m/Δm) can be obtained together with a

lateral resolution of approximately 2 µm due to chromatic aberrations. For high spatial resolution the primary ion beam can be focused down to 300 nm providing only nominal mass resolution. Spectrometry is performed in static SIMS mode by limiting the primary ion dose to <$10^{11}$ ions/$cm^2$. Therefore, less than 1 % of the samples surface is disturbed by the primary ion bombardment. Obtained spectra are calibrated on the $C^-$, $C_2^-$, $C_3^-$, $C_3H^-$, $C_4H^-$ peaks.

## 4.5 Microscopic methods

### 4.5.1 Fluorescence microscopic image analysis

The fluorescence images of the protein gradient in the microfluidic chip are taken by MZ FLIII. The OpenLab software allows rapid and automatic change of filters, so that fluorescent dyes with different spectra can be observed almost simultaneously. Brightness and contrasts are edited by Adobe Photoshop.

As for cell images in chip experiments, Spinning Disc microscope is used. The exposure time is fixed to 500 ms and the laser intensity is selected as 20 %, 90 %, 90 % for 405 nm, 488 nm and 561 nm, respectively. If necessary, z-stacks are chosen with spacing between two slices of 0.29 mm. Each z-stack is used as it is or as combined using "extended focus" function of Axiovision software. ImageJ software (http://rsb.info.nih.gov/ij) is used for counting cells from DAPI images, profiling of gradients, defining intensity in restricted area and roundness of stem cell colonies and subcellular localization of proteins.

### 4.5.2 Scanning electron microscopy (SEM)

To confirm the pore size and porosity of the commercially available polycarbonate membrane which is used in the microfluidic production, scanning electron microscope (SmartSEM™ Supra 55VP, Carl Zeiss) is operated in Center For Nanostructure - Nanostructure Service Laboratory in KIT campus south.

## 4.6 Statistical analysis

Data are addressed in figures as the mean with the standard error of the mean. When error bars are not given, the errors are less than the symbol size.

# 5. Results

## 5.1 Rebuilding a morphogen gradient through a microfluidic system

### 5.1.1 Structure of the microfluidic chip

To generate a two-stacked microfluidic chip that is suitable for analyzing the influence of morphogens on cells, several demands were considered (Fig. 5.1). (1) It should contain a gradient-generating part to create a stable, long-lasting and convenient gradient with different morphogens. Therefore, a zig-zag micro-mixer was used. (2) The microfluidic chip should have a cell culture micro-chamber where cells are exposed to the morphogen gradient. (3) The stability and maintenance of gradients in the gradient reservoir must be guaranteed. Therefore, the gradient reservoir was separated liquid-tight into eight different gradient reservoir channels, offering distinct concentrations of the signal molecule of choice. Cells seeded in the same chamber where the gradient is formed might disturb the gradients and suffer from shear stress. To avoid this problem, the cell culture micro-chamber and the gradient reservoir channels were separated by an ion track-etched porous membrane, supporting cell adhesion and also allowing signaling molecules to pass through it.

The details of the microfluidic chip (Fig. 5.2, Jubert, 2009), revealed that the total surface area ($A_{total}$) is: $A_{total}$ = 76 mm x 26 mm = 1976 mm$^2$. The non-contact areas of the upper part (Fig. 5.2A white, $A_{upper}$) and the lower part (Fig. 5.2B white, $A_{lower}$) are: $A_{upper} \approx$ 410 mm$^2$, $A_{lower} \approx$ 420 mm$^2$. Therefore, the contact areas (gray) when the two parts are thermally bonded are: $A_{upper} \approx$ 1566 mm$^2$, $A_{lower} \approx$ 1556 mm$^2$. Both parts have a 0.5 mm height. Thus, the volume of the upper part is $V_{upper} \approx$ 205 mm$^3$ and that of the lower part is $V_{lower} \approx$ 210 mm$^3$.

In the upper part, the cell adhesion area is considered as $\approx$ 316 mm$^2$ excluding inlet and outlet areas so the approximate volume of cells culture chamber is $\approx$ 158 mm$^3$. The growth area of commercially available 24-well cell-culture plates is 200 mm$^2$ and that of 12-well plates is 400 mm$^2$. With 1 ml medium volume in a 12-well plate, the medium height is 2.5 mm, which is 5 times higher than the 0.5

mm in the micro-chamber.
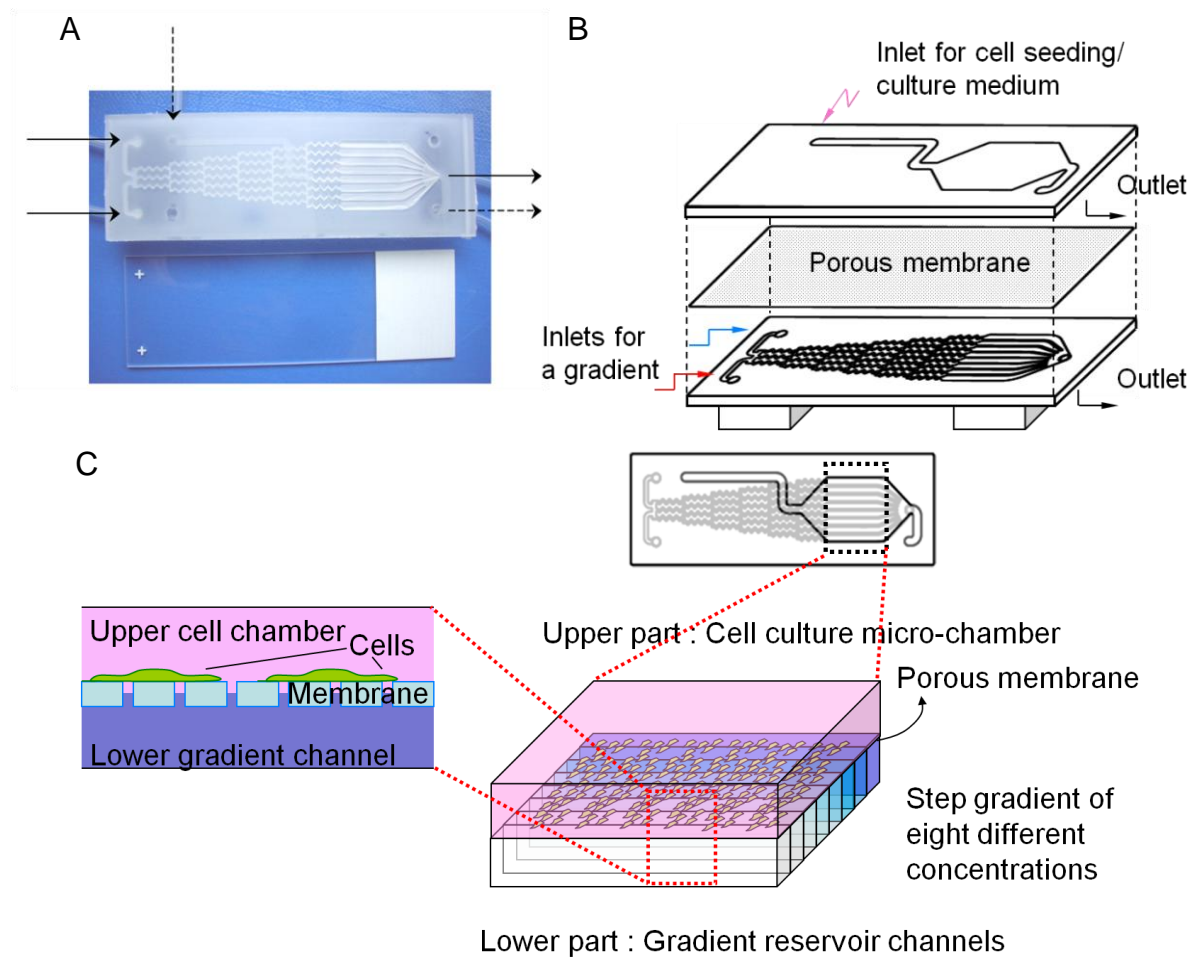


Fig. 5.1 Structure of the two-stacked microfluidic chip. (A) Top view of the complete chip with microscope glass slide (76 mm x 26 mm) for comparison. Inlets and outlets are marked by arrows; solid arrows for the lower part and dotted arrows for the upper part. (B) Schematic drawing of each composition of the microfluidic chip. The upper part is where cells are cultured and the gradient is created in the lower part. The lower gradient is reached to the cells in the upper chamber through the ion track-etched porous ($d$=0.4 µm) membrane. (C) Detailed scheme showing cells are exposed to the separated different concentration in the gradient reservoir channels. Not to scale.
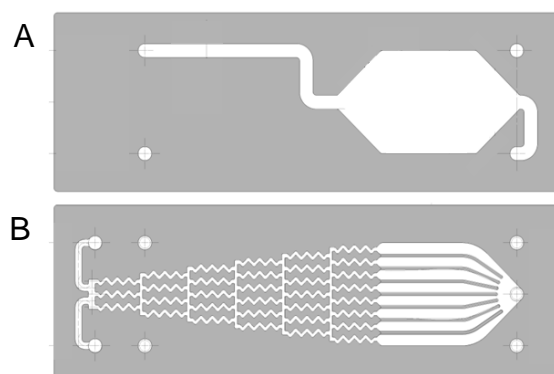


Fig. 5.2 Description of the contact area of the upper (A) and lower (B) part of the chip. Adapted from Jubert, 2009.

5.1.2 Flow operation in a two-stacked microfluidic chip

To expose cells to a gradient from the lower part, the maximal amount of signaling molecules has to pass through the membrane pores into the upper cell chamber. Since the microfluidic chip is a two-stacked system the fluid transport was controlled by flow operation. A flexible control is possible by regulating the flow rates of each part. The structures of the upper part and the lower part are not identical – the lower has eight separated channels the upper does not –, so that identical flow rates in both chambers are expected to expose different hydrodynamic shear stress on the membrane. In different operating modes using crystal violet and BSA solutions, the transport rates from the lower to the upper part were monitored. The initial absorbance of the lower part and the absorbance of the outcome from the upper part were recorded at 590 nm and at 280 nm for crystal violet and BSA solution, respectively (Fig. 5.3).
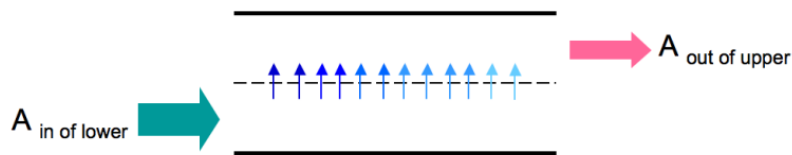


**Fig. 5.3 Scheme of flow operation experiments**

The pressure-driven flow causes a hydrodynamic shear stress on the membrane when it is cell-free or on the cells. Gaver and Kute (1998) calculated the shear stress on a single cell compared to a cell-free wall and found it depends on the relative dimension of the micro-channels to the cells. When an adhered cell has the radius (R) as 1/10 of a micro-channel height (H), i.e. R/H=0.1, the shear stress is increased to three times of that of cell-free wall. In this device, R/H is $\approx 0.02$ when the cell radius is considered as 10 µm, so it is agreed that loading the chamber with cells does not change the shear stress.

A Poiseuille flow model describes the hydrodynamic wall shear stress $\tau$ which is generated onto porous membranes, and the applied flow rate was converted to it following the equation;

$$\tau = \frac{6Q\mu}{bh^2}$$

where $\tau$ is the wall shear stress [dyne/cm$^2$], $Q$ is the flow rate [cm$^3$/s], $\mu$ is the viscosity of liquid (water $\approx$ 0.01) [dyne$^5$/cm$^2$], $b$ is the width [cm], and $h$ is the height [cm].

When $\tau$ is calculated, the different dimension ($b$) of the two parts of the chip was considered and the height is $h$=0.5 mm. For the upper part $b$=15 mm, and for the lower part $b$=1.63 mm (Ch.1 & 8) and $b$=1.375 mm (Ch.2-7). The width of the lower part is taken as 1.375 mm, since a narrower channel gives higher shear stress. Two different operation modes were conducted; (1) Open/Closing mode (2) Open/Controlled closing mode.

Open/Closing mode

As shown in Fig. 5.4A, the outflow rate and the inflow rate of the lower part was identically setup by a digital syringe pump. The pressure difference was introduced by the upper flow rates, resulting in a transport of gradient molecules from the lower to the upper part. The difference of shear stress is $\Delta\tau = \tau_{\text{lower}} - \tau_{\text{upper}}$, where $\tau_{\text{lower}}$ is the shear stress of the lower channels and $\tau_{\text{upper}}$ is that of the upper chamber. When the identical upper flow rate was applied for either BSA or crystal violet molecules, $\Delta\tau$ is positive in all applied flow rates (Fig. 5.4B). Thus, molecules were transported by the pressure difference from the lower to the upper chambers. As the pressure difference is increased about five times, the transported one is increased from 30 % to 50 %, while the transport of dye molecules decreased and maintained as the pressure difference is increased as shown in Table. 5.1.

When crystal violet dye solution was filled in the lower channels and the flow rate from the upper chamber was varied, the difference of shear stress also varied from negative values to positive values. Table. 5.2 summarizes the applied flow rates and the difference of the pressure. Here, as the $\Delta\tau$ is increased with different combination of flow rates, the outcome dye concentration shows increased tendency as well.
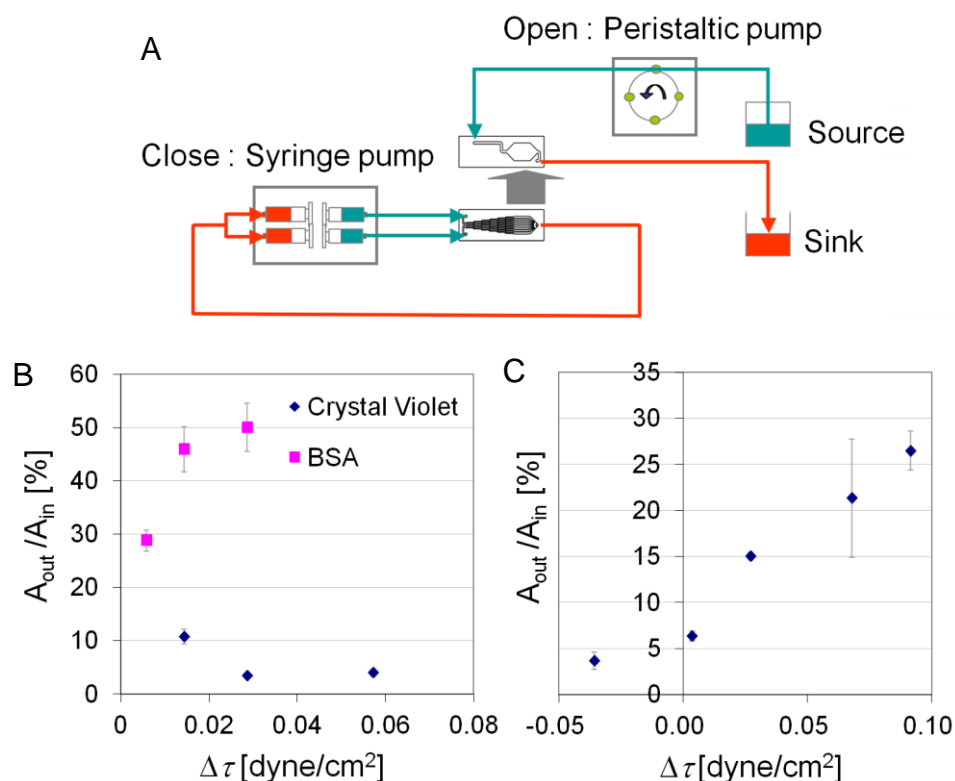
**Fig. 5.4 Open/Closing mode for transporting from the lower channels. (A) Schematic drawing of the setup. The digital syringe pumps are connected in a closed loop having identical inflow and withdrawal setup in the lower channels. Arrows indicate the direction of flows. Green color shows the inflow from the source and red color does the outflow to the sink. (B) The graph shows the outcome of the transported BSA (square) and dye molecules (diamond) from the lower channels when the identical flows were set and (C) in the case of different flow rate setup between the upper chamber and the lower channels.**

**Table. 5.1 The used flow rates and its relation with applied shear stress on the membrane in Fig. 5.4B.**

| Flow rate [mm³/min] | Hydrodynamic shear stress [dyne/cm²] | | |
|---|---|---|---|
| | $\tau_{upper}$ | $\tau_{lower}$ | $\Delta\tau$ |
| 20 | 0.016 | 0.021 | 0.006 |
| 50 | 0.039 | 0.054 | 0.014 |
| 100 | 0.079 | 0.107 | 0.029 |
| 200 | 0.157 | 0.215 | 0.057 |

**Table. 5.2 The applied shear stress on the membrane which is indicating the transport of molecules in Fig. 5.4C.**

| Flow rate [mm³/min] | | Hydrodynamic shear stress [dyne/cm²] | | |
|---|---|---|---|---|
| $J_{upper}$ | $J_{lower}$ | $\tau_{upper}$ | $\tau_{lower}$ | $\Delta\tau$ |
| 100 | 40 | 0.079 | 0.043 | -0.036 |
| 50 | 40 | 0.039 | 0.043 | 0.004 |
| 20 | 40 | 0.016 | 0.043 | 0.027 |
| 50 | 100 | 0.039 | 0.107 | 0.068 |
| 20 | 100 | 0.016 | 0.107 | 0.092 |

Open/Controlled closing mode

To generate the net flow by controlling different inflow and outflow rates in the lower channels two digital syringe pumps were used (Fig. 5.5A). Dye solution was filled in the lower channels without a gradient and the inflow rates were fixed as 40 and 100 µl/min (Fig. 5.5B). The different withdrawal flow rates created the net flow. The transport by generating net flow resulted in over 50 % of recovery of input molecules. In Fig. 5.5C only one inlet of the lower channel was filled with BSA solution to allow a gradient formation. Similar to the previous mode, the outcome was collected from the outlet of the upper chamber. The more net flow applied, the more outcomes out of the initial addition were obtained. For the BSA gradient up to 30% of the molecules inserted in the lower chamber were recovered in the outflow of the upper chamber.

5.1.3 Transport of signaling molecules in a two-stacked microfluidic chip

Importantly, the architecture of our microfluidic chip allowed both diffusion- and convection-based exposure of cells to the signal source. To model the situation that BIO as an activator of Wnt pathway is transported to the upper micro-chamber where culture medium is filled in, cell-free runs were performed using a BSA solution for the upper micro-chamber (culture medium model) and a methylene green dye solution for the gradient reservoir channels (BIO or small molecule model). For the diffusion-based transport (Fig. 5.6A), the output from the upper part was collected and the absorbance was measured to quantify the
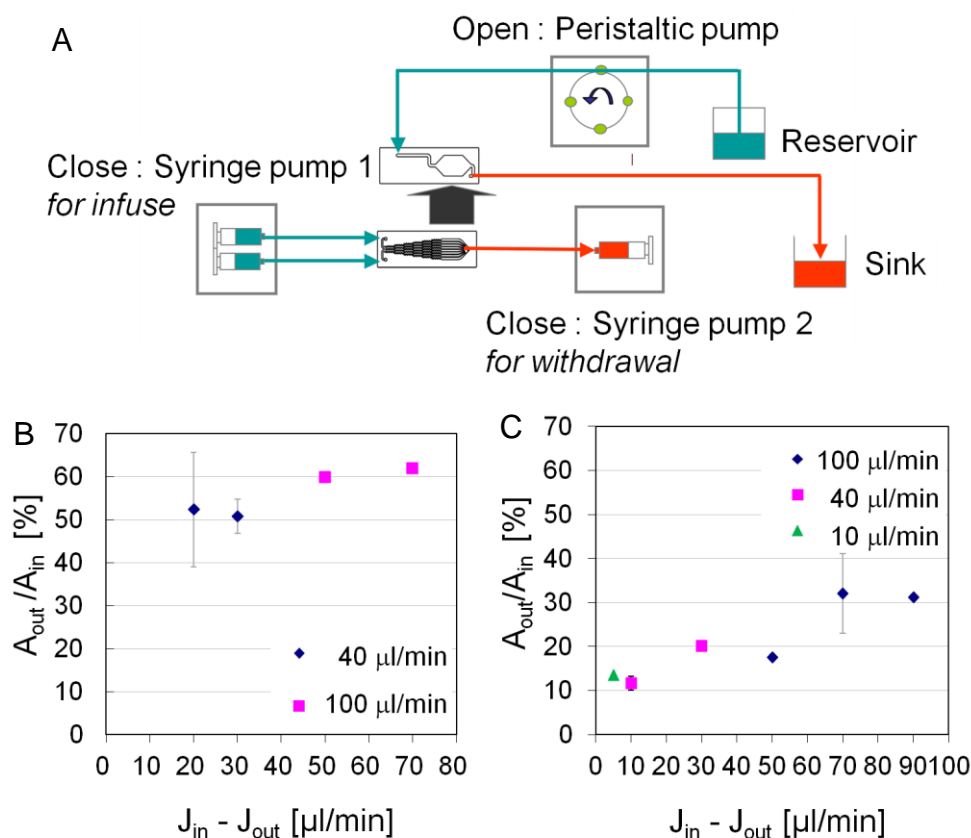
**Fig. 5.5 Open/Controlled closing mode for the net flow generation. (A) Schematic drawing of this setup. The inflow and the withdrawal were separated by the two syringe pumps controlling independently. Arrows indicate the direction of flows. Green color shows the inflow from the source and red color does the outflow to the sink. (B) Dye solution filled in the whole lower channels (no gradient) is transported by the net flow. The inflows 40 µl/min (diamond) and 100 µl/min were tested with varied difference with outflows. The difference is marked as $J_{in} – J_{out}$ in x axis. (C) BSA gradient was formed and transported to the upper chamber. The inflows of the lower were applied as 100 (diamond) / 40 (square) / 10 (triangle) µl/min.**

diffused dye fraction from the lower part. As a result, nearly 15 % of dye was traceable in the outlet of the upper micro-chamber after 24 hrs of diffusion through the cylindrical pores of the membrane (Fig. 5.6A). By closing the inlet of the upper micro-chamber and the outlet of the lower part the convection based transport was modeled by dominant pressure-driven flow. The traces of dye from the lower part in the upper chamber showed that replacement of BSA in the upper chamber started after 4 hours when the flow rate is 5 µl/min. As expected, the methylene green entered the upper compartment by convective flow faster and reached its maximum of about 80% after 21 hrs (Fig. 5.6B).
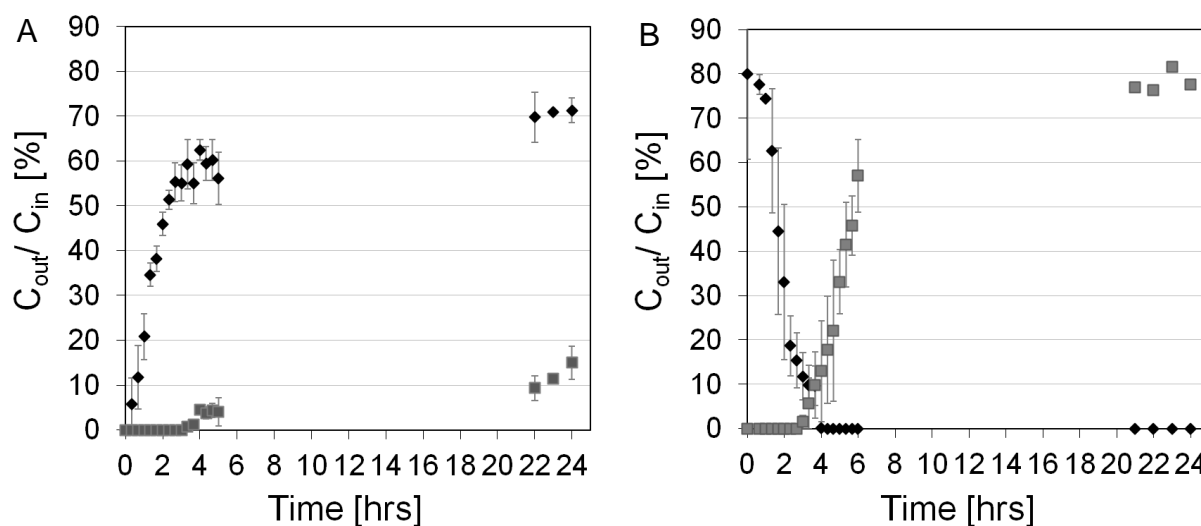
**Fig. 5.6 Two models of a gradient molecule transport from the lower part to the upper part. (A) Diffusion-based transport. Both chambers were filled with distilled water and started perfusion with BSA solution to the upper and methylene green dye solution to the lower part. A set up of different volumetric flows for upper (6.8 μl/min) and lower compartments (5 μl/min) was chosen minimizing the pressure difference (Δτ) in between the two parts. Thereby the different architectures of the upper micro-chamber and the lower gradient channel platform were taken into account. (B) Convection-based transport. The upper part was filled with BSA solution and the lower part with distilled water before running with the flow rate of 5 μl/min. Black diamond dots indicate the outcome concentration of BSA to the initial concentration and gray square dots mean that of methylene green dye solution.**

### 5.1.4  Generation of stable gradients

Jubert (2009) used fluorophore conjugated dextrans (10 kDa) to demonstrate that the zig-zag micro-mixer, in principle, forms gradients. Analysis of such a gradient revealed that in the mixing cascade 1 and 2 the homogeneous mixing is completed and gradually changed to more sigmoid shape in the mixing cascade 3 to 6 (Fig. 5.7). The mixing in each cascade is considered to be completed.

Prior to testing morphogens, the purified GST tagged green fluorescence protein (GST-GFP) was used as a model protein. A coomassie brilliant blue stained SDS-PAGE demonstrates that in addition to the protein of interest several unspecific proteins were co-eluted from the Glutathion sepharose (Fig. 5.8). Because GST-GFP with the molecular weight as ≈ 54 kDa is much bigger than dextrans, the flow rate was adjusted to 10 µl/min. Indeed, a linear gradient was formed (Fig. 5.9).
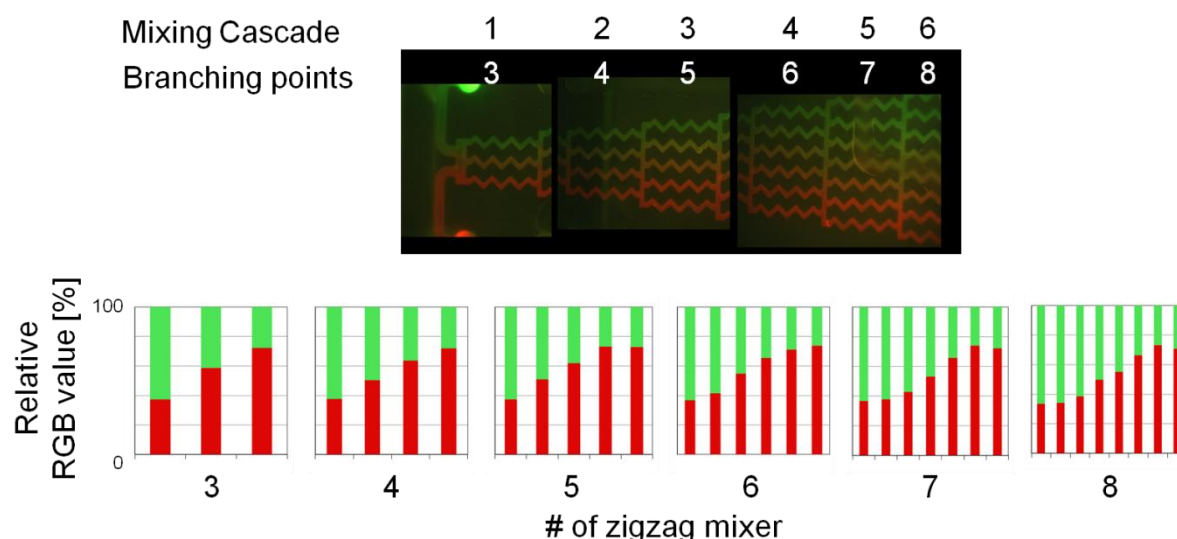
Fig. 5.7 Mixing cascade of the zig-zag mixer. The two fluorescent dextran solutions confirmed the formation of a gradient through six mixing cascades. The relative RGB value was plotted in each cascade. The conjugated dextrans are 10 kDa and the applied volumetric flow rate was 0.125 ml/min per inlet (Image: Jubert, 2009, analysis: in this work).
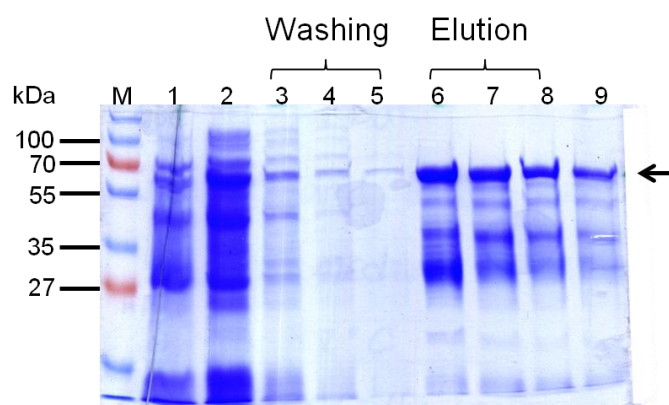


Fig. 5.8 GST-GFP purification. Aliquots of different steps of GST-GFP purification were separated on a 10 % SDS PAGE and stained with coomassie brilliant blue. M: marker, 1: crude cell extract, 2: the aliquot after 2 hours binding to Glutathion-sepharose, 3-5: aliquots after each washing step, 6-8: aliquots eluted with 10 mM glutathion after 5, 10 and 20 min, respectively, 9: proteins remained on sepharose. The arrow indicates the expected size of GST-GFP.

To decipher whether proteins unspecifically adsorbed on hydrophobic polycarbonate surfaces, the gradient reservoir channels were filled with GST-GFP for 2.5 hours and washed with water for 2.5 hours. Washing completely removed all GST-GFP, indicating that unspecific adsorption is negligible.

The volumetric inflow rates and the size of molecules that differs diffusivity are expected to define the gradient profile in the gradient reservoir channels. To estimate the maximum flow rate for homogenous mixing mainly by diffusion which is linked to the size of molecules, two time scales are introduced. One is the diffusion time scale ($T_d$) which covers the time for molecules to diffuse along the half of the channel width. The other is the travel time scale ($T_v$) when molecules travel along the zigzag channel ($L$) and reach the end of it (Fig. 5.10).
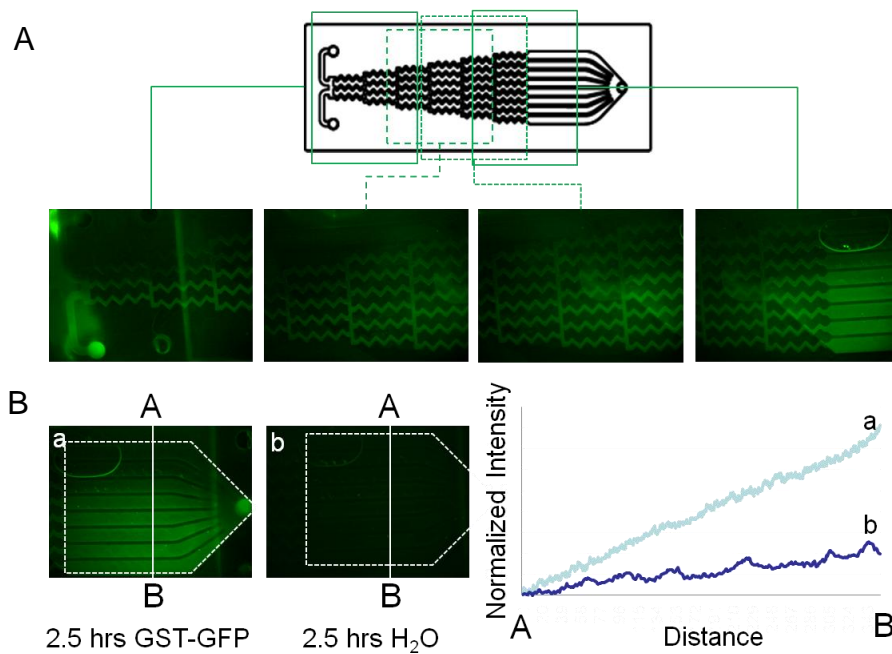


**Fig. 5.9 Formation of a linear gradient GST-GFP in the gradient reservoir channels. (A) GST-GFP was applied into one inlet to create a single GFP gradient. (B) The GFP linear gradient was shown from an intensity profile of the image after 2.5 hours input (a). After washing for 2.5 hours, drastically decreased normalized intensity was observed (b).**

One-dimensional diffusion time is defined as,

$$T_d = d^2 / 2D$$

where $d$ [μm] is half the width of a zig-zag channel, $d=w/2$, and $D$ [μm²/s] is the diffusivity. Using the Stokes-Einstein equation and the Wilke-Chang correlation (Cussler, 2009), the diffusion coefficient was estimated for small molecules and for proteins. The travel time along zigzag channels is defined as,

$$T_v = BV / J$$
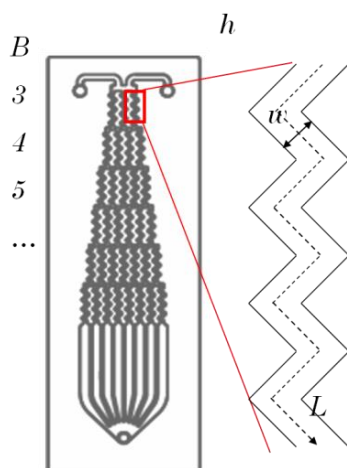
**Fig. 5.10 The dimension of one zig-zag channel. In this microfluidic chip, height *(h)* is measured as 0.5 mm, width *(w)* as 0.4 mm and length *(L)* as 9.53 mm.**

where $V = wLh$ is the volume of each zig-zag channel [mm³], $w$ is the width [mm], $L$ is the length of zig-zag channel [mm], $h$ is the height of the channel [mm], $J$ is the volumetric flow rate [mm³/min] and $B$ is the number of branches of the cascade. The travel time through a single cascade was calculated by the speed of streams and volumes. For the first cascade, $B$ is 3 and $J$ is divided by three to obtain the volume per minute in one zig-zag of the first cascade. Then, the time is obtained by dividing by the zig-zag channel volume. To assure mixing mainly by diffusion, the diffusion time should be shorter than the travel time at the first cascade. With a flow rate of 5 µl/min, small molecules which have $D \approx 500$ µm²/s diffuse over half of the channel width in $\approx$ 40 s and travel through the first cascade in $\approx$ 70 s. This permits homogeneous mixing in each cascade through diffusion. Thus, small molecules can diffuse across zig-zag channel before reaching the end of the zig-zag channel of the first cascade, which means before homogeneous mixing is achieved. Therefore, eight distinct gradient reservoir channels were built to guarantee a linear step gradient concentration. Depending on this concentration, transport of BIO was conducted either in diffusion-base or convection-base.

For larger molecules including proteins, the diffusivity $D$ necessarily has to be considered under some assumptions. Diffusivity, i.e. diffusion coefficient depends on the hydrodynamic radius comprised by the size and shape of molecules, the viscosity of diluents and the interaction with the solvent (Tinoco *et al.*, 2002). To estimate $D$ of proteins, the following assumptions were considered; (1) mean value of protein density is taken as 1.43 g/cm³ (Quillin & Matthews, 2000), (2) temperature is 20 ºC, and (3) proteins are globular in water.

The Diffusion coefficient, $D$ is defined as,

$$D = (1/f)kT$$

$$f = 6\pi\eta r$$

where $f$ is frictional coefficient, k is Boltzman constant [J/K], T is absolute temperature [K], $\eta$ is viscosity [dyne s/cm$^2$], r is radius of sphere [cm]. For BSA-FITC with a molar mass of 66 kg per mole, the density is calculated with 66000 g divided by the mean value of protein density, 1.43 g/cm$^3$ and the volume of a single molecule, which is obtained by dividing by Avogardro's number, assuming molecules are perfectly packed. Under the assumption of that single molecule is sphere, the radius is defined by its volume. Therefore, diffusivity of BSA-FITC is assumed as $\approx 80$ µm$^2$/s in this work. The value of $f$ will be increased in the case of asymmetric shape of molecules or non-elastic interaction with diluents (Tinoco *et al.*, 2002). This is matched the lower value of 60.7 µm$^2$/s (Muramatsu & Minton, 1988) compared to the obtained value. Based on these estimations, the gradient profiles were analyzed differing volumetric inflow rates by digital syringe pumps using BSA-FITC.

To determine optimal flow rates for proteins of the size of FITC-conjugated, different flow rates were applied and the shapes of the resulting gradients were detected by monitoring mean fluorescence intensity (Fig. 5.11). Total volumetric flow rate is marked in each image in the upper line. When the BSA-FITC solution was added at the flow rate 100 µl/min, the fluorescence intensity showed that no linear gradient was formed. Instead, a one step gradient between channel four and five was visible (Fig. 5.11). Decreasing the flow rates to 40 µl/min, 10 µl/min and 5 µl/min changed the gradient profile as expected. The slower the gradient molecules were filled in, a more linear-shaped gradient was formed. At 5 µl/min the measured BSA-FITC fluorescence intensity in the channels nearly approached the theoretically calculated linear line after 120 min. Therefore this flow rate was used for protein application in this microfluidic chip.
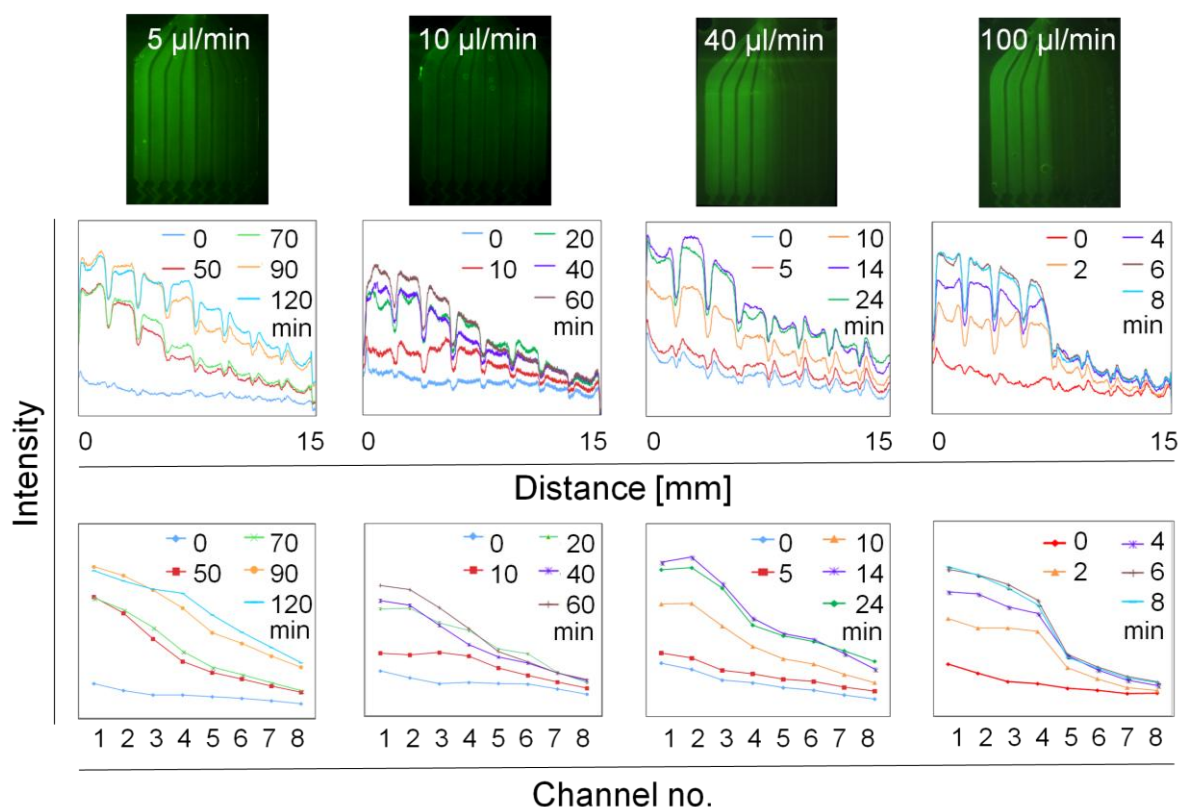
**Fig. 5.11 The shape of step gradients of BSA-FITC depending on the inflow rates. Total volumetric flow rate is 5 / 10 / 40 / 100 µl/min (from left to right). The upper line images were taken at the last time point for each case. In each time point the fluorescence images of whole area of the gradient reservoir channels were used for intensity profiling showing step-like gradient (the middle line). The pixels in each channel were summed up and averaged to make plots simple (the lower line).**

As shown in Fig. 5.12, the stability was confirmed for 24 hours along the channel, as almost gradient application is within 24 hours. This was necessary because the channels are 7.5 times longer than wide and cells on each position should be exposed to the same concentration during experiments.

To check the reliability and flexibility of the microfluidic chip, the two different gradients were exchanged (Fig. 5.13). After opposite gradients of BSA-FITC and BSA-tetramethylrhodamine conjugates reached equilibration, the two inlets were exchanged to switch the gradient. During the exchanging time the superimposed fluorescence microscope images showed the decayed overall gradients and allowed quantification of relative green-red intensities. The upcoming gradient became completely replaced to recover the highest relative green intensity in the opposite position (Fig. 5.13).
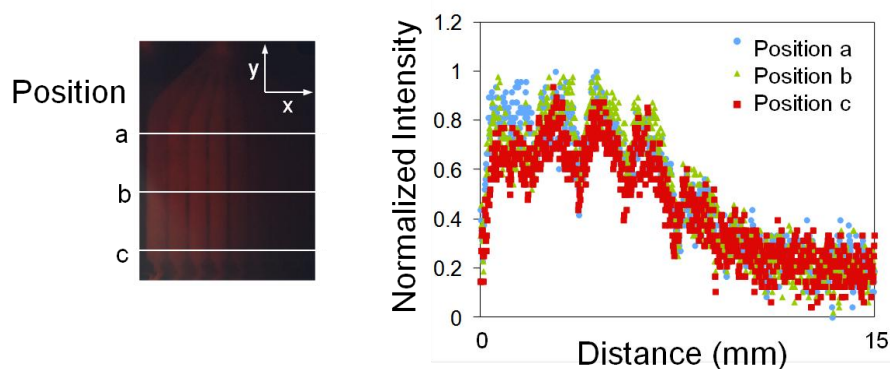
**Fig. 5.12 The stability of a gradient. The gradient profiles of each position along y-axis (from inlet to outlet) are superimposed that means the gradient maintained stable for 24 hrs with negligible difference along the positions in y-direction (y/x = 7.5). Three positions were checked along the y-axis and they were mostly superimposed each other showing negligible differences in normalized intensity.**
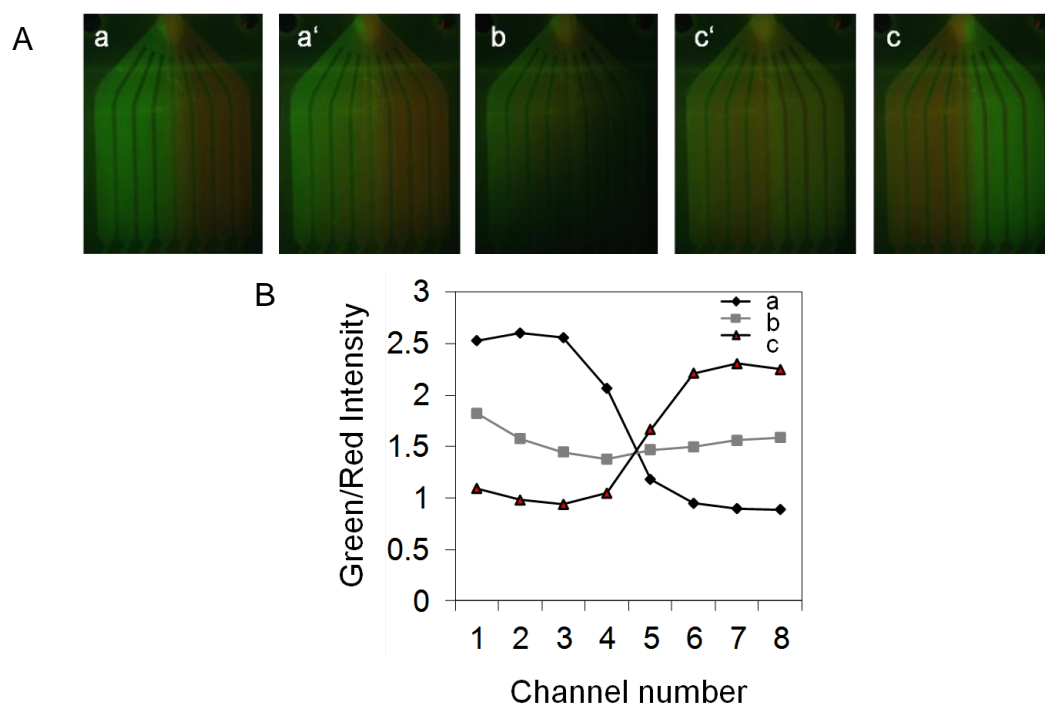


**Fig. 5.13 The capacity to switch two different gradients. BSA-FITC (green) and BSA-tetramethylrhodamine (red) were used to prove the microfluidic chip has the capacity to switch gradients. (A) Fluorescent images were merged at each time point; (a) after 25 min of the first green-red gradient, (a') after exchanging the inlets, (b) after 5 min (b) 15 min and (c) 30 min of the second red-green gradient. The flow rate was applied as 40 µl/min. (C) Images were analyzed by green/red relative intensity showing the green-red gradient (a) was replaced with a red-green one (c) within one hour without washing steps.**

To demonstrate the flexibility of the device BSA-FITC was also used to form a single gradient with the flow rate of 5 µl/min. The fluorescence image was captured after 120 min (Fig. 5.14A). Surface plot was performed to scan 2-dimensional intensity difference (Fig. 5.14B). Instead of summing up all pixels, five profiling lines were chosen along the channel and the intensity was normalized to that of Area 5 (Fig. 5.14C). The difference between Area 1 and 5 of channel 1 is 0.45 which is comparable to that between channel 1 and 5 of Area 5 (0.54).
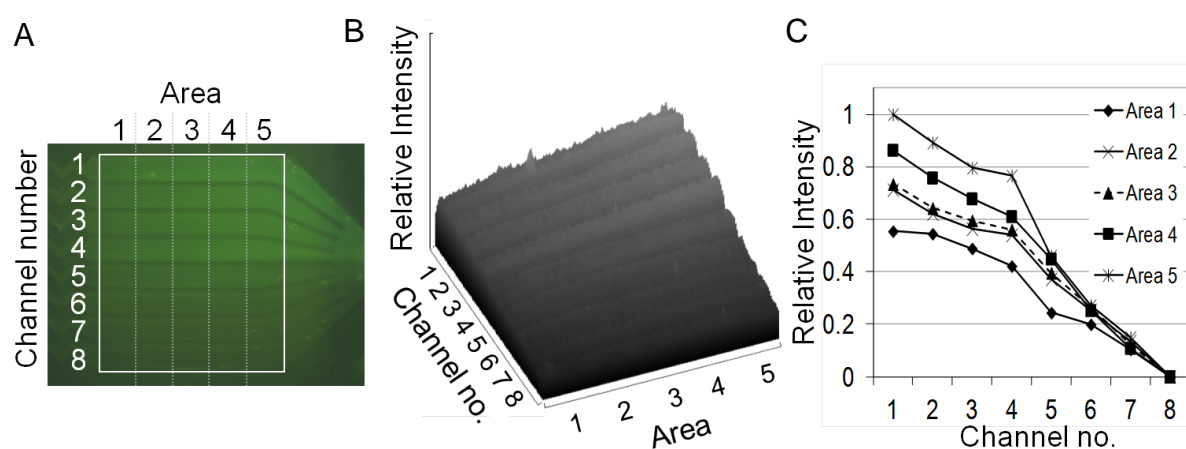


**Fig. 5.14 Observation of 2-dimensional gradient in a short time. (A) The single gradient of BSA-FITC was formed with 5 µl/min for 120 min. The five areas were taken of each channel for profiling intensity. (B) Surface plot of whole area. (C) Normalized intensity profiles of Area 1-5 to that of Area 5.**

5.1.5  Cell adhesion on ion-track etched polycarbonate membranes

Cell adhesion on porous membrane in the microfluidic chip should be ensured. To check which substrates were suitable for cell attachment, HeLa cells were seeded on different pore-sized polycarbonate membranes. Compared to control glass slides coated with Alcian blue, no significant differences in cell shape were observed (Fig. 5.15). Indeed, HeLa cells spread on the polycarbonate membrane independently of the pore size. However, after 48 hours cultivation more cells significantly remained on 0.2 and 0.4 membranes compared to those with bigger pores (Fig. 5.15).
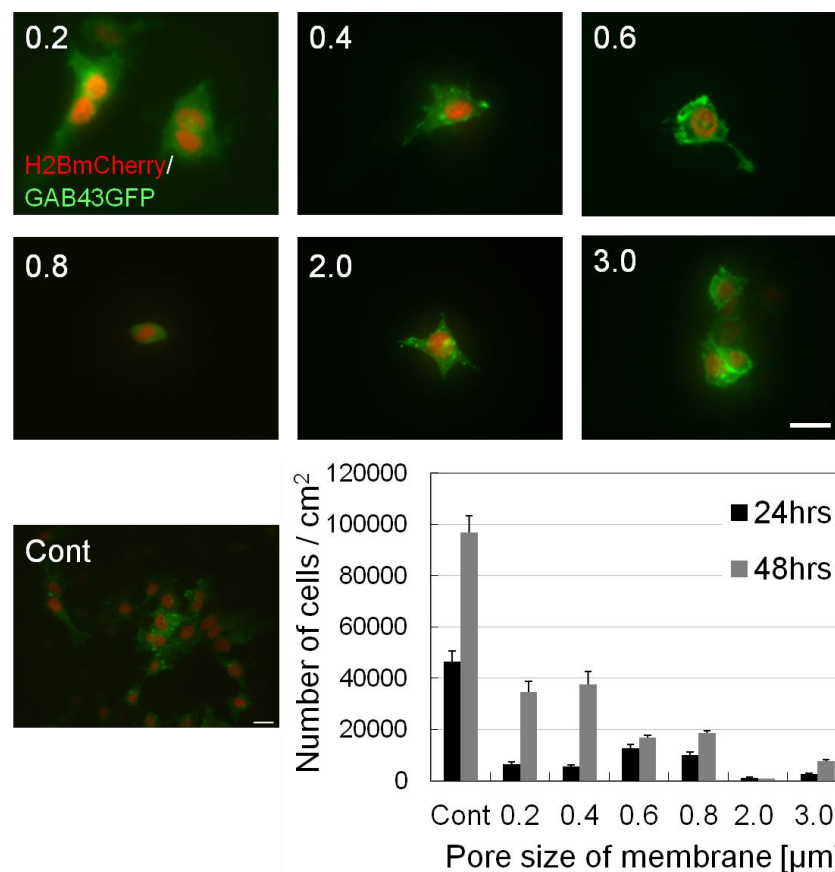
**Fig. 5.15 HeLa cells on different sized ion-track etched polycarbonate membranes. The cells were transfected with H2BmCherry/GAB43GFP and incubated for 5 days on membranes. The 0.2, 0.4, 0.6, 0.8 membranes were from Millipore and 2.0, 3.0 from Pieper. None of the membranes was treated. The number of cells was counted by DAPI number in 10x low magnified images after 24 hours and 48 hours incubation. Bar = 20 μm.**

The same effect was also observed with MCF-7, human breast adenocarcinoma cells. Again, the cell morphology was independent of the pore size, but the cell number decreased with increasing pore size (Fig. 5.16).
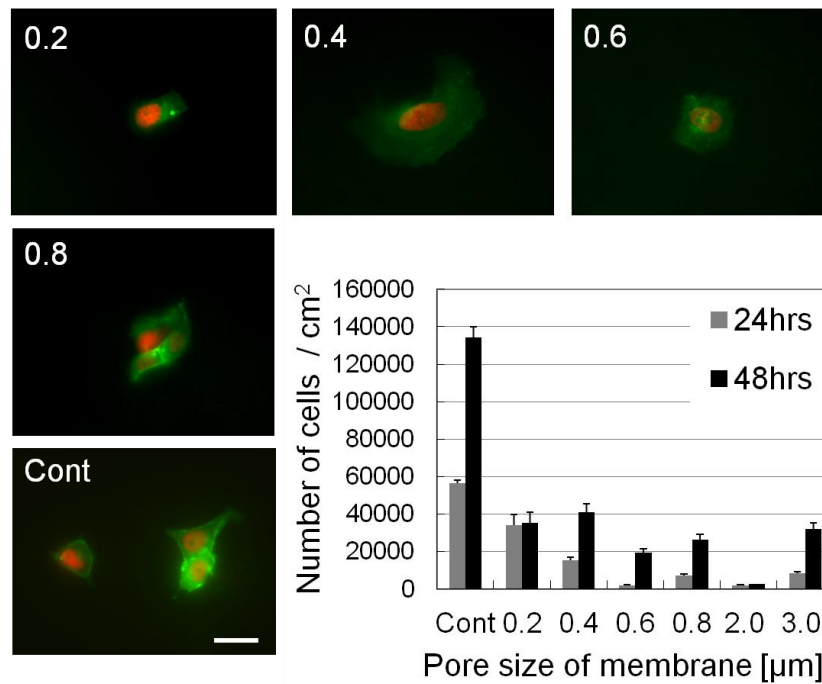
**Fig. 5.16 MCF-7 cells on different sized ion-track etched polycarbonate membranes. The cells were transfected with H2BmCherry for nuclei and GAB43GFP for cell membranes and incubated for 3 days on membranes. The 0.2, 0.4, 0.6, 0.8 membranes were from Millipore and 2.0, 3.0 from Pieper. The control glass slide was treated with Alcian blue and none of the membranes was treated. The cells were incubated for 24 hours and 48 hours and DAPI number was counted. Bar = 20 μm.**

To increase the attractiveness of the polycarbonate substrate, the membranes were treated. First the membranes were treated with UV light of short wavelengths (λ= 185 nm) as described elsewhere (Welle & Gottwald, 2002). Indeed, after six days cultivation the number of MCF-7 cells on the UV-treated membrane was higher than on the untreated membrane (Fig. 5.17). Importantly, on the UV-treated membranes cells still could spread. However, the number of cells adhering on the membrane was still low compared to control glass cover slides (Fig. 5.17).
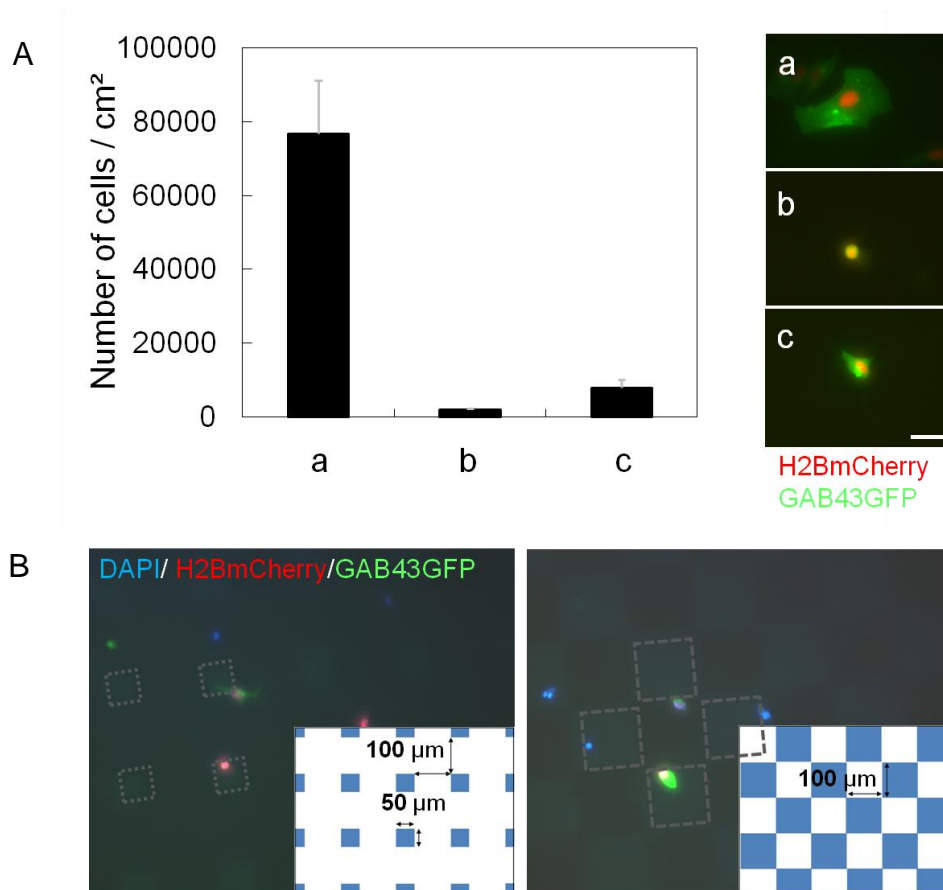
Fig. 5.17 UV treatment on polycarbonate membrane. Cells were transfected with H2BmCherry for nuclei and GAB43GFP for cell membranes and cultured for 6 days. (A) The number of cells and selected cell images for each condition. a. non-treated glass slide, b. non-treated membrane, c. whole area UV-treated membrane. Bar = 20 µm. (B) UV treatment in patterned areas by using masks. The areas exposed to UV are marked as blue which indicates dashed squares in fluorescent images of cells. Nuclei were counterstained with DAPI.

Finally, different coatings were examined to enhance cell adhesion on different sizes of porous membranes. Most of these proteins did not significantly enhance cell adhesion, apart from poly-l-lysine and fibronectin. They led to an increased number of adhered cells compared to no coating (Fig. 5.18).
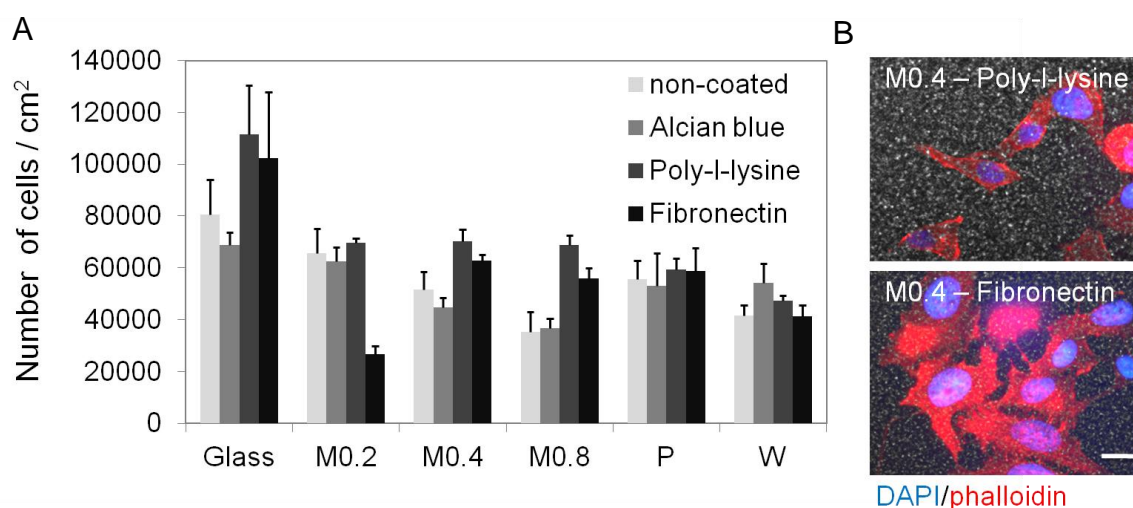
**Fig. 5.18 Different coatings on membranes. (A) The number of attached HeLa cells for 2 days in culture on glass, 0.2, 0.4, 0.8 (M:Millipore), 1.0 (P:Pieper, W:Whatman) µm with different coating molecules; Alcian blue (1 w/v%), poly-l-lysine (100 µg/ml) and fibronectin (10 µg/ml). (B) Representative figures of spreading cells on poly-l-lysine and fibronectin coated membranes with 0.4 µm pores. DAPI for nuclei and phalloidin for actin filaments were used. Bar = 15 µm.**

Although coating of the membrane with proteins did not enhance cell growth, it was found to be necessary for the following experiments. On untreated membranes BSA-FITC was highly adsorbed (Fig. 5.19), making it likely that any protein, including morphogens, unspecifically binds to these membranes. Pre-incubation of the membrane with FCS-containing medium completely prevented unspecific protein adsorption (Fig. 5.19). Therefore, in-chip experiments, the upper and lower parts of the microfluidic chip were pre-incubated with culture medium.
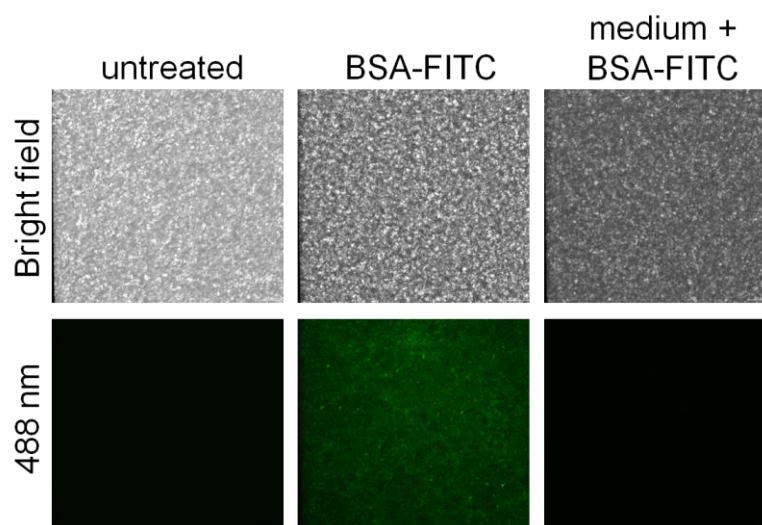


(Figure legend is in the next page.)

**(Figure in the previous page) Fig. 5.19 Protein adsorption on porous (0.4 µm, Millipore) polycarbonate membranes. BSA-FITC (12.5 µg/ml) was highly adsorbed after 1 hour incubation at room temperature. Pre-incubation with culture medium for 1 hour at 37 ℃ resulted in blocking the membrane with a complex protein mixture filled before BSA-FITC incubation for 1 hour. Three times washing with PBS was followed by each incubation step.**

5.1.6  Cell culture condition in micro-scale

To study cellular responses to morphogen gradients in a micro-sized chamber, cell viability should be validated since critical factors arise, e.g. shear stress, limited gas exchange, when cells are cultured in micro-scale condition compared to traditional petri-dish culture. In Leibovitz' conditioned medium cells were viable for at least overnight to six days (Fig. 5.20A). Similarly, DAPI staining revealed mitotic nuclei in RPMI conditioned medium after four days in culture (Fig. 5.20B), indicating that the cells are healthy and continuously proliferating. Thus, either HEPES buffered Leibovitz' medium or conditioned RPMI medium can be used to culture cells in the micro-sized chamber in perfusion condition.
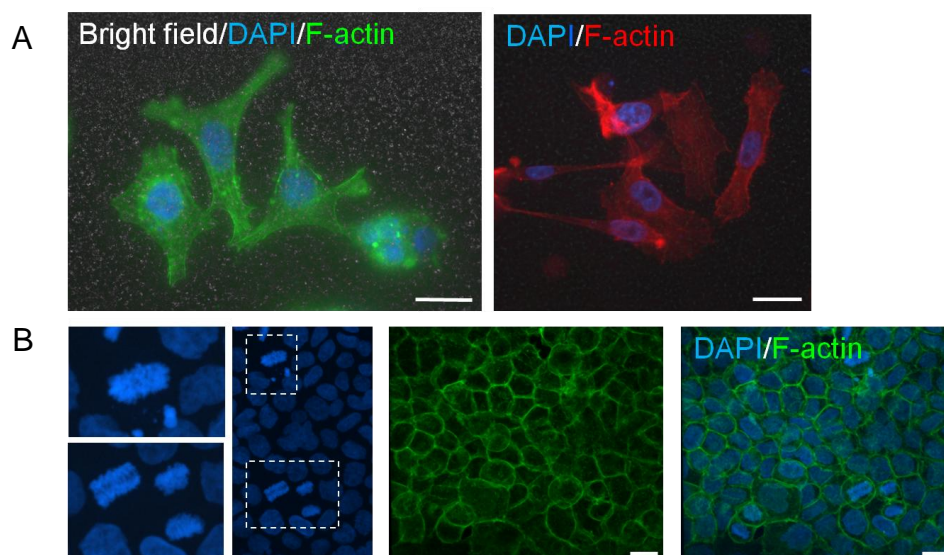


**Fig. 5.20 HeLa cell cultivation in the micro-chamber of the microfluidic chip. (A) After incubation in Leibovitz's conditioned medium overnight (left) and for six days (right), cells were found well spread (actin-phalloidin counterstained with DAPI). (B) After four days of cultivation in RPMI conditioned medium cells were viable and underwent mitosis (mitotic nuclei were enlarged). Bar = 20 µm.**

Since the culture medium was perfused into the upper chamber by a digital syringe pump in the microfluidic chip, the hydrodynamic shear force generated by flows and an appropriate perfusion rate should be evaluated in order to avoid loss of nutrients and cell damages by shear forces.

The effective culture time (ECT) introduced by Walker *et al.* (2004) was calculated to define the maximal static cultivation time in the micro-scale culture. It is the time related to a proper media change interval, which should be given under the micro-scale culture condition.

Damkohler number, $D_a$, the ratio between reaction and diffusion time scales (Zeng *et al.*, 2006) is defined as,

$$D_a = \frac{K_m h \, \sigma}{D \, C_0} = \frac{h^2/D}{C_0 h / K_m \, \sigma} = \frac{T_d}{T_r}$$

where $K_m$ is uptake rate [mol/min], $h$ is chamber height [mm], $\sigma$ is cell density [/mm], $D$ is diffusivity [$\mu$m/s$^2$], $C_0$ is initial concentration [mol/mm$^3$], and $T_d$ is diffusion time [min], $T_r$ is reaction time [min].

Small molecules are known to enter cells through facilitated diffusion by the concentration difference. Facilitated diffusion also follows the enzyme-substrate kinetics (Cussler *et al.*, 1989) based on Michaelis-Menten equation. The total reaction time not only depends on the uptake rate but also on the diffusion of molecules in the medium. Lowering the height of the fluid level shortens the diffusion time. Due to the small dimension of the micro-device the total time scale for activation of a signaling pathway e.g. canonical Wnt/ß-catenin signaling pathway indicates that the reaction is time limiting.

As shown by the $D_a$ equation, diffusion time is an order of magnitude higher than reaction time and $h$ in upper chamber ($h = 0.5$ mm) is five times smaller than that in the in-well culture system ($h = 2.5$ mm), which is comparable to the culture flask condition.

$$ECT = T_r = \frac{C_0 \, h}{K_m \, \sigma}$$

$T_r$ is equivalent to ECT in diffusion-dominant system, which is linearly proportional to $h$. HeLa cells are cultured in culture flasks with 25 cm$^2$ in 5 ml

volume of 2 mm medium height and medium is changed every three days (72 hours). As $h$ of the upper cell micro-chamber is 0.5 mm, ECT for the microfluidic chip should be 18 hours. Therefore, it was considered to limit the static incubation time in the chip to 18 hours, in this thesis, < 16 after seeding cells. From this concept, critical perfusion rate (CPR) was introduced (Young & Beebe, 2010), which is combined with ECT and micro cell chamber dimension.

$$U_m = \frac{V}{T_c}$$

$$\kappa = \frac{T_c}{T_r} = \frac{(V/U_m)}{(C_o h/K_m \sigma)} = 1$$

$$U_m = \frac{V K_m \sigma}{C_o h} = \frac{V}{T_r}$$

where $U_m$ is CPR [mm³/min], $V$ is volume of upper cell chamber [mm³], $T_c$ is residence time or convection time [min], $\kappa$ is the ratio of convection and reaction time scales. The volume of the upper cell chamber is about 205 mm³ thus CPR for the chip is considered as 0.19 µl/min. The perfusion rate was kept above 0.19 µl/min to avoid nutrient depletion and waste accumulation.

The expected parabolic flow profile allows the estimation wall shear stress by Newton's law of viscosity in 2D Poiseuille flow systems as described previously (5.1.2). The practically measured height of adherent HeLa cells by a confocal microscope is around 2-10 µm and the micro-channel height is 500 µm. Therefore, it was considered that the fluid stress is nearly same with that when the micro-channel has no adherent cells.

Although different cell types accept a range of shear stress, most cells are resistant up to 1 dyne/cm². HeLa cells are resistant even up to 4 dyne/cm² (Ranjan *et al.*, 1996; Lee *et al.*, 2006). When a perfusion rate of 5 and 6.8 µl/min is applied for the upper micro-chamber in the microfluidic chip, wall shear stress can be estimated as 0.0013 and 0.0018 dyne/cm², respectively. Therefore, the range from 5 to 6.8 µl/min used throughout the experiments agrees critical perfusion rate (0.19 µl/min) thus introduces negligible shear stress.

5.1.7 Concentration-dependent Wnt/ß-catenin pathway activation in-well control

To compare the activity on Wnt/ß-catenin signaling pathway with that in the microfluidic device and to determine the concentration range of Wnt pathway regulators for in-chip experiments, precedent in-well control experiments were conducted.

The small molecule, 6-bromoindirubin-3'-oxime (BIO) (Fig. 5.21) as an inhibitor of glycogen synthase kinase-3 (GSK-3), activated the Wnt/ß-catenin pathway but the inactive compound MeBIO didn't (Meijer *et al.*, 2003; Sato *et al.*, 2004).
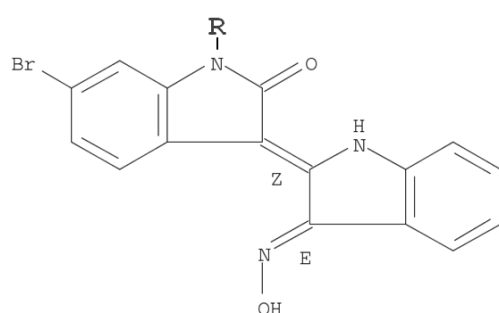


BIO: R = H
MeBIO: R = CH$_3$

**Fig. 5.21 Chemical structures of BIO and MeBIO. (Modified from SciFinder database; https://scifinder.cas.org)**

In HeLa cells treated for 16 hours with 5 µM BIO dissolved in DMSO, the amount of ß-catenin positive nuclei was significantly increased (Fig. 5.22A). Importantly, staining of ß-catenin at the membrane remained unchanged. Western blot analyses revealed that even at approximately 3 µM BIO, an increase of hypophosphorylated active ß-catenin was observed. Concentrations between 2 µM and 5 µM revealed a dose-dependent increase of active ß-catenin (Fig. 5.22B).

Similarly, also the nuclear accumulation of ß-catenin depended on the BIO dose (Fig. 5.23). However, an increase of nuclear ß-catenin was already observed by fluorescent images at 1 µM BIO, indicating that this readout system is approximately three times more sensitive than detecting active ß-catenin in western blot. Thus, in-chip concentrations of BIO should be adjusted to low micro-molar ranges. Additionally, the minimal time for BIO-treatment was tested. 2 µM BIO was not sufficient to induce nuclear ß-catenin accumulation after eight hours incubation (data not shown).
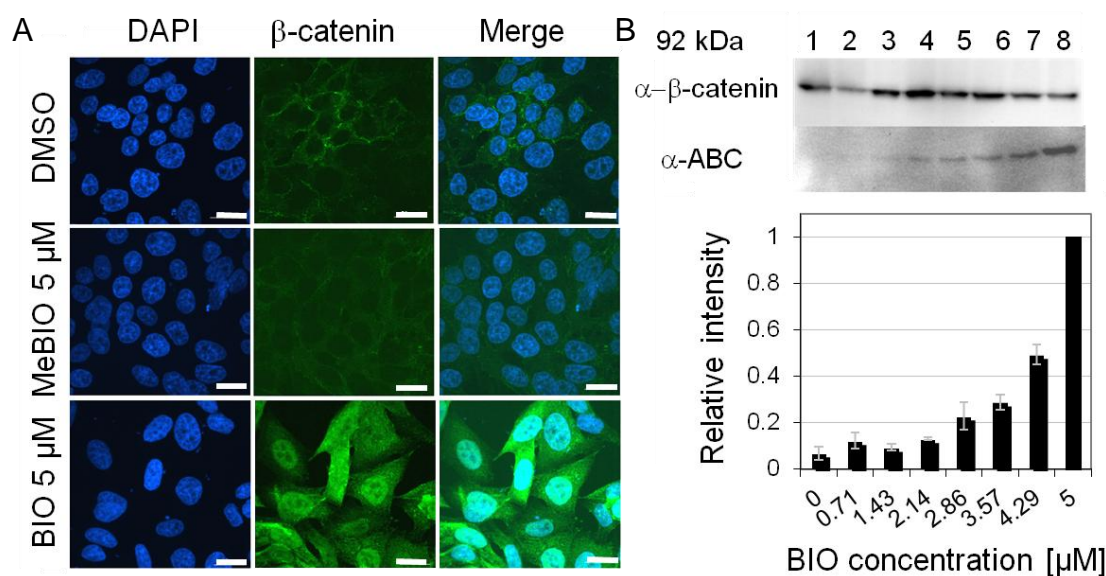
**Fig. 5.22 Analysis for the subcellular localization of β-catenin under BIO treatment. (A) Compared to MeBIO and solvent only treated HeLa cells, 5 µM of BIO treated cells induced nuclear localization of β-catenin. Total β-catenin was immunofluorescently stained together with DAPI for nuclei visualization. Bar = 20 µm. (B) HeLa cells were treated with different BIO concentrations for 24 hours and analyzed in western blots for the presence of total β-catenin (α-β-catenin) and active-β-catenin (α-ABC). Bio concentrations: 1=0 µM, 2=0.71 µM, 3=1.43 µM, 4=2.14 µM, 5=2.86 µM, 6=3.57 µM, 7=4.29 µM, 8=5.0 µM. The densitometry was obtained from the relative intensity of ABC bands to that of total β-catenin and normalized to the value of 5 µM BIO.**
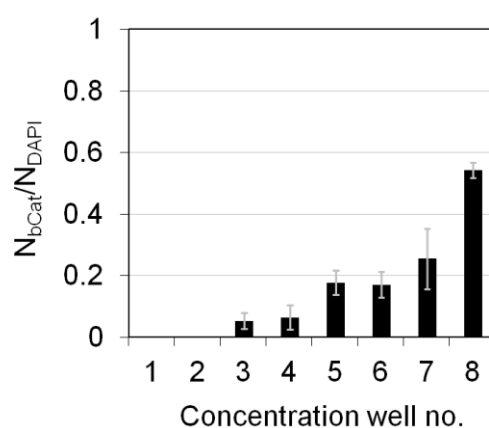


**Fig. 5.23 Nuclear β-catenin fraction ($N_{bCat}/N_{DAPI}$) by BIO treatment of in-well condition for 16 hours. Concentration well number indicates as follows; 1=0 µM, 2=0.29 µM, 3=0.57 µM, 4=0.86 µM, 5=1.14 µM, 6=1.43 µM, 7=1.71 µM, 8=2.0 µM. In each experiment three immunocytometric images were taken per each condition to count the total number of cells ($N_{DAPI}$) and β-catenin nuclear accumulated cells ($N_{bCat}$) by intensity. The average of total counted cells per each condition was 937 cells and that of cell density in each image was 1.3 x $10^5$ /cm².**

The activity of commercially available Wnt3a protein and the inhibitory effect of commercially available Dkk-1 were examined in similar experiments. Immunofluorescence analyses revealed that ß-catenin accumulated after treatment with more than 100 ng/ml (Fig. 5.24). Similarly, an increase of active ß-catenin was observed after treatment with 100 ng/ml Wnt3a (Fig. 5.25A). The antagonistic effect of Dkk-1 was proven by the dose-dependent decrease of hypophosphorylated ß-catenin in Wnt3a stimulated cells (Fig. 5.25B). As few as 10 ng/ml Dkk-1 decreased the amount of active ß-catenin. This inhibitory effect of ß-catenin was also observed by immune fluorescence studies. Here, 350 ng/ml Wnt3a induced accumulation of ß-catenin in the nuclei, an effect which was completely reverted by adding 500 ng/ml Dkk-1 (Fig. 5.25C).
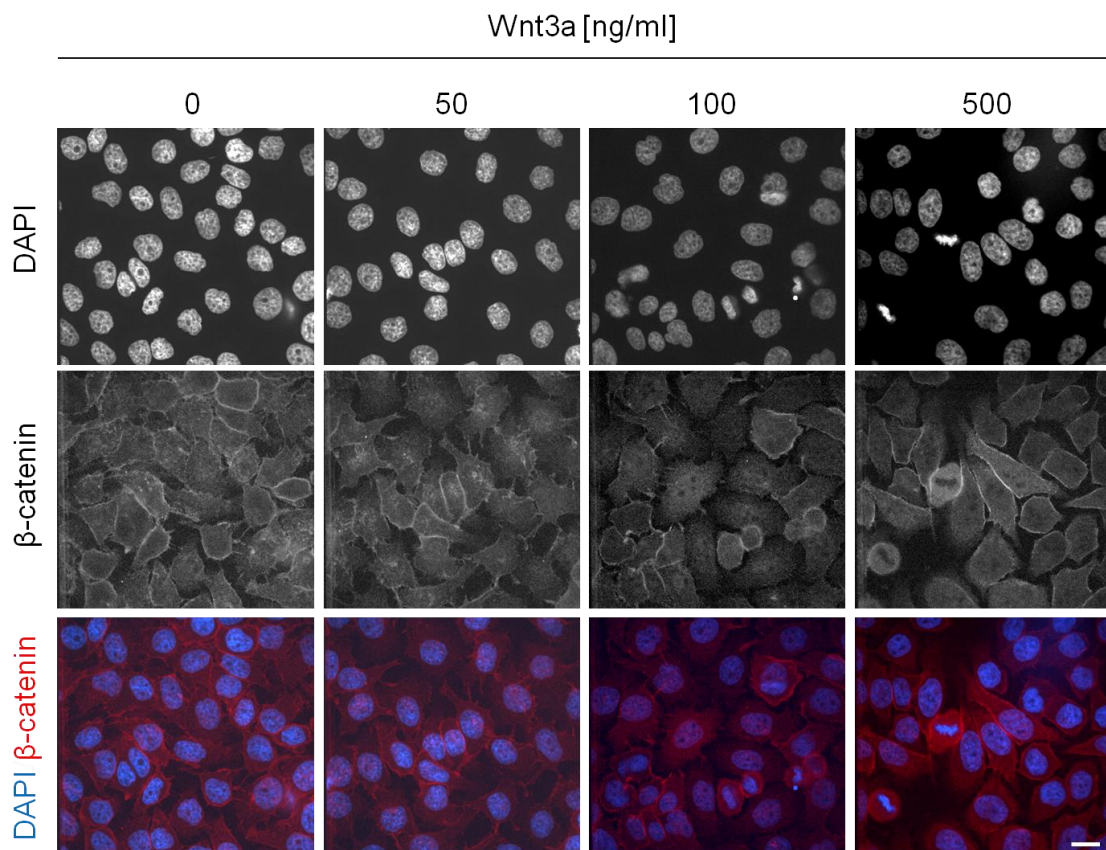


**Fig. 5.24 Recombinant Wnt3a activates Wnt signaling pathway in HeLa cells in a concentration-dependent manner. The cells were exposed to each concentration of Wnt3a for 24 hours. In unstimulated cells β-catenin localizes mostly at cell-cell contact sites whereas in stimulated cells an additional localization in the nuclei was seen. Upper line: DAPI staining, middle line: anti total β-catenin staining, Lower line: merge. Bar = 20 µm.**
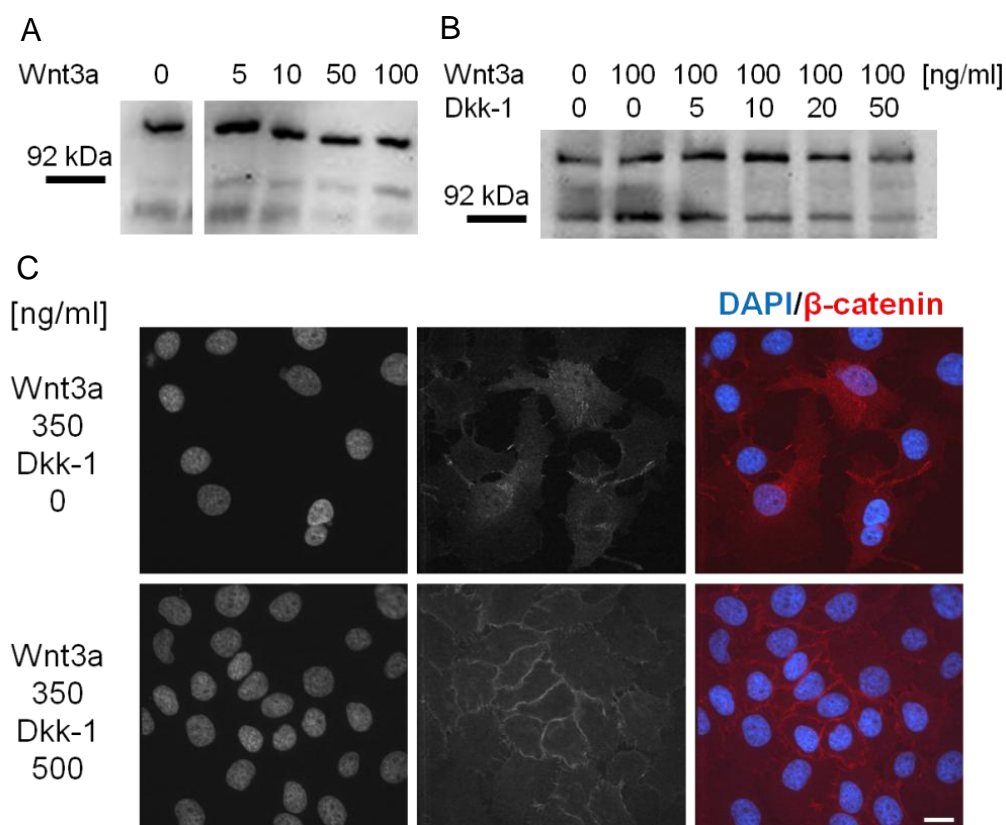
**Fig. 5.25 Recombinant Wnt3a and Dkk-1 to activate or inhibit Wnt/β-catenin signaling pathway. Only Wnt-treated (A) and treated with Dkk-1 (B) HeLa cells for 24 hours in-well culture were analyzed by Western blot. Dkk-1 has inhibiting ability to attenuate the detection of anti active β-catenin bands by increased concentration (B). The bar indicates 92 kDa. At 148 kDa and 65 kDa unspecific binding was detected. (C) Immunofluorescence analysis. At the increased concentration to 350 ng/ml of Wnt3a for 24 hours the signaling was activated and deactivated by addition of 500 ng/ml Dkk-1. Bar = 20 µm.**

5.1.8 Activation of Wnt/ß-catenin pathway by BIO in the microfluidic chip

The cellular response to a gradient of BIO was studied in the microfluidic chip by monitoring the nuclear translocation of ß-catenin. HeLa cells in the upper observation micro-chamber were exposed for 20 hours to a linear gradient from 0 and 2 µM BIO. In the convection-based mode of the chip, BIO induced a dose-dependent accumulation of ß-catenin (Fig. 5.26). The threshold was between channel 2 and channel 3 with calculated concentrations of 0.29 µM and 0.57 µM, respectively. Thus, the response of the cells in the microfluidic chip (Fig. 5.26) was similar to their response in the in-well culture (Fig. 5.23).
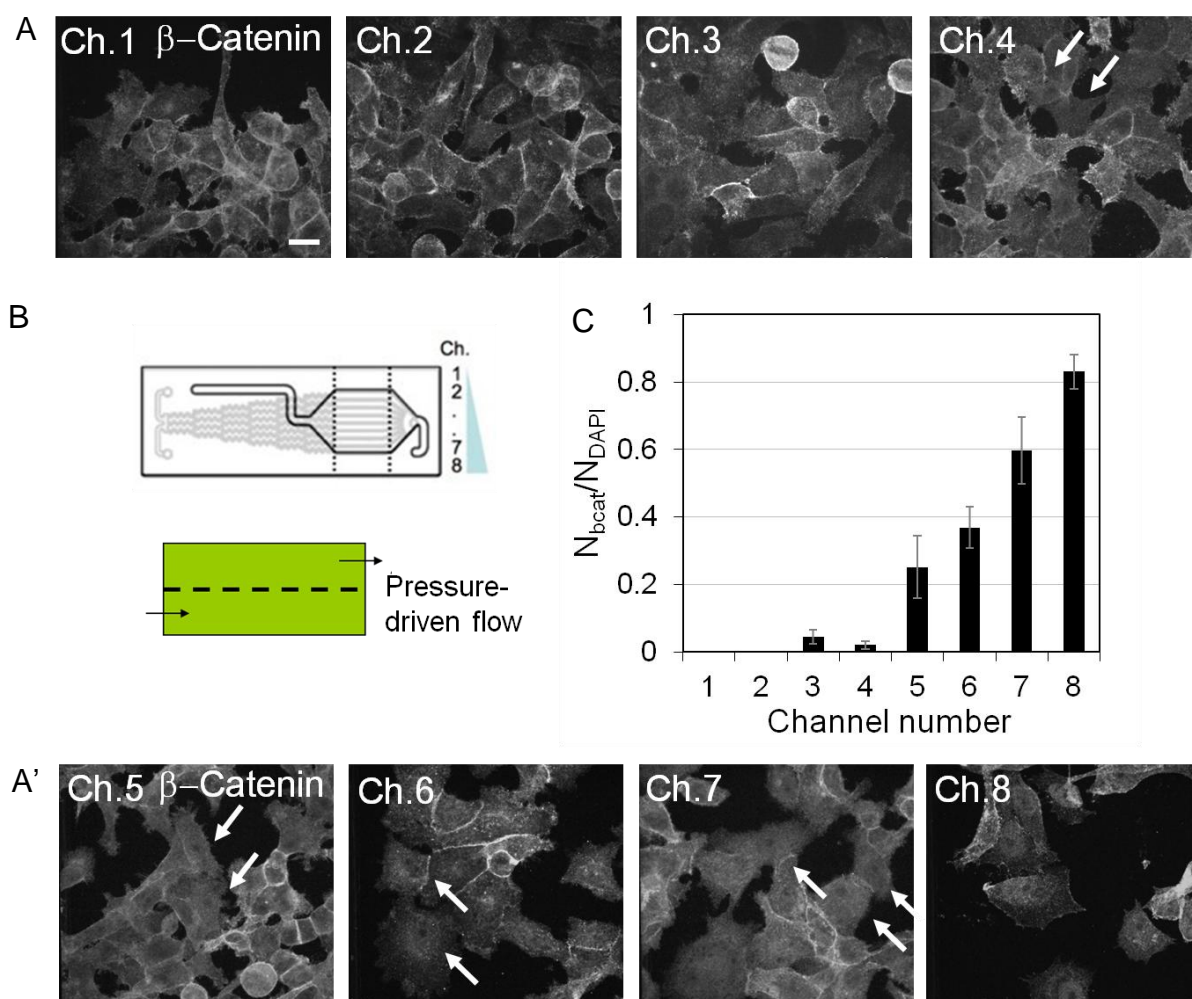
**Fig. 5.26 Selectively activated canonical Wnt/β-catenin signaling transduction in the microfludic chip in convection-based mode. (A-A') The white arrows indicate the representative β-catenin positive cells in nuclei shown from channel 4 (Ch.4) to channel 8 (Ch.8). Bar = 20 μm. (B) Higher numbered channel (Ch.8) has a higher concentration of BIO (2 μM). (C) Relative number of the cells with β-catenin accumulation in nuclei out of the total number of DAPI stained cells. After BIO gradient was applied for 20 hours in total, cells were analyzed as follows. Five images were taken from each channel. Average cell density of each image was $5.8 \times 10^4$ /cm². Total 678 cells ($N_{DAPI}$) were counted from 40 images and β-catenin nuclear accumulated cells ($N_{bcat}$) were selected by intensity difference in the images.**

Next, diffusion-based transport of BIO was investigated with the same readout. A diffusion-based extracellular signal transport is the most plausible suggested model that explains how a morphogen gradient is generated and reaches the cells (Lander *et al.*, 2002). When the diffusion mode was applied, the experimental time scale was divided in three steps (Fig. 5.27A).
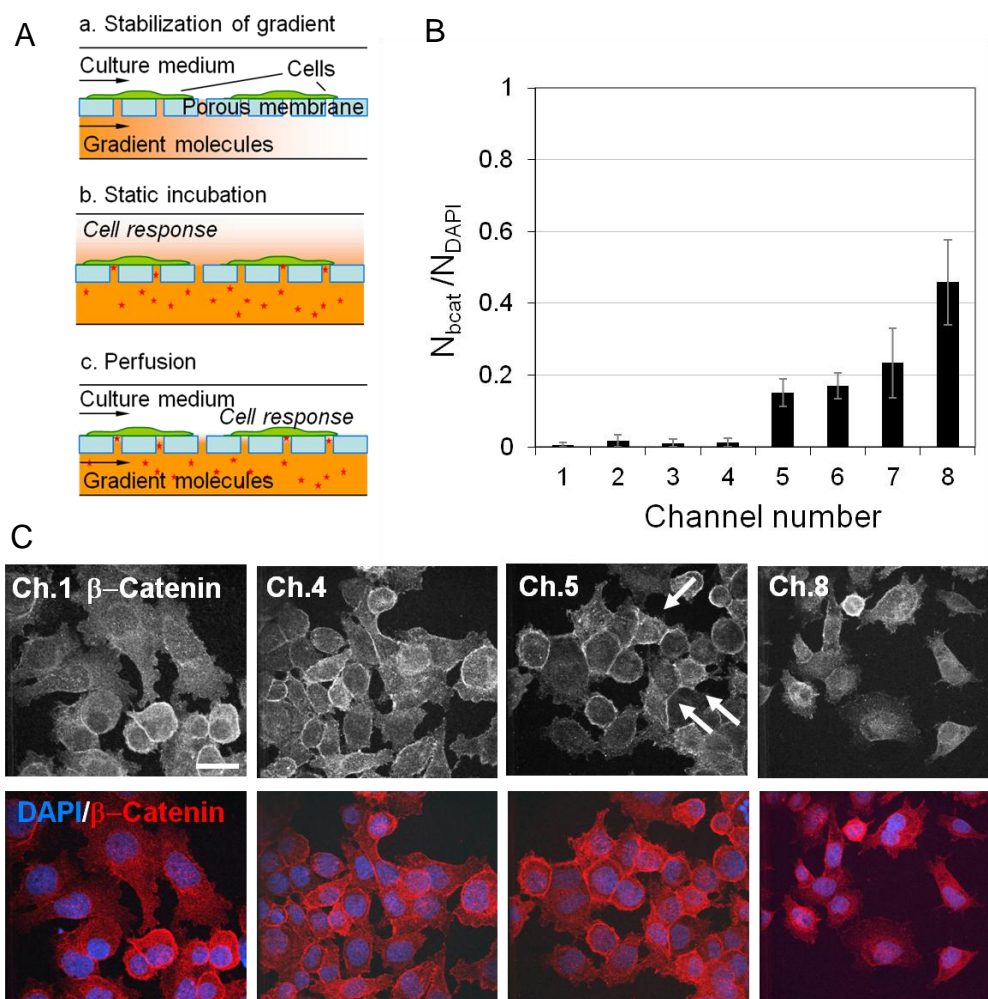
**Fig. 5.27 Selective activation of Wnt/β-catenin signaling pathway induced by diffusion-based transport of BIO. (A) Schematical drawing of the diffusion-based transport mode. The cells on the perforated membrane were supplied by culture medium and contacted *via* diffusion with a morphogen gradient generated on the lower side of the membrane. Not to scale. (B) Distribution of responding cells to BIO by diffusion-based mode. The highest concentration was 5 μM. Five images were taken from above each channel. Average cell density of each image was 5.4 x 10$^4$/cm$^2$. Total 632 cells (N$_{DAPI}$) were counted from 40 images and β-catenin nuclear accumulated cells (N$_{bcat}$) were selected by intensity difference in the images. (C) Through the diffusion-based exposure of BIO, strong β-catenin accumulation in the nuclei was shown only in the channels above the threshold concentration to turn canonical Wnt/β-catenin pathway on (arrows). Bar = 20 μm.**

First the BIO gradient solution was applied and formed a stabilized state along the gradient reservoir channels for four to six hours (a.stabilization of gradient). Once the gradient reservoir channels were filled up, cells were exposed to BIO by diffusion with no flow in both compartments for zero to four hours (b.static incubation). To mimic a bipolar physiological environment, the upper micro

chamber was perfused with conditioned medium for 14-18 hours to feed the cells and to continuously remove the morphogen from the cell culture medium. Simultaneously cells responded to BIO diffusing from the gradient reservoir (c.perfusion). To analyze the activation of Wnt/ß-catenin pathway, the accumulation of nuclear ß-catenin was scored (Fig. 5.27B). To account for the lower net-transport compared to the convection-based mode, the maximum concentration of BIO (channel eight) was increased to 5 µM.

In the channels with low concentration of BIO ß-catenin was located almost exclusively at cell-cell contacts. The threshold for ß-catenin accumulation in the nuclei was between 2.1 µM calculated for channel 4 and 2.9 µM calculated for channel 5 (Fig. 5.27), thus an order of magnitude higher than in the convection-based mode. However, the concentration that cells sense in the upper micro-chamber might be less than the calculated 2.1-2.9 µM due to the smaller contact area (porosity: 5-20 % provided by Milllipore, ≈ 13 % measured by SEM) and a set of fluidic resistance of the porous membrane (VanDersarl *et al.*, 2011).
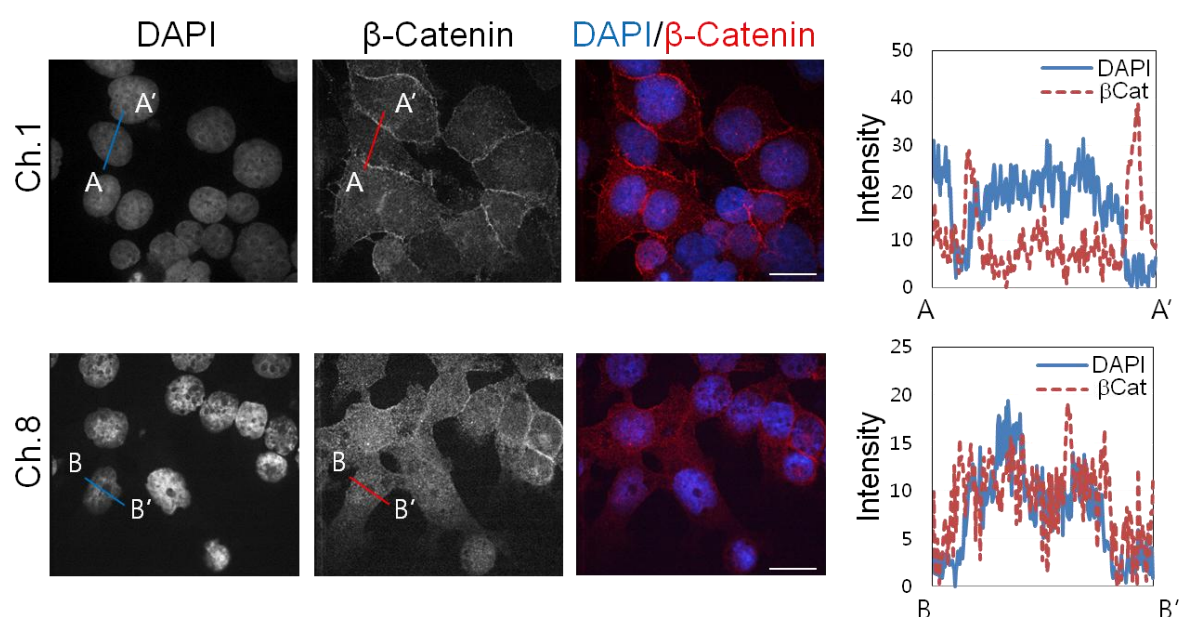


**Fig. 5.28 The representative images of channel one and channel eight in a higher magnification (63x) of the activation by diffusion-based transport of BIO. The cross-sectional intensity profile shows the significant difference of localization of β-catenin in nucleus between the two channels. Bar = 10 µm.**

In higher magnified images, the comparison of the intensity profile of DAPI to that of ß-catenin shows the significant increase of nuclear ß-catenin in BIO-treated cells (Fig. 5.28).

It was also necessary to confirm the proper distribution of cells seeded in the upper cell micro-chamber in order to interpret the cellular response on each position in a reliable control. Regardless of the different transport modes, most of the chips showed evenly distributed cells as exemplified with three different chips in Fig. 5.29.
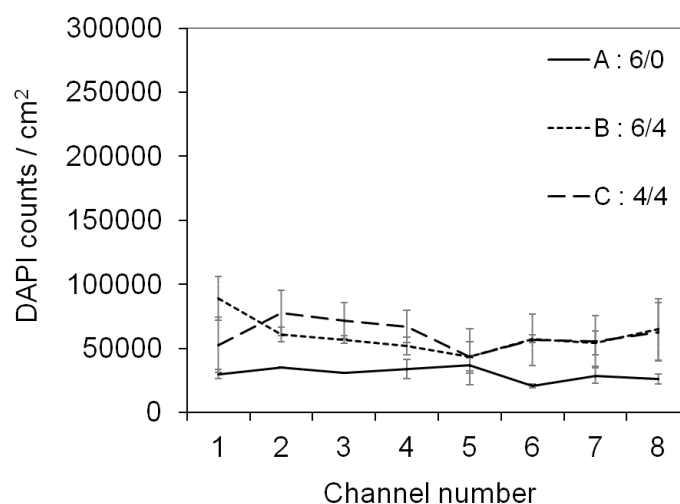


**Fig. 5.29 Distribution of cells in chip in diffusion-based experiments under different static incubation time (Fig. 5.27A). After 6 hours for a gradient, static incubation time varied as 0 hour (A:6/0) and 4 hours (B:6/4). The gradient time was decreased to 4 hours and static incubated for 4 hours in C:4/4. Total running time after a gradient was 24 hours for each case. DAPI stained cells were counted from five images per each channel per each chip. For all three, overall distribution was well established as such reliable cellular response was possible. A, without static incubation time showed less cells over all area in the upper micro-chamber while B and C with 4 hours static incubation time have comparable DAPI counts.**

Interestingly, longer static incubation time increased not only the DAPI counts but also the number of cells with ß-catenin positive nuclei in higher number of channels (Fig. 30). The longer static incubation helped to increase the exposure time of BIO to cells. Four experiments which have 4 hours static incubation time among independent microfluidic chips were averaged of positive number of nuclear ß-catenin. It revealed a dose-dependent increase of the readout with the channel number (Fig. 5.30C).
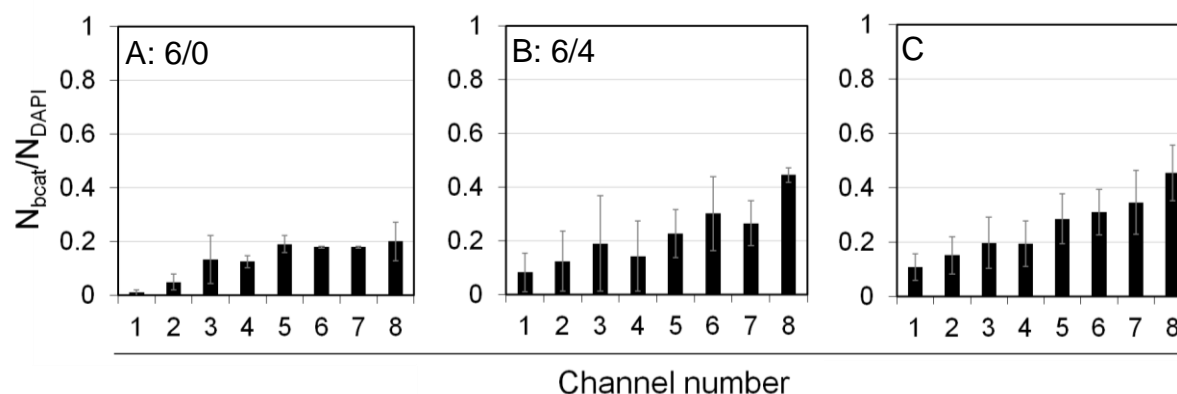
**Fig. 5.30 The relative number of cells with nuclear β-catenin to that of DAPI stained cells in differently operated diffusion-based activation of Wnt signaling pathway. As indicated in Fig. 5.29, after 6 hours for a gradient, static incubation time varied from 0 hour (A:6/0) to 4 hours (B:6/4). Total 755 cells (A) and 1557 (B) cells from two independent chips were counted. Five images were taken from each channel of each chip. Forty images per chip were used for selecting the number of β-catenin nuclear accumulated cells ($N_{bcat}$) out of DAPI stained cells ($N_{DAPI}$) by intensity difference in the images. (C) The average of activated cell number among four independent chips that were statically incubated for four hours. It showed nearly linearly increased tendency by the channel number. Total 2965 cells were counted from four independent microfluidic chips.**

5.1.9 Cellular reactions on Wnt3a/Dkk-1 protein gradients in chip

The addition of 500 ng/ml Wnt3a concentrations resulted in a moderate activation of the Wnt pathway throughout all eight channels (Fig. 5.31). This high Wnt3a concentration was chosen for two reasons: (1) strong pathway activation allows better to analyze the counter gradient of the antagonist Dkk-1 and (2) out of chip, nuclear accumulation of ß-catenin in response to high Wnt3a concentrations was completely reverted by high doses (500 ng/ml) of Dkk-1.

Although the Wnt dose was very high, a dose-dependent response was seen from channel five to channel eight (Fig. 5.31B, gray bars). Co-application of recombinant Dkk-1 protein *via* the second inlet drastically reduced the fraction of ß-catenin positive nuclei (Fig. 5.31B, black bars). Under these conditions Wnt responding cells were found only in the channels with highest Wnt3a concentrations (500 ng/ml) and virtually no Dkk-1. The high magnified representative fluorescent images of channel one and channel eight are shown in Fig. 5.31C and those of all channels are shown in Fig. 5.32.
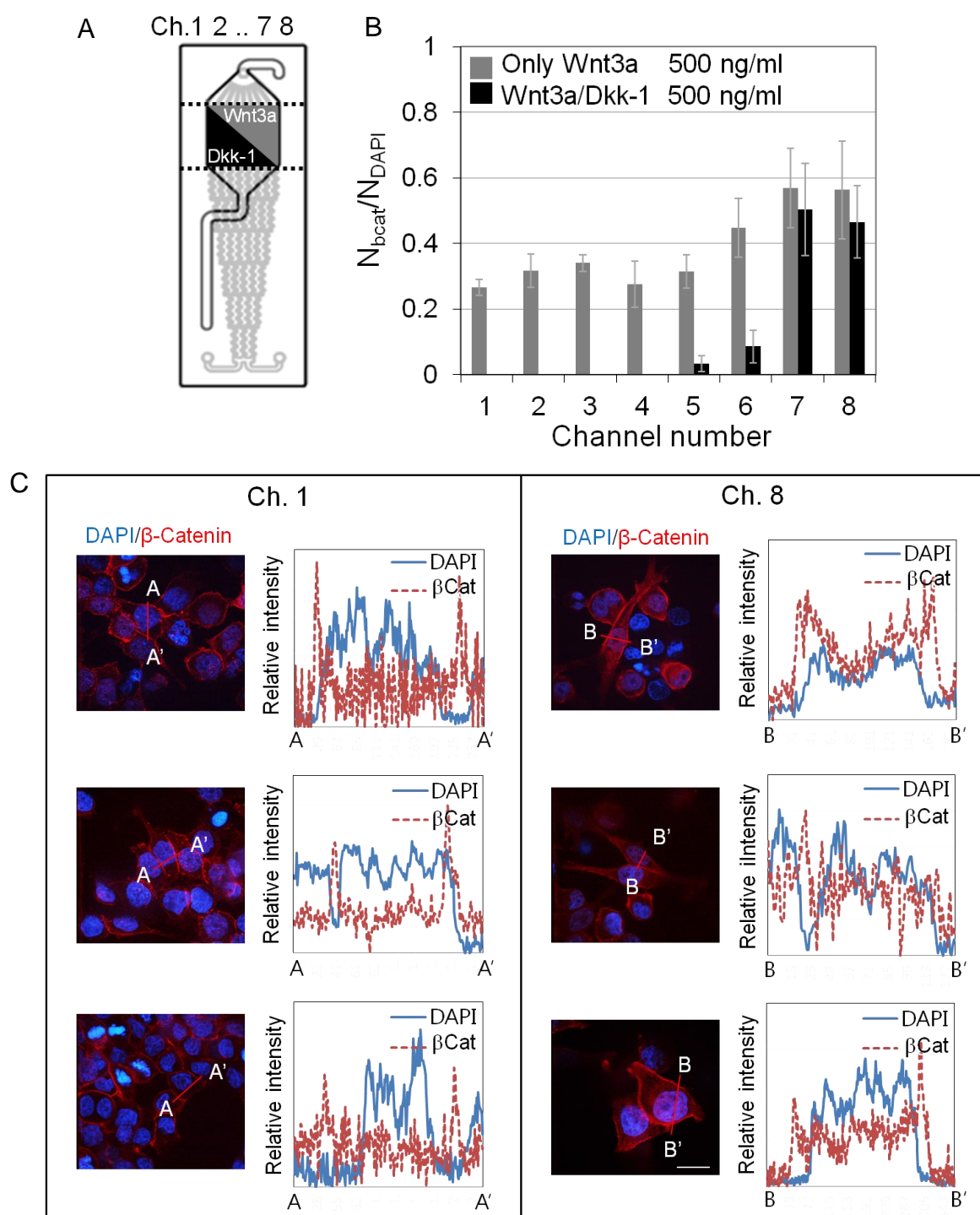
Fig. 5.31 Pathway activation by gradients of a morphogen and its inhibitor. (A) Recombinant Wnt3a and its repressor Dkk-1 were added into two inlets. Channel eight has highest concentration of Wnt3a (500 ng/ml) and lowest concentration of Dkk-1, *vice versa* for channel one. (B) Wnt3a treatment leads to a moderate accumulation of β-catenin in all channels (gray bars). Dkk-1 counter gradient does not allow for Wnt pathway activation in channel one - six (black bars). The fraction of β-catenin positive nuclei ($N_{bcat}$) was analyzed out of total 984 and 676 cells ($N_{DAPI}$), respectively. (C) Higher magnified images (63 x) of the cells exposed to the bipolar gradient. The cross-sectional intensity profiles illustrate the significant difference of β-catenin localization between channel one and eight. Bar = 10 μm.

Thus, the two-chambered microfluidic chip allows simultaneous application of a morphogen gradient and a counter gradient of its inhibitor.
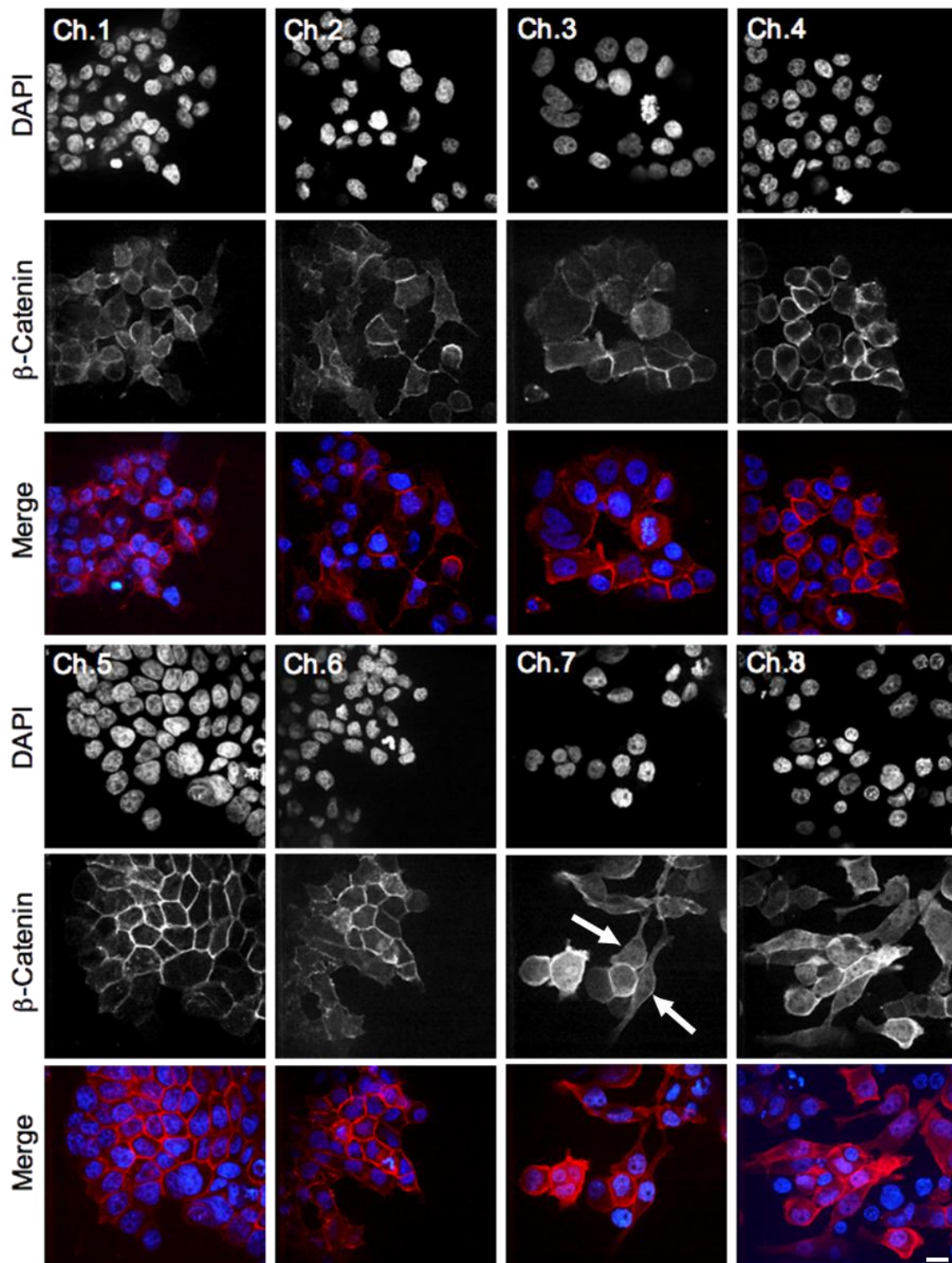


**Fig. 5.32 Fluorescent images of each channel of the bipolar Wnt3a and Dkk-1 gradient application. Channel one is supposed to have 500 ng/ml concentration of Dkk-1 with no Wnt3a and channel eight contains 500 ng/ml Wnt3a with no Dkk-1. In channel seven and eight accumulation of β-catenin (arrows) is shown as overlapped with DAPI. Bar = 20 μm.**

In collaboration with the Institute of Microstructure Technology, further microscopic observation for cellular response in long-term was tested with a long-distance objective. To ensure *in situ* monitoring of high magnified observation, the chip surfaces were polished or the additional process was conducted to increase transparency (Kreppenhofer, 2012). Fig. 5.33 shows the clear fluorescent image of transfected HeLa cells living on the membrane in #168 chip. This opens the possibility to continuously monitor cellular responses on morphogens in higher magnification (e.g. sub-cellular localization of a single cell) for long term without opening chips.
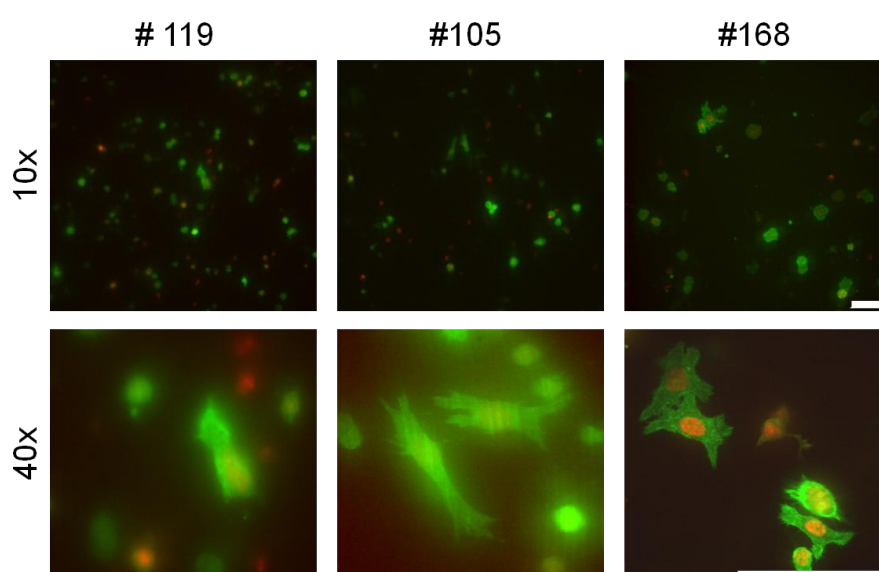


**Fig. 5.33 The use of a long-distance objective at a spinning disc microscope. HeLa cells were transfected with LifeAct-TagGFP and H2BmCherry to visualize F-actin and nuclei in living cells, respectively. Cells were seeded at 1 x 10⁶ /ml into the poly-l-lysine-coated and medium pre-incubated upper chamber of each chip. They were then incubated for 48 hours without perfusion. Three chips (#119, 105, 168) were independently fabricated and surface-treated resulting in different transparency. At 40x long-distance objective, the adhered cells were observed in all three chips but #119 and #105 show as blurred. In #105 some vertical lines were also found, which were from one of the manufacturing steps. The transparent #168 gave clear observation of the attached cells on the membrane. Bar = 100 µm.**

## 5.2 Murine embryonic stem cells (mES) in chip

### 5.2.1 Maintenance of pluripotency in Oct4-GFP mES by extracellular soluble factors

For maintenance of mES cells pluripotency a two factor coctail consisting of BIO and LIF was applied. BIO inhibits GSK3 and thereby activates ß-catenin-driven transcription, resulting in active pluripotent network (Wray *et al.* 2011). LIF drives self-renewal by activating the transcription factor STAT3 in combination with bone morphogenetic proteins (Ying *et al.* 2003).

By using these two soluble extrinsic factors, Oct4-GFP mES were cultured in serum-containing medium for 6 days and morphology of the grown colonies was analyzed on day 2/4/6 by image processing software. Morphological observation was chosen because it is one of the practical readout systems when mES is monitored in the microfluidic chip.

Compact colony growth of mES cells points to pluripotency. Therefore, the roundness of colonies was calculated by encircling a colony. The software defined a roundness as $4*area/(\pi*major\ axis^2)$ (http://rsbweb.nih.gov/ij). That means roundness of a perfect circle with radius, r is assigned with $4*\pi r^2/\pi*(2r)^2 = 1$, while a linear shape received the value "0" (area=0). This analysis revealed that LIF supplement induced circle-like colonies on day 4 and day 6 in both absence and presence of BIO treatment (Fig. 5.34A). The additional BIO treatment (LIF+/BIO+) attenuated the morphological change to spreading colonies, while in absence of LIF supplement the change was accelerated especially when BIO was lacking (LIF-/BIO-). BIO supported the maintanence the circle-like morphology of mES colonies regardless of LIF presence. Representative images are shown in Fig. 5.34B. After 6 days of incubation, the colonies were found dispersed and Oct4-GFP expression was almost lost in absence of both, LIF and BIO (Fig 5.34, upper line). LIF alone was able to maintain the round morphology of colonies (LIF+/BIO- , middle line) but the most compact colonies with highly expressed Oct4-GFP were only found under the condition of LIF+/BIO+ (bottom line).
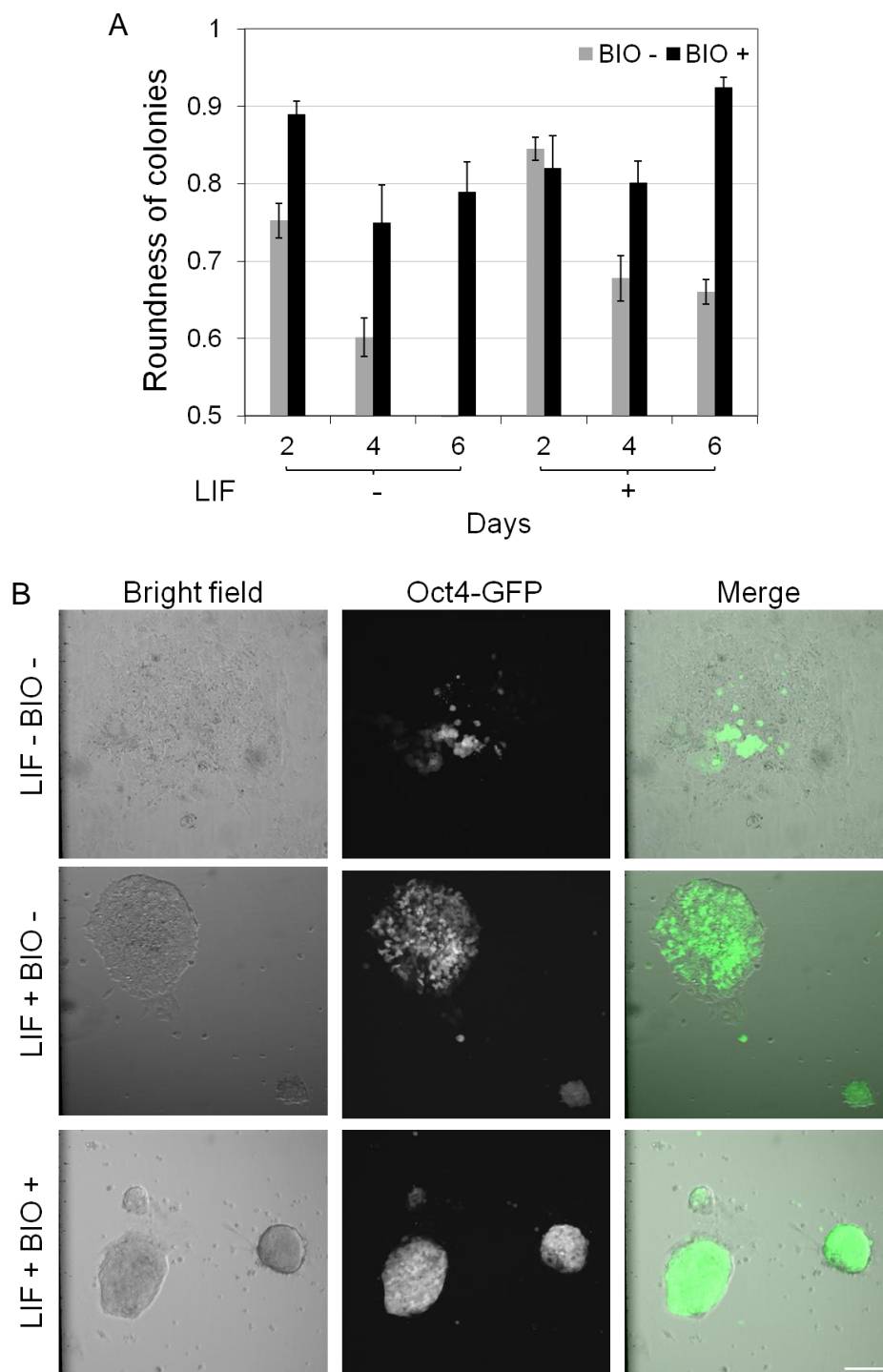
**Fig. 5.34 Roundness of Oct4-mES colonies in presence or absence of LIF or BIO. (A) The roundness was maintained as being over 0.8 under the condition of LIF (+) 1.6 v/v %, BIO (+) 5 µM. (B) The bright field and fluorescent representative images of Oct4-GFP mES grown in serum-contatining media for 6 days. The colony-like morphology was lost in the absence of LIF and BIO, while compact colonies with high Oct4 expression were found in LIF and BIO supplements. Bar = 100 µm.**

To extend this observation into a concentration dependent manner, LIF treatment was varied with different volume per volume ratio out of culture media in presence or absence of BIO. When mES maintained self-renewal state, colony size increased and the morphology appeared more globular-like. Therefore, the diameter of colonies and the number of colonies were analyzed. With a lack of BIO (Fig. 5.35, left row, BIO-), there was no significant change in the distribution of small colonies ($d$: 10-50 µm) over time. For colonies with a diameter 100 µm and more, the tendency was observed that larger colonies were formed with increasing incubation time. This tendency was even more pronounced in the presence of BIO (Fig. 5.35 right row, BIO+). The longer mESs were incubated, the larger colonies were generated and the less number of colonies was detected.

To figure out whether the LIF and BIO supplements change cadherin expression, western blot analysis was performed against E-Cadherin and N-Cadherin, since E-Cadherin as cell adhesion protein is preserved at pluripotency state (Larue *et al.*, 1996; Cavallaro & Christofori, 2004) and its replacement to N-Cadherin is considered as an indicator for neural differentiation (Eastham *et al.*, 2007; Spencer *et al.*, 2007; Redmer *et al.*, 2011).

The LIF and BIO treatment on wild type of mES, W4 differed the expression of E-Cadherin and N-Cadherin (Fig. 5.36). Western blot analysis clearly indicates that E-Cadherin expression is enhanced under the LIF positive condition on 7 days incubation. Regardless of BIO presence, N-Cadherin is suppressed when LIF is supplemented.
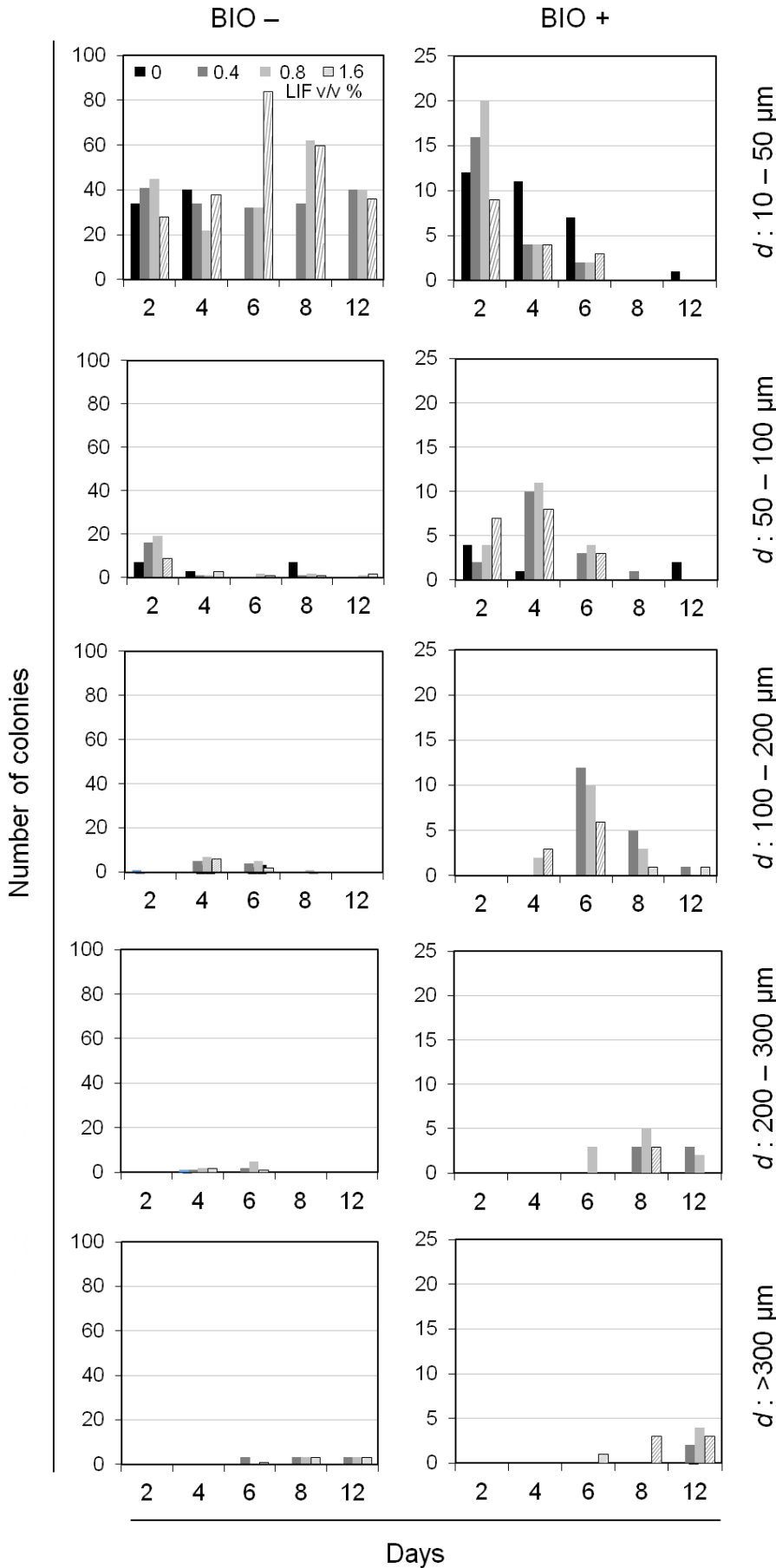
Fig. 5.35

**Oct4-GFP mES colonies changes in size and number at different conditions of LIF and BIO. BIO positive means the concentration is 5 μM. Culture medium was replaced every two days in each condition.**
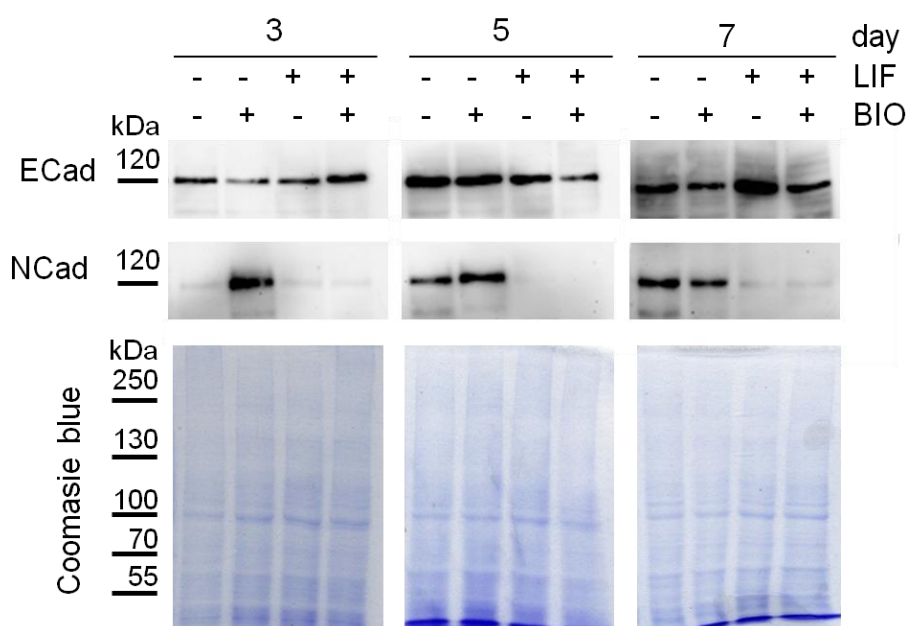
**Fig. 5.36 Cadherins expression after treatment with LIF and/or BIO. BIO positive means treatment with 2 µM and LIF postive indicates 1.6 v/v %. Culture medium was replaced every two days. Normalized proteins amount were loaded in 8 % SDS gel.**

5.2.2  Initiation of differentiation by hanging drop method

To induce *in vitro* differentiation of mES, hanging drop method was used. After 2 days of hanging and 3 days of culture in bacteriological dishes (5 days), embryoid bodies (EBs) were seeded on gelatin-coated dishes to be expanded. Western blot with antibodies against Oct3/4 and the heart tissue marker Connexin 43 revealed that whenever the differntiation marker Connexin 43 is expressed, Oct3/4 is not detectable (Fig. 5.37A). Indeed, only in the mES + LIF control cells strong Oct3/4 expression was detected. Connexin 43 expression in EBs increased with time starting from 5+4 days.

The exclusive expression of either a differentiation marker or the pluripotency marker Oct3/4 and the ongoing differentiation in EBs was confirmed by immunofluorescence studies (Fig. 5.37B/C). Immunofluorescence images are shown of those after 5+2 days (B) and 5+11 days (C) since differentiation has been induced. After 5+2 days, the loss of Oct3/4 was observed in dispersed colonies in which spontaneous differentiation was already initiated. That was shown by the expression of Connexin 43, Troponin T as cardiac differentiation indicators and of ßIIITubulin, Nestin as neuronal markers. After 5+11 days,

Oct3/4 was drastically repressed and cardiac or neuronal differentiation markers became more enhanced. E-Cadherin at cell-cell contact was expressed when colony growth was maintained.

### 5.2.3 Maintenance of pluripotency of Oct4-GFP mES in chip with modified structure

A further developed second microfluidic chip with structural and material changes (Fig. 5.38B, Krepenhofer, 2010) was also tested for stem cell biocompatibility. (1) In this device the PMMA supporter below the complete chip which enabled the connection with tubing was removed. Therefore, the inlets and outlets of the upper and lower part were extended to the end of the part, not having L shape but straight flow micro-channels (a, b). (2) The cell observation chamber was modified possessing eight separated channels (c). (3) The porous membrane was changed to a partially perforated membrane. SEM images proved that the original designed device was consisted of a totally perforated polycarbonate membrane (Fig. 5.38A'). It caused unexpected diffusion from the last cascade of zig-zag mixer in the triangle areas (Fig. 5.38A inset, black triangles). In the modified design, the membrane contained a selectively perforated area (P) and a non-perforated area (NP), as SEM images confirmed the different porosity (Fig. 5.38B')
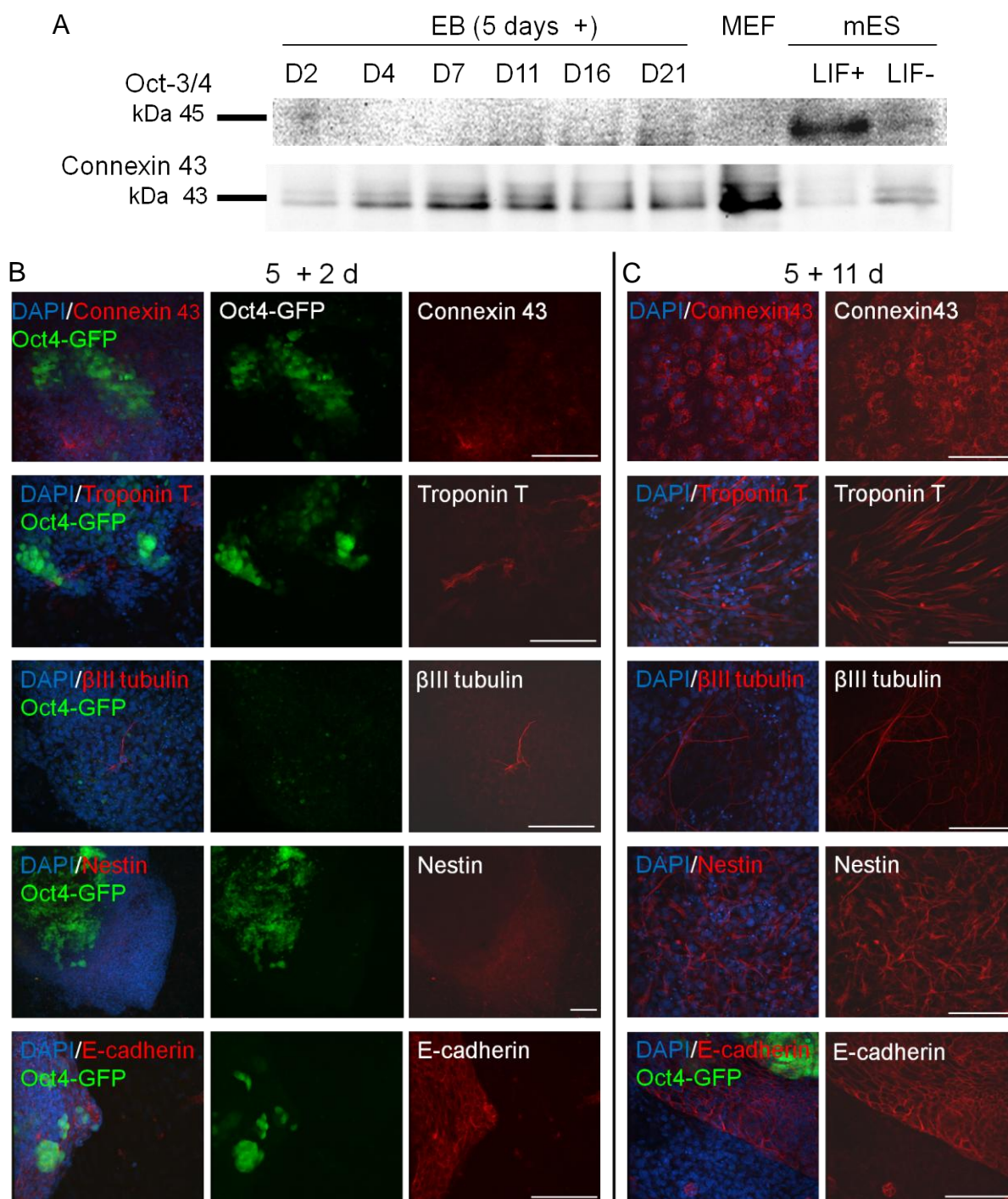
Fig. 5.37 Spontaneous differentiation from embryoid bodies (EBs) formation method. (A) Western blot analysis of Oct3/4 and Connexin 43 over increasing days of differentiation. EBs were formed for 5 days in suspension culture and transferred to gelatin-coated substrates for further incubation. In presence and absence of LIF mES were cultured for 7 days and were cultured with MEF (passage 5) for control. Immunofluorescence assay was performed against Connexin 43, Troponin T, βIII Tubulin, Nestin and E-Cadherin after 5+2 days (B) and 5+11 days (C). Bar = 100 µm.
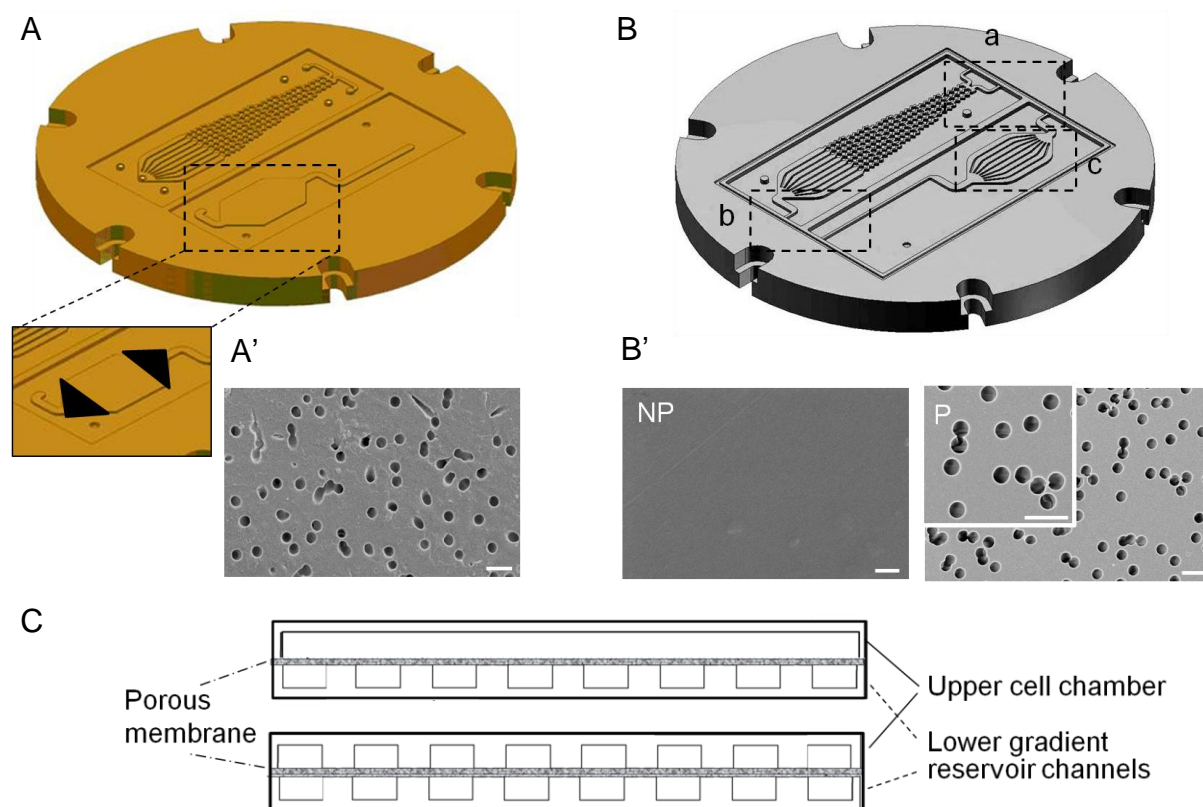
**Fig. 5.38 Comparison of two different designs of the developed microfluidic chip. (A) The insert mold image of original design of the two-stacked microfluidic chip with totally perforated membrane. The upper cell micro-chamber area is enlarged to show the triangle areas where unexpected diffusion occurs. (A') SEM image demonstrates that the pores (0.4 µm) of the totally perforated membrane was preserved after thermal bonding process. (B) The insert mold of the secondly developed device with structural and material changes resulting in a partially perforated membrane. SEM images confirm the different porosity of the membranes. NP, non-perforated area ; P, perforated area. Bar = 1 µm (schemes of the insert molds were provided by the Institute of Microstructure Technology, Karlsruhe Institute of Technology). (C) The sectional views of the original (upper) and post-developed (lower) structure. Not to scale.**

Oct4-GFP mES were cultivated in the modified chip, where the cell observation chamber was separated in eight channels (Fig. 5.39). The chamber was perfused with 5 µl/min which gives negligible shear stress of approximately 0.005 dyne/cm². CPR is regarded as 0.28 µl/min and ECT ≈ 12 hours. Consistently, only few colonies were found at the membrane. Instead, large Oct4-GFP positive colonies formed in the gap between porous membrane which was not bonded on the polymer sheet and the cell observation chamber (Fig. 5.39A). These mES cells maintained Oct4-GFP and divided.
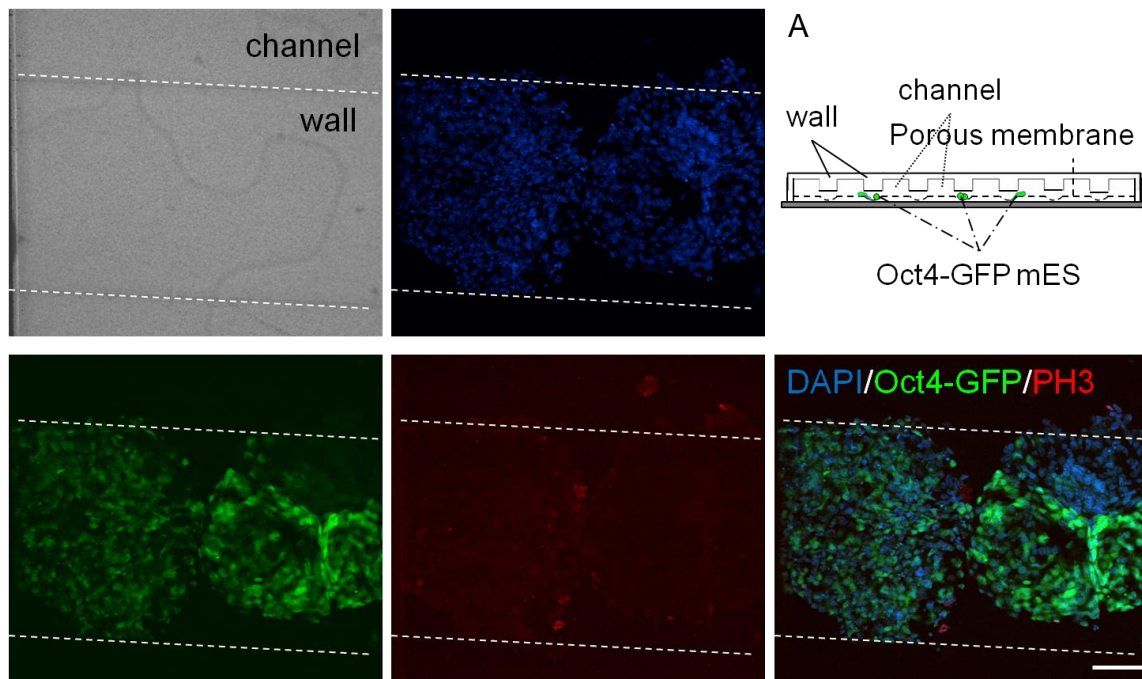
**Fig. 5.39 Oct4-GFP mES were cultured in the chip with only upper part and porous membrane. (A) Incomplete bonding allowed mES residing under the wall, changing their morphology. The seeded Oct4-GFP mES were supplemented with LIF (1.6 v/v %) in the microfluidic chip and after 6 days the chip was opened for immunofluorescence detection of the proliferation marker phosphohistone H3 (PH3). Images were obtained followed by DPAI nuclei staining. Bar = 100 µm.**

Hence, it was switched to the completely liquid-tight bonded microfluidic chip. The cultured Oct4-GFP mES colonies grew in size and maintained the round morphology as well for 7 days (Fig. 5.40). At day one, most of cells were highly dispersed with a few cells forming small colonies within a diameter 10-50 µm. With increasing incubation time, the relative number of larger colonies increased as well (Fig. 5.40B). As colony size is grown, the length of the micro-channel affect on the distribution of soluble factor by fluid flow from left to right (Fig. 5.40D).

A  Perfusion culture



B



C



D



→ Direction of flow
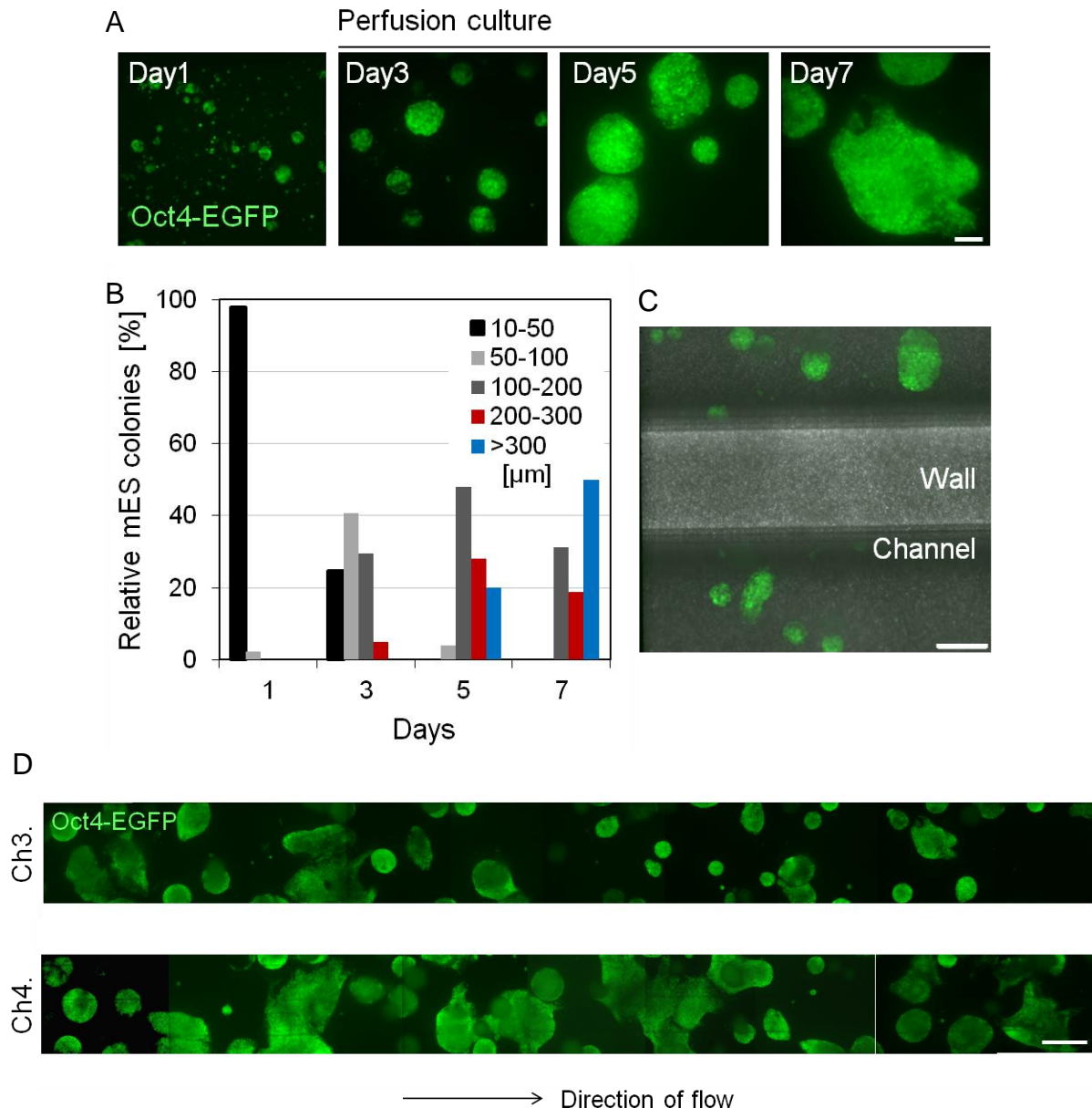
**Fig. 5.40 Oct4-GFP murine embryonic stem cells in the second type of microfluidic chip. (A) Oct4-GFP mES were seeded seeded at 2 x 10⁶ /ml on gelatin pre-coated upper chamber in medium supplemented LIF (2 v/v %). After overnight static incubation, the medium was perfused (5 µl/min) only in the upper part. In the separated upper channels cells were cultured in perfusion with the medium supplemented by LIF to maintain pluripotency for more than 7 days. When the colonies were monitored by Oct4-GFP signal at the low magnification (10x), perfusion was temporarily stopped. Confocal microscope confirmed the height of colonies is on average ≈ 150 µm (globular shape). Bar = 100 µm. (B) Relative number of mES colonies was counted by the diameter using ImageJ software. (C) The channels separated by walls in the cultivation chamber help to culture mES at discrete concentrations of a gradient. The image was taken after 5 days of perfusion. The bright field and green fluorescent images were merged. Bar = 200 µm. (D) The fluorescent images of the whole length of channel three and four were overlapped to overview the distribution of the colonies. Bar = 500 µm.**

## 5.3 Direct surface modification by nanografting

Nanografting is an approach of scanning probe lithography to structure self assembled monolayers (SAMs) - here thiols on a gold substrate - with a high resolution. This process includes two subsequent steps: (1) First the molecules of the thiol SAM are shaved by the AFM tip which has a diameter of tens of nanometers that provides the resolution from hundreds of µm² squares to tens of nanometer lines (Ngunjiri *et al.*, 2008). This shaving is carried out in a solution containing thiol molecules different from those forming the SAM. (2) In the second step the shaved molecules are substituted by the thiol molecules solved in the liquid. In this work, as a proof-of-concept the square patterns of 15x15, 10x10 and 5x5 µm² were prepared by this method (Fig. 5.41). As a background (non-patterned area) ethylene glycol (EG) unit containing SAMs were pre-formed to be used for avoiding unspecific protein adsorption (Lee *et al.*, 1989; Pale-Grosdemange *et al.*, 1991; Desai *et al.*, 1991). After pattern areas are shaved by AFM tip in contact mode, benzyl guanine (BG) containing thiols as ink molecules self-assembled on uncovered areas immediately and simultaneously. The spacing between two patterns varied from 15 µm to 20 µm (Fig. 5.41).
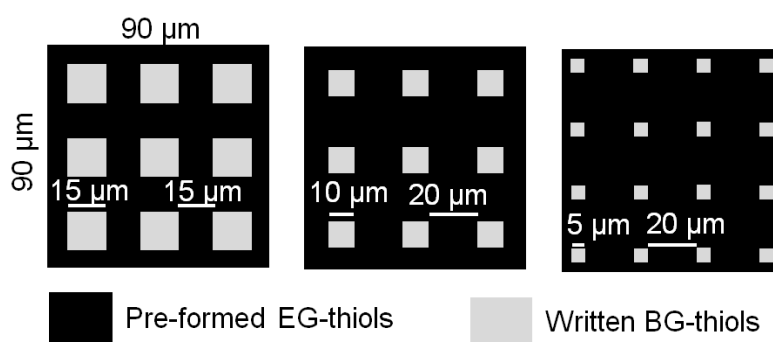


**Fig. 5.41 Pattern dimensions. The whole scanning area is 90x90 µm². Micropatterns were made by grafting resulting in benzyl guanine (BG) thiol patterns out of pre-formed ethylene glycol (EG) thiols.**

### 5.3.1 Characterization of grafted patterns

#### 5.3.1.1 *In situ* analysis by AFM

One of the significant advantages of nanografting is the *in situ* examination of the structured surface areas without exchanging AFM tips and the necessity to refind the patterns. As such topographical and phase information of the patterns

were determined (Fig. 5.42). The topographical profile of BGT:EG$_4$OH written in 15x15 µm² out of pre-formed EG$_3$OMe revealed that the height difference of patterns to the background is approximately 1.2 nm (Fig. 5.42A). The profiling line was chosen in the perpendicular direction to scanning direction. The height difference between the 10x10 µm² BGT:EG$_6$OH grafted area and the pre-formed EG$_3$OMe is increased to 1.6 nm (Fig. 5.42B). The approximate 0.4 nm difference is well comparable to the theoretical SAM thickness of EG$_4$OH and EG$_6$OH (Valiokas *et al.*, 1999, Harder *et al.*, 1998).
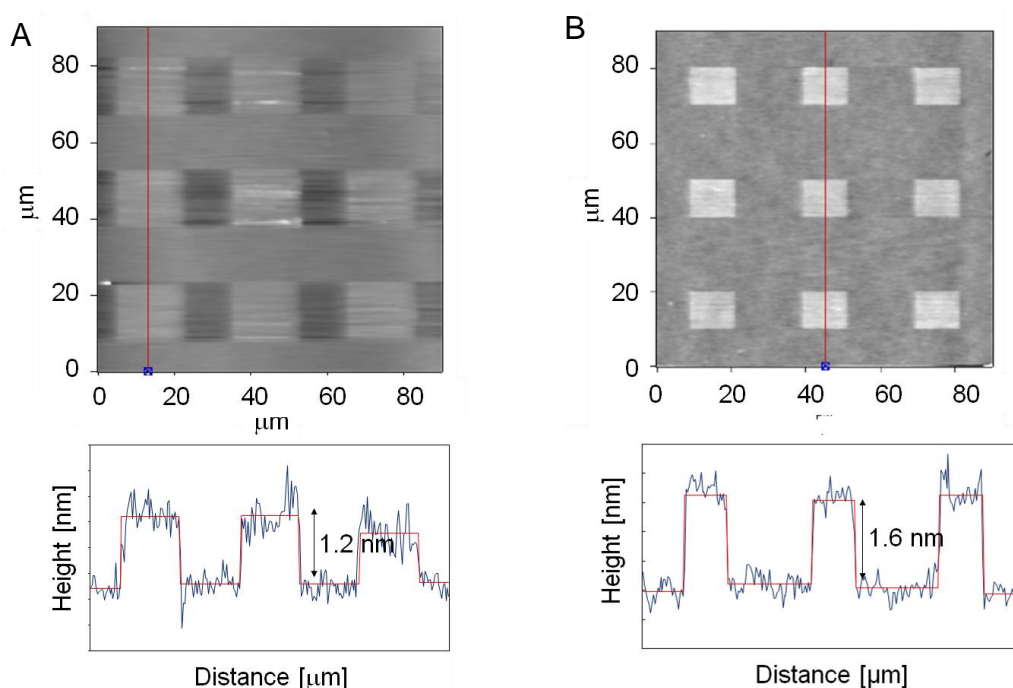


**Fig. 5.42 *In situ* topography distinguishes different pattern molecules. (A) 15x15 µm² of BGT:EG$_4$OH out of pre-formed EG$_3$OMe. (B) 10x10 µm² of BGT:EG$_6$OH out of pre-formed EG$_3$OMe. Bottom line shows the corresponding topography profiles along the red line.**

5.3.1.2 ToF-SIMS analysis

ToF-SIMS analysis provided characteristic chemical information of the patterns. By using this approach, SAM compounds can be identified especially by indicating and characteristic molecular ions. The lateral distribution of some indicating secondary ion counts results in images of each secondary ion in 100x100 µm² (Fig. 5.43). There was a concern that the very low amounts of BG thiol could be detected when using a concentration ratio BGT:EG$_6$OH = 1:100. To increase the detected chemical contrast, pure BG thiol was used for the grafted

area 50x50 µm², omitting EG$_6$OH. As expected, only in the grafted area contains BG thiol indicators as CN$^-$, C$_5$H$_3$N$_5$O$^-$, C$_5$H$_4$N$_5$O$^-$, where the spectral peaks appear at 26, 149, 150 amu, respectively. Additionally SOx species e.g. SO$_3^-$, SO$_4$OH$^-$ where the peaks are detected at 79.96 and 96.96 amu were enriched in the grafted areas, indicating spontaneous oxidation occurred in the sample.

Such images of Fig. 5.44 were corresponded with the lateral distribution of selected secondary ions, which can be obtained as spectra of peaks. The whole experiment time including scanning, grafting, and examining covered 2 hours and samples were kept immersed in ink molecule solution during this time. Therefore, it was necessary to confirm that no spontaneous substitution or invasion of ink molecules to the pre-formed SAM takes place. First, on Au surface EG$_3$OMe SAM was formed for 24 hours. As a kind of simulation of non-grafted area, pure BG thiol solution immersed the pre-formed EG$_3$OMe SAM for 2 hours. After thoroughly washing ToF-SIMS measurement was performed. Fig. 5.44A shows the spectra between ≈ 10-160 amu and ≈ 650-790 amu. The upper blue graph is EG$_3$OMe SAM for comparison to the bottom red graph (EG$_3$OMe + BGT) of that substitution sample prepared as mentioned. The peaks in the region 740-750 amu are corresponded to molecular ion of EG$_3$OMe, [Au$_2$SC$_{18}$H$_{37}$O$_4$]$^-$. For BG thiol indicating region at 146-154 amu is marked in a black rectangle and zoomed in Fig. 5.44B. The weak peak at 150 amu was appeared in EG3OMe + BGT sample, indicating very low amount of pure BG thiol was incorporated in pre-formed EG$_3$OMe.
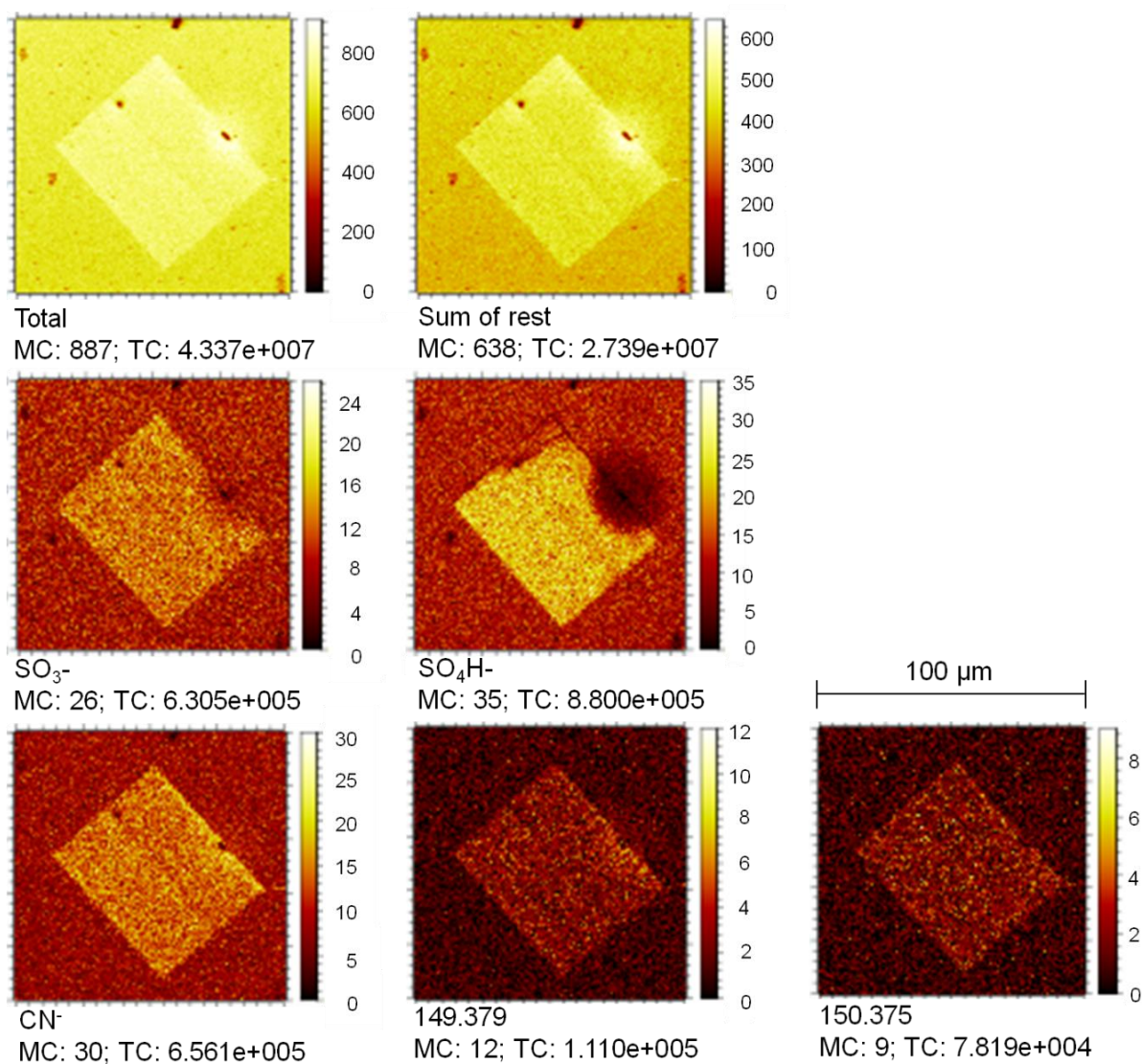
**Fig. 5.43 ToF-SIMS images of a 50x50 µm² grafted area (100 µM pure BGT grafted on pre-formed EG₃OMe). The indicators of photo oxidized SAM (SO₃⁻ and SO₄H⁻) were detected in the area shown in the middle line. The bottom line indicates the characteristic secondary ions for BGT ; CN⁻ at 26 amu, C₅H₃N₅O⁻ at 149 amu and C₅H₄N₅O⁻ at 150 amu (Kwok *et al.*, 2011).**
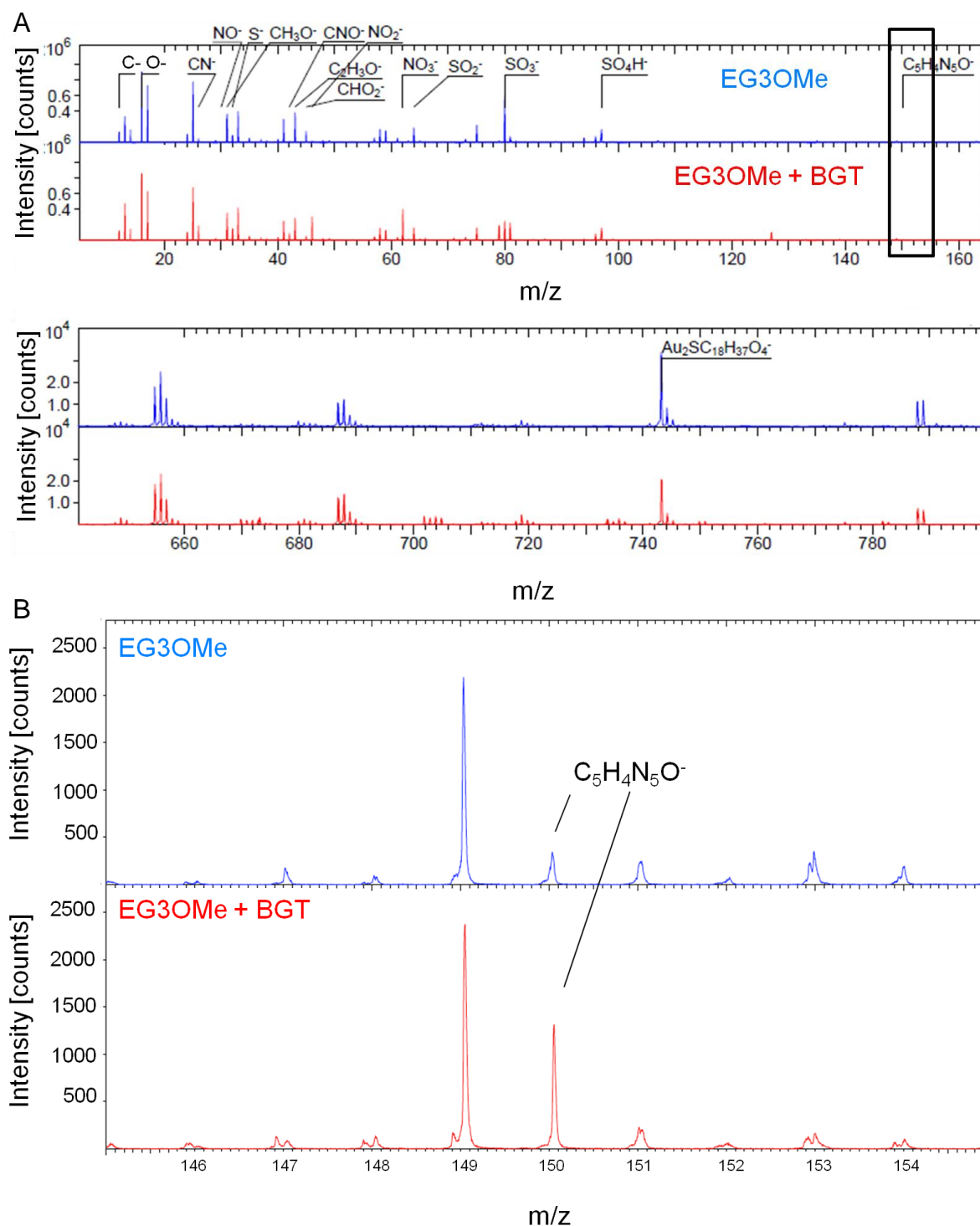
Fig. 5.44 Comparison between EG₃OMe SAM and that incubated BG thiol for 2 hours. (A) Selected secondary ion spectra at ≈ 10-160 amu and ≈ 650-790 amu. Several secondary ions indicating each mass are marked. (B) The region between 146 and 154 amu of BG indicator peaks was zoomed in. Upper line in blue: EG₃OMe SAM as a control, bottom line in red: BGT exposed to EG₃OMe SAM for 2 hours followed by washing, simplified as EG₃OMe +BGT.

Similarly, the question about the substitution of BGT:EG$_6$OH against pre-formed SAM, EG$_3$OMe and EG$_6$OH was analyzed by ToF-SIMS spectra. The EG$_3$OMe and EG$_6$OH SAM were prepared for controls and Fig. 5.45 shows their identification. The molecular ion for EG$_3$OMe, Au$_2$SC$_{18}$H$_{38}$O$_4$ simplified as [Au2-EG3]$^-$ at 740-750 amu was detected only on EG$_3$OMe SAM and that for EG$_6$OH, AuSC$_{23}$H$_{48}$O$_7$ simplified as [Au-EG6]$^-$ was found only on EG$_6$OH SAM.
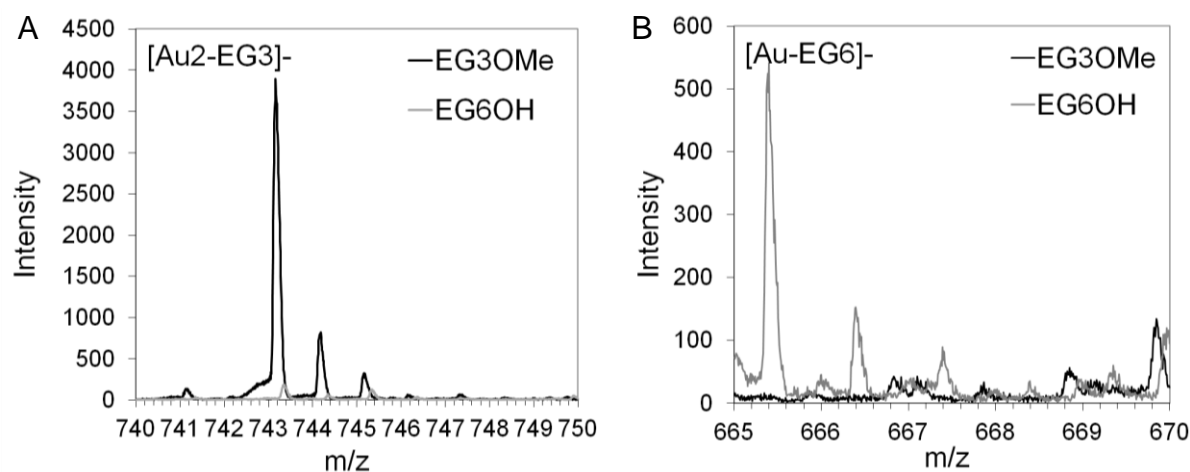


**Fig. 5.45 Selected secondary ion mass spectra of negative polarity. (A) Only EG$_3$OMe SAM produced the molecular ion [Au2-EG$_3$]$^-$ detected between 740 and 750 amu. (B) Only EG$_6$OH SAM possesses the molecular ion peak [Au-EG6]$^-$ at 665-670 amu.**

Fig. 5.46 shows the comparison of the peaks at the region 149 and 150 amu. The BG thiol specific peak at 150 amu was determined only for BGT:EG$_6$OH SAM which served as a positive control, but not for BGT:EG$_6$OH incubated on EG$_3$OMe (Fig. 5.46A, dashed line) and on EG$_6$OH (Fig. 5.46B, dashed line). Hence, the ink molecule, BGT:EG$_6$OH did not substitute pre-formed SAM, neither EG$_3$OMe nor EG$_6$OH. Additionally, the peaks at 149 and 150 amu are considered as BG thiols indicators. However, one should note that EG$_3$OMe has also a detected peak at 149 amu. It will be discussed in the discussion chapter.
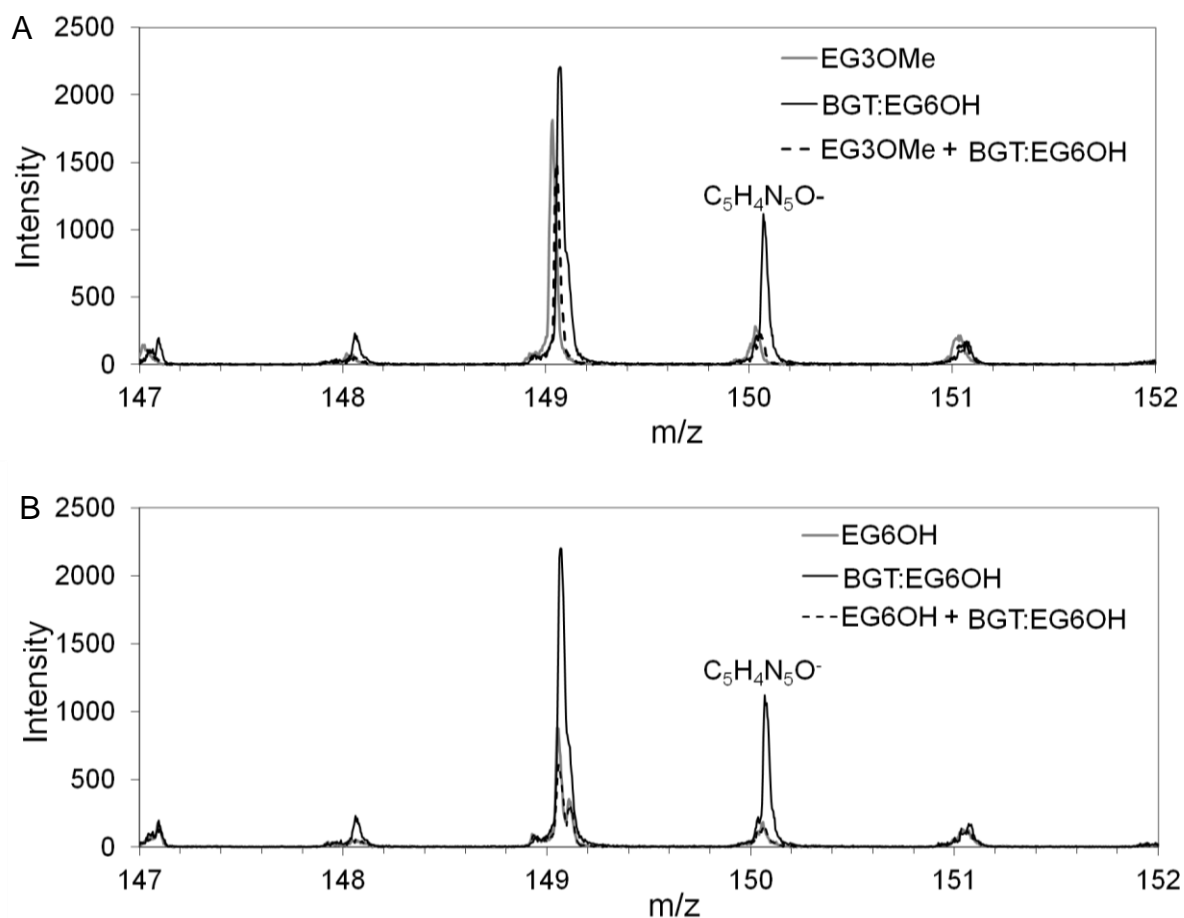
**Fig. 5.46 Negative secondary ion spectra of the substitution experiments. BG thiol indicating peak at 150 amu was only found in a positive control, BGT:EG₆OH SAM. No substitution was found by 2 hours incubation of BGT:EG₆OH ink molecule on EG₃OMe (A) nor on EG₆OH (B).**

### 5.3.2 Selective immobilization of proteins on grafted patterns

### 5.3.2.1 SNAP-GFP on grafted patterns

Affinity purified His-SNAP-GFP protein (Fig. 5.47) was used to functionalize the patterned surfaces. Analyses of the purified proteins revealed that SNAP and GFP positive fractions co-eluted. However, in addition to a protein of the expected size (50 kDa), the anti GFP antibody detects also a smaller protein (29 kDa). Interestingly, such a smaller band was also detected in a silver-stained gel but not with the anti-SNAP antibody, indicating that parts of fusion protein were degraded.
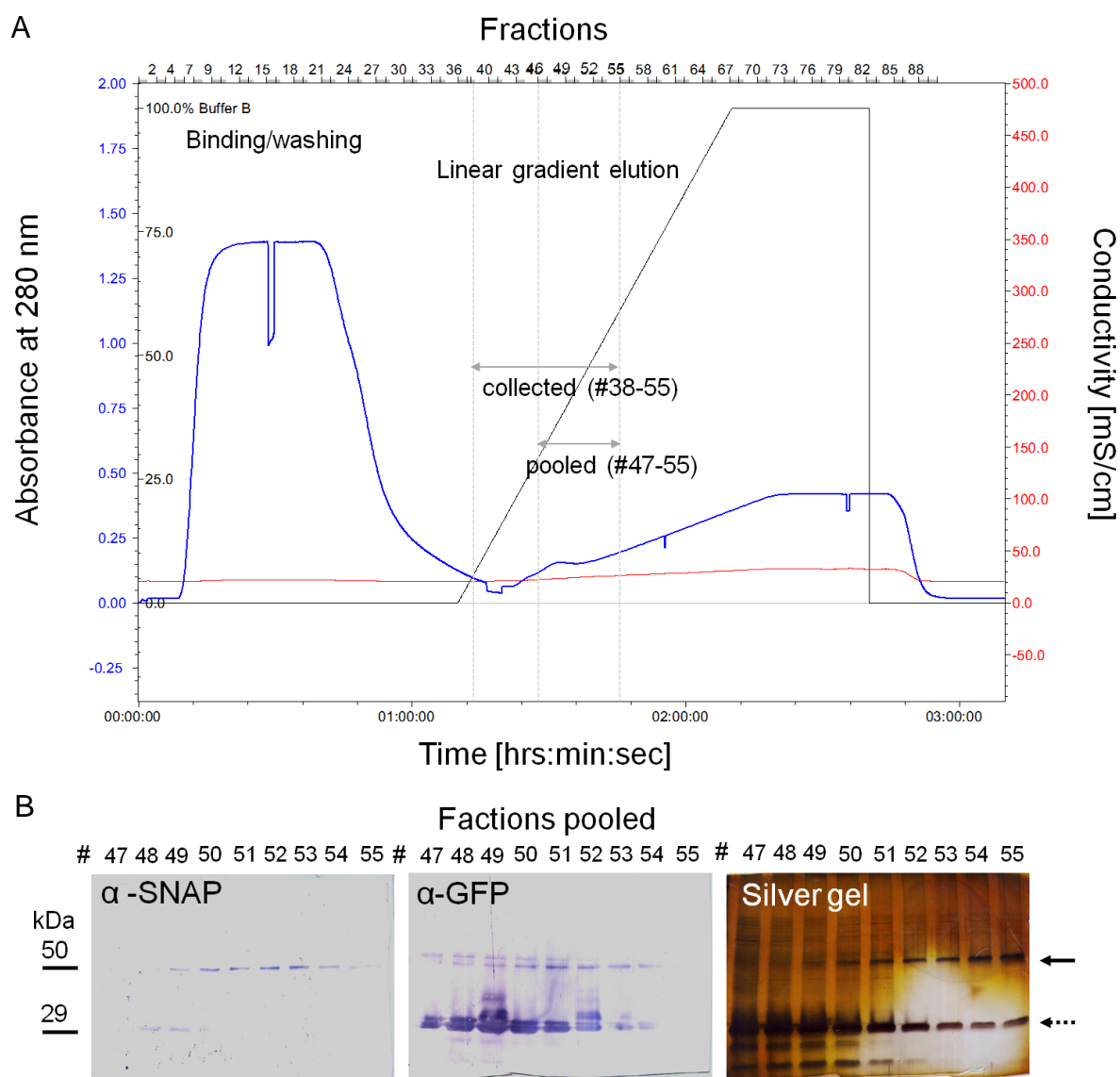
**Fig. 5.47 Purification of SNAP-GFP by Ni²⁺-NTA affinity chromatography. (A) The FPLC chromatogram demonstrated the purification process of His-SNAP-GFP extract from *E. coli*-BL21-AI™. Blue curve indicates absorption at 280 nm of non-specifically (#1-37; binding/washing) and specifically bound (#38-55; linear gradient elution) proteins. Black curve shows the increasing imidazol concentration during linear gradient elution step. Red curve describes constantly maintained conductivity. (B) The collected fractions (#38-55) were analyzed by SDS-PAGE followed by silver gel staining and western blot against SNAP and GFP. Only GFP and SNAP positive fractions (#47-55) were selected to pool. Visible bands against GFP at smaller size (29 kDa) were detected. By silver gel staining total proteins were traced at 50 kDa (solid arrow) as well as at 29 kDa (dotted arrow).**

The purified SNAP-GFP was coupled through the enzymatic activity of SNAP tag to the micro-patterned benzyl guanine substrate (Fig. 5.48). This covalent protein immobilization was successfully applied on the grafted 15x15 µm² pattern. The

green fluorescence intensity difference between the patterns and the background was clearly distinguishable, indicating that the EG₃OMe SAM blocked unspecific protein binding. The used samples' topography (Fig. 5.48A) and phase contrast (Fig. 5.48B) also supported the defined patterns.
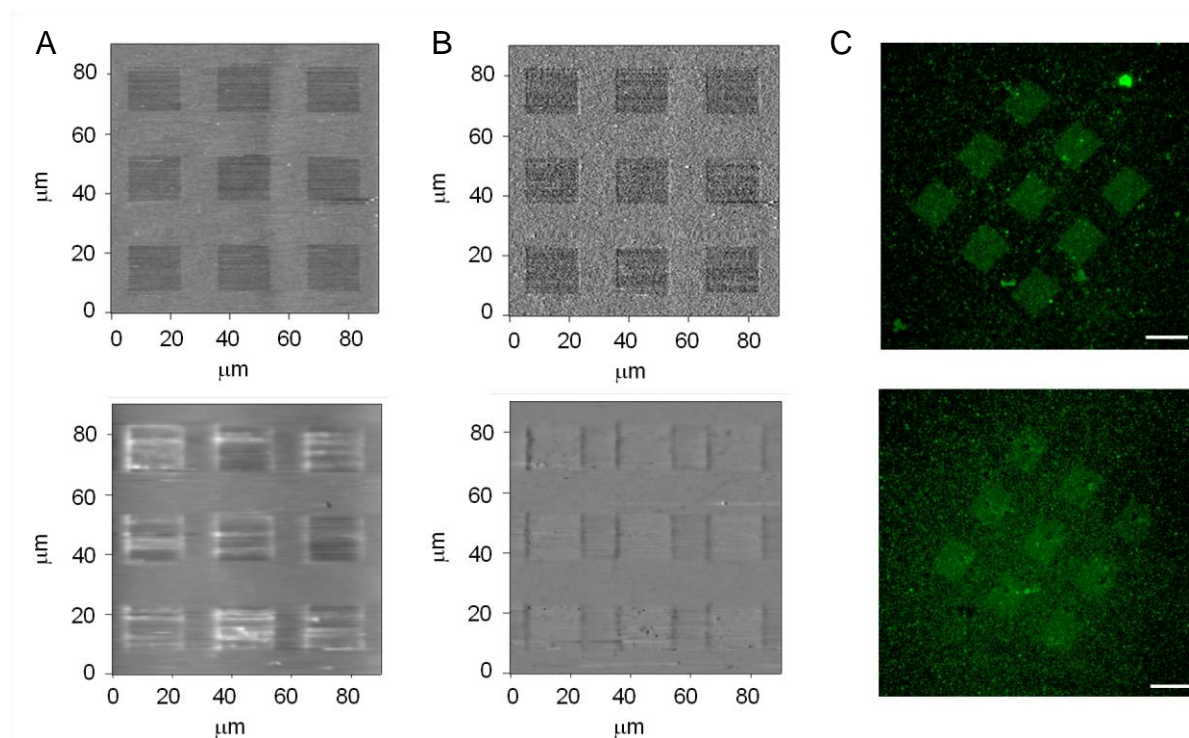


**Fig. 5.48 Analysis of the micropattern created by grafting method. (A) Topography and (B) phase contrast images which were examined simultaneously by AFM. (C) shows the fluorescence images of SNAP-GFP selectively immobilized on the formed micropatterns. Bar = 20 μm.**

5.3.2.2  SNAP-E-Cadherin functionalization on grafted patterns

To extend the application of the grafted micropattern to cell adhesion, the affinity of purified extracellular domains EC1-5 of E-Cadherin fused to a SNAP tag (Engin *et al.*, 2010) was used for surface functionalization. Western Blot analyses with anti-SNAP and anti-E-Cadherin of the fractions from the purification revealed a protein of the expected size of 120 kDa (Fig. 5.49). The fractions showing this 120 kDa protein with both antibodies were used for coupling to the functionalized surfaces.
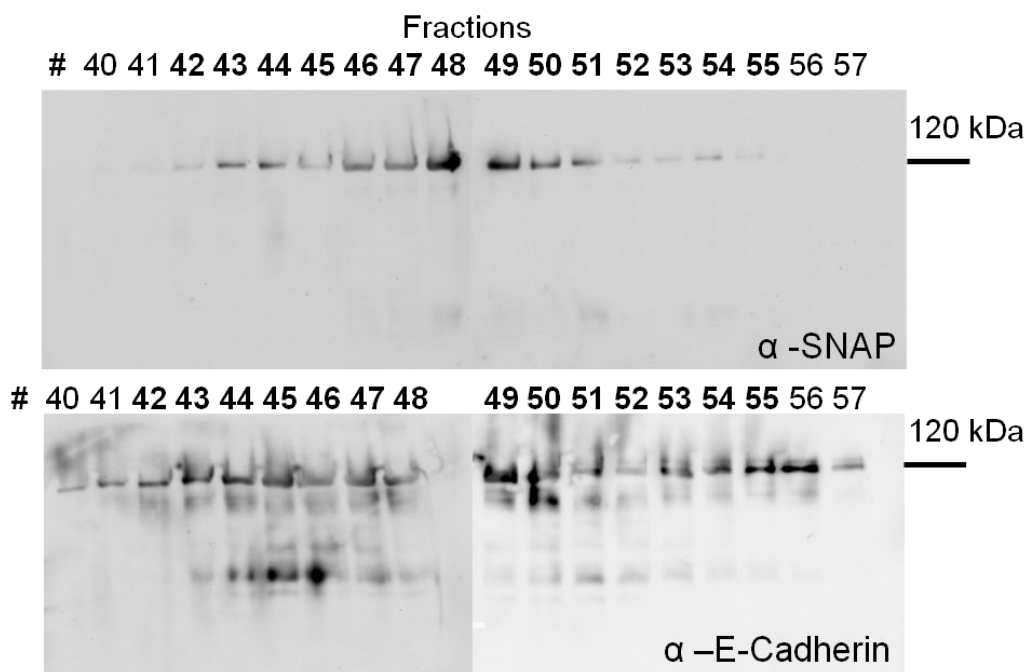
**Fig. 5.49 Purified SNAP-ECad-EC1-5 by Ni²⁺-NTA affinity chromatography. The supernatant was collected from the culture of HEK cells stably transfected with ECad_EC1-5_SNAP_12His. Collected fractions (#40–57) were analyzed by western blot against SNAP and E-Cadherin. The purified interest of protein was visualized at 120 kDa. Both SNAP and E-Cadherin positive fractions (#42-55) were pooled and used for further experiments.**

The nine square patches of 15x15 µm², 10x10 µm² and 5x5 µm², respectively were established in the whole scanning area 90x90 µm² and functionalized with SNAP-E-Cadherin EC1-5 (Fig. 5.50). AFM topography (left row) and AFM phase contrast (middle row) images indicate the height difference and molecular composition difference between the ink molecules BGT:EG$_6$OH (1:100, volume ratio) and the pre-formed EG$_3$OMe SAM. Unlike SNAP-GFP, the immobilized E-Cadherins were detected indirectly by antibodies. Immunostaing of the 15 x 15 µm² squares demonstrate that EC1-5 of E-Cadherin is bound to the structured surface.

However, the several controls of the immunostaining unraveled possibilities of unexpected unspecific binding. This relied on the attenuated passivating capacity of EG$_3$OMe backgrounds, for instance, in the case of 10x10 µm² in Fig. 5.50. In the case of the relatively small squares of 5x5 µm² it seemed that topographical information is hard to be proven, however, the significant phase difference confirms the contrast between the patterns and the background. The slightly

different unspecific binding of the E-Cadherin EC1-5 to EG$_3$OMe compared to EG$_6$OH was observed using microcontact printing (Fig. 5.51). EG$_6$OH was used as an ink molecule for the pattern area and EG$_3$OMe was backfilled as a background. Afterwards the patterned substrate was incubated in a solution of E-Cadherin EC1-5. The resulting fluorescence image in Fig. 5.51 shows a lower fluorescence (and with that a weaker unspecific binding of the E-Cadherin) on top of the EG$_6$OH areas compared to the areas terminated with an EG$_3$OMe SAM.
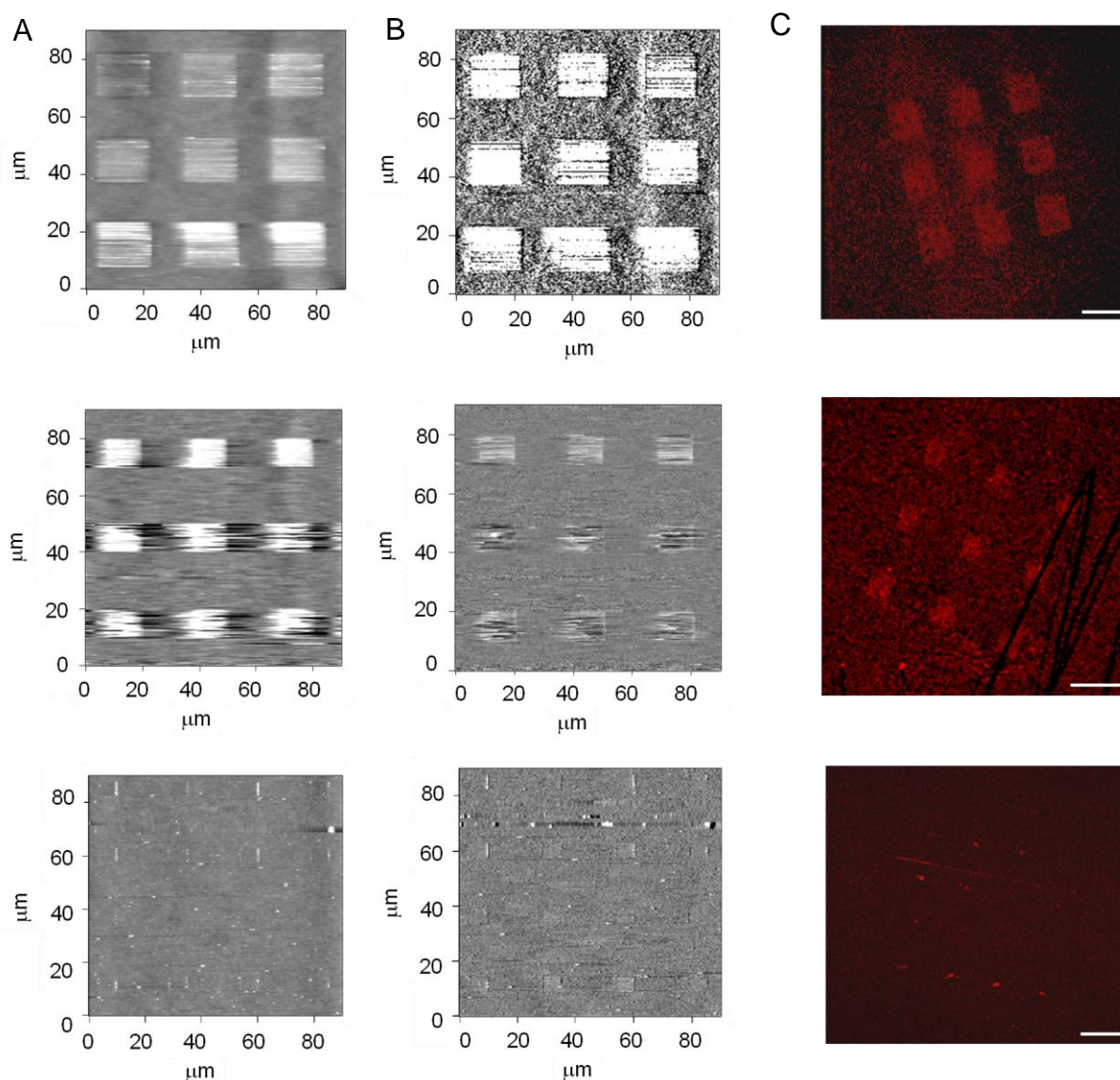


**Fig. 5.50 AFM Topography (A) and AFM phase contrast images (B), and fluorescence microscopy images of the patterns after SNAP-E-Cadherin functionalization (C). BGT:EG$_6$OH (1:100 volume ratio) as an ink molecule and EG$_3$OMe as a pre-formed SAM were used for different pattern sizes; 15x15 in the upper line, 10x10 in the middle line and 5x5 µm$^2$ in the bottom line. The generated surfaces were washed with HBS buffer and incubated with the purified SNAP-E-Cadherin EC1-5 proteins for 2 hours at room temperature. Immunostaining was performed against E-Cadherin followed by cy3-conjugated secondary antibody to visualize. Bar = 20 µm.**
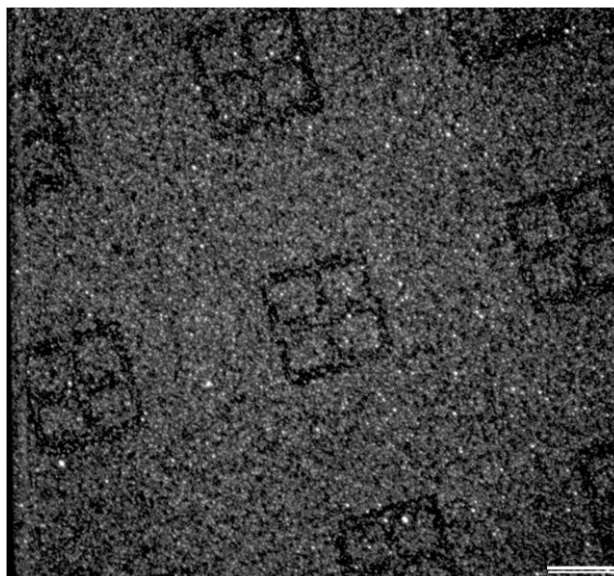
**Fig. 5.51 The immunofluorescently visualized E-Cadherin EC1-5 pattern by microcontact printing method. PDMS stamp was incubated with EG$_6$OH 100 µM for 5 min and transferred to Au-substrate for 2 min. EG$_3$OMe 100 µM was filled in the background for 45 min. After thoroughly washing with isopropanol followed by HBS buffer, 2 µM of E-Cadherin EC1-5 was incubated for 2 hours at room temperature. Immunostaining was performed to detect E-Cadherin on the substrate. Although BGT exists nowhere, EG thiol with methoxy end group allowed slight unspecific binding of E-Cadherin while EG thiol with hydroxyl end group showed less binding. Bar = 20 µm.**

### 5.3.3 ECad-EGFP L-cells on the functionalized patterns

To analyze, whether living cells, indeed, accept EC1-5 functionalized and patterned surfaces as substrates for cell adhesion, stably transfected L-cell with hECadEGFP (Fichtner, 2012) were seeded on the 15 x 15 µm² squares. Indeed, a L-cell expressing hECadEGFP adhered specifically in a functionalized square (Fig. 5.52). Topography and phase confirmed the quality of the pattern area (Fig. 5.52B/C). The artificial cell shape adapting a square boundary supported that the binding resulted from the site-directed functionalization. Another cell was captured at the boundary of 90x90 µm² whole scanning area, showing artificial L-shape following the pattern boundary. This observation confirmed the possibility using non-contact mode of AFM after the pattern formation.
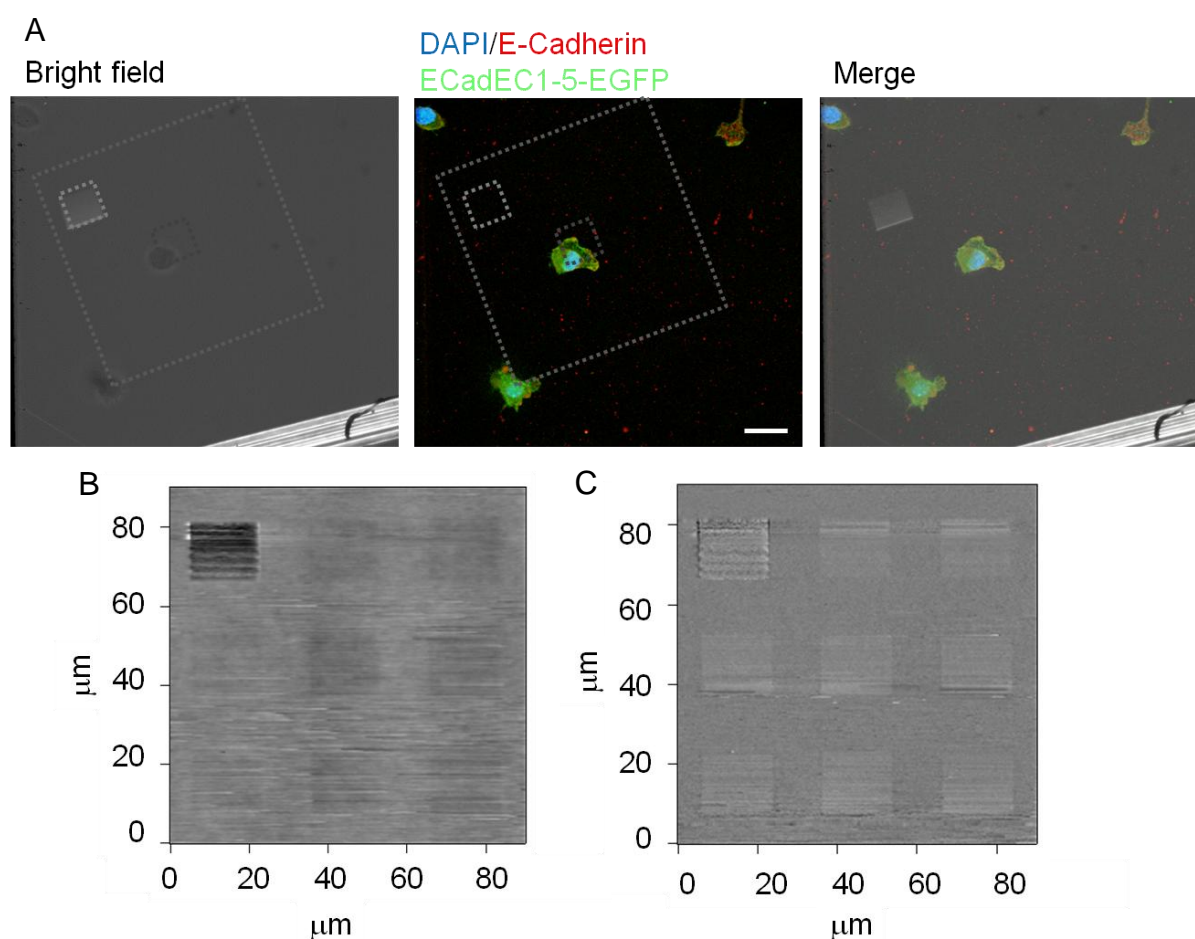
**Fig. 5.52 Stably transfected with ECad_EC1-5_EGFP L-cells seeded on the grafted patterns with BGT:EG$_6$OH 1:100 out of EG$_3$OMe pre-formed SAM. One cell recognized one of the 15x15 µm$^2$ grafted patterns (A). The micropattern was generated by grafting and washed with HBS followed by the 2 hours incubation with the purified SNAP-E-Cadherin EC1-5. The ECad_EC1_5 _EGFP L-cells were detached with separation media and seeded on the E-Cadherin immobilized surface at a concentration of 1.1 x 10$^5$ /ml. After 2 hours incubation in serum-free culture medium, they were fixed and immune-staining was performed against E-Cadherin followed by DAPI staining for nuclei visualization. (B, C) This micropattern was analyzed by topography and phase difference in non-contact mode. The shaved area was able to superimpose of bright field to the fluorescent images. Bar = 20 µm.**

To figure out whether the density of immobilized E-Cadherin affect the specific cell adhesion, the mixing ratio of the ink molecules BGT:EG$_6$OH was changed from 1:100 (Fig. 5.52) to 1:500 (Fig. 5.53) with the same pre-formed SAM.

Like the previous trial, two squares were shaved to detect the site easily at microscopic observation (Fig. 5.53A, white dashed squares). None of the adhered L-cells was found on 15x15 µm$^2$ patterns where E-Cadherins were supposed to be immobilized. Instead, cells were found at the boundary of 90x90 µm$^2$ as shown in

the fluorescent image. The created nine patches were verified by AFM height and AFM phase information (Fig. 5.53B/C).
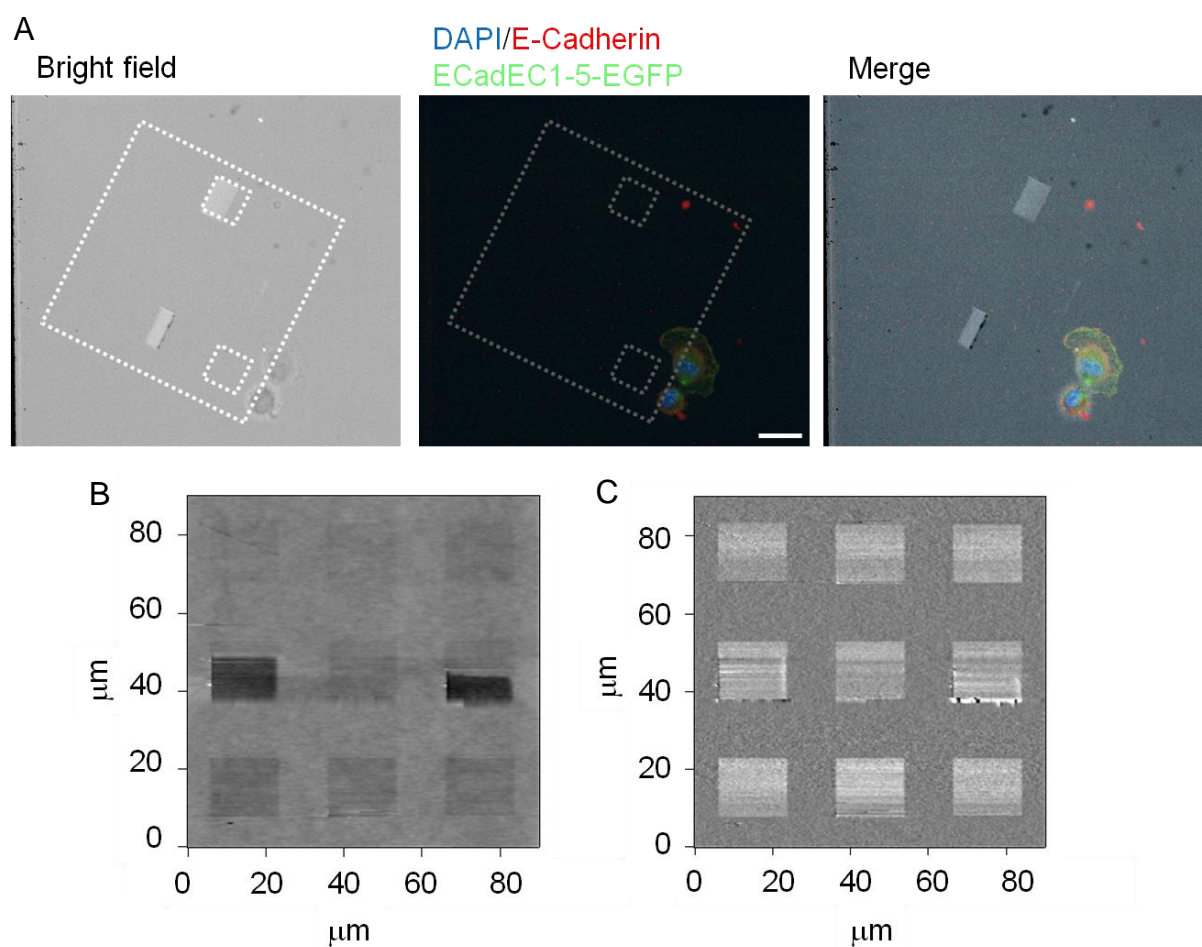


**Fig. 5.53 Stably transfected with ECad_EC1-5_EGFP L-cells seeded on the grafted patterns with BGT:EG$_6$OH 1:500 out of EG$_3$OMe pre-formed SAM. E-Cadherin expressing L-cells attached on the boundary of the whole grafted region (90x90 µm$^2$)(A). Immunostaining was achieved against E-Cadherin followed by cy3-conjugated secondary antibody to visualize and nuclei were stained by DAPI. The area was examined by topography (B) and phase (C) in non-contact mode. Bar = 20 µm.**

# 6. Discussion

Stem cell renewal and stem cell differentiation in the niche is triggered by external factors, including local morphogen concentrations, composition of the extracellular matrix and contact to neighboring cells (Fuchs *et al.*, 2004; Scadden, 2006; Peerani *et al.*, 2007). Thus, an experimental design for controlled application of these external factors is desired (Kobel & Lutolf, 2010; Saha *et al.*, 2011).

In this work, two approaches for controlling stem cell niche were developed and tested. In the first approach, a two-stacked gradient generating microfluidic chip was developed in collaboration with the Institute of Microstructure Technology (Jubert, 2009; Kreppenhofer, 2010; Kreppenhofer, 2012). With the novel device, a set of gradients of small molecules and proteins was generated by an integrated zig-zag micro-mixer and the local response of cells to small inhibitor- and morphogen gradients was analyzed.

In the second approach, micro-patterns of E-Cadherin EC1-5 were created by AFM-based nanografting and the attractiveness of these surfaces for cells was analyzed.

## 6.1 Two-stacked structure of a microfluidic chip and its flexibility

The main achievement of the developed microfluidic chip is the combination of a stable gradient with a cell culture chambers separated by a porous membrane. Powers *et al.* (2002) and Morel *et al.* (2012) utilized a similar two-stacked structure to have a limited shear stress on cells below a physiologically significant range ($<2$ dyne/cm$^2$) or nearly zero for cell applications. Others introduced two-stacked micro-systems to re-create *in vivo* situations, including air-liquid two-phase flows to mimic respiratory injuries (Huh *et al.*, 2007), intestinal tissues (Kimura *et al.*, 2008; Kim *et al.*, 2012), vascular environments (Neeves & Diamond, 2008) and intravascular steps in metastasis (Song *et al.*,

2009). However, a microfluidic device combining a gradient generating part with a cell culture micro-chamber has not been used so far. Thus, a device that combines the advantages of the two-chambered chip with a micro-mixer was developed and examined.

A zig-zag micro-mixer (Jeon *et al.*, 2000; Dertinger *et al.*, 2001) enables to define the concentration profile and steepness of the gradient simply by controlling the flow speed and the number of incoming channels. A cell monitoring channel is usually located at the end of the mixer (Jeon *et al.*, 2002; Walker *et al.*, 2004; Gunawan *et al.*, 2006). However, a disadvantage of such devices often relies on gradient blurring due to lateral diffusion along the monitoring channel when the continuously provided source is missing. The gradient gets even more disturbed when cells are cultivated in the same channel (Chung *et al.*, 2005; Park *et al.*, 2009; Cimetta *et al.*, 2010). Thus, the unstable profile along the area of interest might cause misleading results. To improve the stability of the gradient, the gradient mixer flow streams were separated into eight gradient reservoir channels. Liquid-tight seals protected the channels from lateral diffusion. The formed step gradients in this device are stable and easy to manipulate. Moreover, in the post-developed design this separation was mirrored to the upper cell chamber so that cells are exposed to the distinct concentration diffused from the lower gradient channels avoiding lateral diffusion in the cell chamber.

## 6.2  Formation of gradients in a microfluidic chip

When scaled down to micro-scale, the fluid regime is changed to laminar flow where mixing is dominantly achieved by molecular diffusion (Sia & Whitesides 2003; Capretto *et al.*, 2011). Since diffusive mixing is a slow process, different approaches are known to improve mixing in micro-channels. Passive micro-mixers do not use an external energy source to introduce perturbation. Instead, the channel geometry is designed in a manner to increase the surface area between the different fluids and to decrease the diffusion path. For instance, the two flows experience the sequential processes of splitting, recombination, and flow rearrangement by different geometries (Lee *et al.*, 2006; Fang & Yang 2009; Sip *et al.*, 2011). T- or Y shaped micro-mixers (Kamholz *et al.*, 1999; Erbacher *et al.*, 1999; Bessoth *et al.*, 1999; Park *et al.*, 2009), the introduction of obstacles

and/or grooved patterns in the micro-channel (Stroock *et al.*, 2002; Yang *et al.*, 2008), serpentine (Vijayendran *et al.*, 2003; Jiang *et al.*, 2004) and zig-zag channels (Mengeaud *et al.*, 2002) have been widely used to induce chaotic advection. Out of these passive micro-mixers, a zig-zag mixer was selected based on the initial work of Jubert (2009) in his diplom thesis. In such a setup, mixing is provided by laminar recirculation that induces transverse velocity components localized at each channel angle (Mengeaud *et al.*, 2002). In this work, to find an appropriate range of volumetric flow rate to have homogeneous mixing in the zig-zag mixer, diffusion time was compared to travel time to apply with different molecules that have different diffusion coefficients. It was based on that molecules simultaneously diffuse across the zig-zag channel and travel along the channel by fluid flow. For the flow rates below 8.5 µl/min small molecules with $D$=500 µm$^2$/s diffusion is completed before the molecules reach the end of the channel. Under these conditions, small molecules are mixed homogeneously. This homogenous mixing allows predicting the linear step gradient and the local concentration in each of the eight reservoir channels.

Since the diffusion coefficient depends on the hydrodynamic radius of a molecule, a term which can be calculated exactly only for spherical proteins, the local concentrations of proteins are less predictable solely by estimation. Therefore, different flow rates between 5 and 100 µl/min were applied by digital syringe pumps. For the given channel geometry, the Reynolds number is considered as <2300 for 5 µl/min ($\approx$ 420) and 10 µl/min ($\approx$ 830) while as >2300 for 40 µl/min ($\approx$ 3300) and 100 µl/min ($\approx$ 8300) flow rates in aqueous solutions. By the estimation of diffusivity of globular proteins ($D_{BSA}\approx$80 µm$^2$/s, 66 kDa), complete mixing is calculated for flow rates below 1.3 µl/min. However, the empirical result showed that a BSA-FITC step gradient formed nearly linear-likely already at 5 µl/min. This discrepancy between calculation and experiment might be due to intrinsic properties of the zig-zag mixer. If the mixing behavior is caused not only by diffusion in cross sectional but also by laminar recirculation i.e. chaotic advection in zig-zag geometry, diffusion is not longer rate-limiting. Similarly, the ion-track etched porous membrane, which is embedded on the lower mixer part, might induce additional chaotic advection by its not-flattened surface like by grooved patterns in micro-channel (Stroock *et al.*, 2002; Yang *et al.*, 2008).

Compared to BSA, the poor characterized properties of Wnt proteins in solution, including its hydrophobicity due to fatty acid modifications (van den Heuvel *et al.*, 1993; Kadowaki *et al.*, 1996) and its tendency to dimerize (Janda *et al.*, 2012) could add even more complexity. To reflect a concentration-dependent and long-range signal of Wnt morphogen (Zecca *et al.*, 1996; Strigini & Cohen 2000), the commercially available recombinant Wnt3a protein was used. The purification of recombinant Wnt proteins (Willert *et al.*, 2003; Schulte *et al.*, 2005; Sousa *et al.*, 2010) is noted as a breakthrough in the field since they are known as highly hydrophobic. Wnt proteins are palmitoylated in the endoplasmic reticulum (van den Heuvel *et al.*, 1993; Kadowaki *et al.*, 1996) and the palmitate is known as important for signaling. Although it is not defined how the palmitate affects Wnt transport from secreting cells to receiving cells, a Wnt without the lipid modification is not secreted (Couso & Arias 1994; Willert *et al.*, 2003). To reduce the hydrophobic interaction between the proteins and the polymer surface, the whole chip was pre-treated with serum-containing medium to block unspecific binding.

The tendency of Wnts to form dimers (Papkoff 1989; Smolich *et al.*, 1993; Burrus & McMahon 1995; Schryver *et al.*, 1996) hinders an exact calculation of the diffusion coefficient, even more, because the ratio of dimers to monomers is not defined. This forces a careful interpretation of the concentration in each gradient reservoir channels in the microfluidic chip. Nevertheless, the different cellular response to Wnt3a or Wnt3a/Dkk-1 gradients showed the potential of the microfluidic chip to study how a gradient of soluble morphogens controls cell response.

## 6.3 Transport of signaling molecules in a microfluidic chip

Basically, the structure of a combined two separated micro-chambers with a porous membrane allows diffusive mass transport and minimizes convective transport through the membrane (Ismagilove, *et al.*, 2001; Atencia *et al.*, 2009; Kim *et al.*, 2009). Minimizing convective flow is achieved by a low pressure gradient across the separator (Saadi *et al.*, 2007; Mosadegh *et al.*, 2007; Abhyankar *et al.*, 2008) and by a high resistance to fluid flow across the separator (Ismagilove, *et al.*, 2001).

In such two-chambered systems, numerous studies tracked the quantified diffusive transport by indirect detection. To visualize two fluids diffusion contact, Ismagilov *et al.* (2001) used different sets of stimulator-reactant e.g. $CaCl_2$-fluo-3 or substrate-enzyme pairs, including BCIP/NBT-alkaline phosphatase, 5-bromo-4-chloro-3-indolyl galactoside (X-gal)/ß-galactosidase and ELF-97 acetate-esterase. The dominant difference between diffusion and convection was observed by the proliferation kinetics of cells in micro-channels (Yu *et al.*, 2005). More indirectly, cellular uptake could be also one of the indicators of diffused signaling small molecules as Kim *et al.* (2009) reported.

More quantitatively, in a simple device finite element method (FEM) simulation is used to predict diffusive delivery mechanisms (VanDersarl. *et al.*, 2011). Their two-stacked PDMS chip with a zig-zag micro-mixer at the bottom and a static cell monitoring chamber can be opened or closed by a glass slide. Fluid flows only in the lower channel, thus diffusion is the primary delivery mechanism for molecules to enter the cell monitoring chamber. In this setup, the measured dye concentration matched the FEM simulation. Also the dye staining of the cells sitting in the cell monitoring chamber were consistent with the gradients. The integrated cylindrical porous membrane minimizes convective flow by its fluidic resistance that depends on the membrane porosity and thickness. An analytical model of a total resistance of that device for diffusive delivery properties based on an electrical analogue (corresponding to electric resistance; Oh *et al.*, 2012) is suggested.

In the two-stacked microfluidic chamber used in this work, in addition to diffusion dominant transport, convective transport is possible as well. The Open/Closing mode and Open/Controlled closing flow operation modes indicate convective transport from the lower to the upper micro-chamber by pressure difference. In these systems, the fluids in both chambers are flowing with different flow rates. The flexibility of convective transport by tuning pressure difference was confirmed by these experiments.

Besides, the flexibility from convective to diffusive transport was also achieved with slower flow rates to be closer to the cell application. Methylene green dye solution was added as a model-molecule of the small inhibitor BIO into the lower gradient channels. After 24 hours application, the traceable outputs contain

approximately 15 % in diffusion-based mode and almost 80 % in convection-based mode. Therefore, the net transport of BIO, and thus the cellular response to this small inhibitor should be much higher in the convection based transport than in the diffusive transport. Indeed, application of 2 µM BIO in the convection mode resulted in 84 % β-catenin positive nuclei whereas the same concentration in the diffusion mode led to less than 2 % β-catenin positive nuclei. This opens the possibility to utilize the microfluidic chip with flexible fluid operations to mimic more complex and polar environments like epithelial surfaces.

## 6.4 Readout systems suitable for a in chip observation

Microfluidic approaches generate more defined, controllable, complex gradients, even with more than two kinds of molecules and allow investigating gradients of different choice, including interleukins (Jeon *et al.*, 2002; Kim *et al.*, 2009), growth factors (Wang *et al.*, 2004; Chung *et al.*, 2005), chemokines (Walker *et al.*, 2005; Frevert *et al.*, 2006; Haessler *et al.*, 2011), anti-cancer drugs (Fujii *et al.*, 2006), toxins (Du *et al.*, 2008), extracellular matrix proteins (Gunawan *et al.*, 2006) and fetal bovine serum (Park *et al.*, 2007). With these kinds of gradients, however, cellular responses have been mostly studied in regard to cell viability or chemotaxis behavior. Recently, Moledina *et al.* (2012) reported the representing local signaling environments, focusing on the effects to pluripotent cells by a microfluidic control of autocrine and paracrine signaling.

Since different signaling pathways regulate cell mitosis, apoptosis, cell migration, polarization and differentiation, a smart readout system that is suitable for in-chip analysis of Wnt pathway activation would be helpful for further studies. As a putative readout system, Wnt-responding cells transient transfected with Top-dsRed were co-cultured with transient transfected Wnt2b-EGFP cells as a Wnt-source (Fig. 6.1). Although the Wnt ligand was delivered to responding cells and activated the Top-dsRed reporter gene, several limitations hindered the application to the developed microfluidic chip. (1) The quantification of the secreted signaling molecules is almost impossible. Indeed, it is likely that in this system the Wnt2b-EGFP is rather handed over from cell to cell instead of being secreted in the medium (Holzer *et al.*, 2012). (2) To form a gradient, producing and responding cells should be separated into the two chambers. The

supernatant of the Wnt- producing cells then should feed the gradient in the lower channels. This gradient would not be controllable. (3) The experiments depend too much on the transfection efficiency of both the Wnt receiving and the Wnt producing cells. This problem might be overcome simply by using stable transfectants.
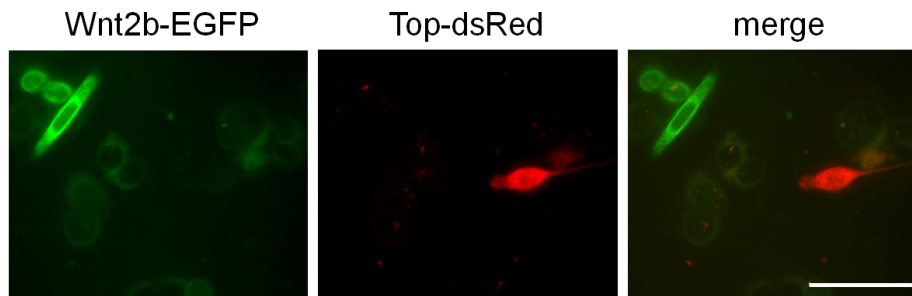


**Fig. 6.1 Transient transfected Wnt-producing and responding Top-dsRed MCF-7 cells. Wnt2b-EGFP secreted from Wnt2b-EGFP transfected cell induced Top-dsRed on after 48 hours co-incubation. Bar = 10 µm.**

Due to the above mentioned concerns immunohistochemical analysis of nuclear ß-catenin accumulation as response to Wnt pathway activation appeared as a suitable alternative readout system. Indeed, with the determination of the subcellular localization of ß-catenin a dose-dependent response to BIO, Wnt3a and Dkk-1 gradients was observed. However, prior to high resolution imaging the chip had to be destroyed. To avoid opening of the chip and to allow monitoring living cells at high magnification in the cell observation chamber, long-distance objectives with high magnification (40x, LD Plan-NEOFLUAR, Zeiss) were tested in collaboration with the Institute of Microstructure Technology.

With a correction collar, the objective is adapted for the use on polymer substrates in the 0 to 1.5 mm range (www.micro-shop.zeiss.com). It enables the observation of the cells in chip across the 500 µm height through 500 µm of polymer substrate. The surfaces of the polycarbonate-based chips were burnished with polishing papers, polishing paste and an additional process for transparency of the chip was developed (Kreppenhofer, 2012). Indeed, these treatments and/or development allowed monitoring of fluorescent signals in the cell observation chamber. It opens the possibility to continuously monitor cellular responses on morphogens in higher magnification (e.g. sub-cellular localization of a single cell)

by using robust reporter cells like 12x TCF/LEF-GFP (Cimetta *et al.,* 2010) for long term without opening chips.

When Oct4-GFP mES were seeded in the microfluidic chip, morphological and Oct4-GFP intensity observation were chosen as readout systems of maintenance of pluripotency (Peerani *et al.*, 2007; Ying *et al.*, 2008; Lyashenko *et al.*, 2011; Wray *et al.*, 2011). For these experiments, high magnification was not essential because mES colonies have a diameter of hundreds of micrometers. The extrinsic soluble factors LIF and BIO regulate JAK/STAT and Wnt pathway, respectively. LIF is one of the cytokines that bind to the receptor gp130, which leads to the response to tyrosine phosphorylation of STAT3. It is known that signaling through STAT3 is sufficient but not necessary to assure pluripotency in mES cells (Niwa *et al.*, 1998; Nichols *et al.*, 2001; Sato *et al.*, 2004; Noggle *et al.*, 2005). BIO inhibits GSK-3 and thereby induces nuclear accumulation of ß-catenin (Sato *et al.*, 2004).

Taken together, the morphological changes to compact round colonies and larger colonies obviously are increased in both treated condition by the two signaling pathways. The effect of reduced E-Cadherin expression in mES associated with the loss of pluripotency was stronger in absence of LIF than in absence of BIO. Regarding to colony growth under shear stress, Kim *et al.* (2006) experimentally proved that large colonies of mES were formed at >0.01 dyne/cm$^2$ for 4 days incubation. I observed in the post-developed microfluidic chip that Oct4 mES colonies were grown mostly within the diameter 10-200 µm after 3 days incubation under ≈0.005 dyne/cm$^2$ in agreement with the report. Further incubation time up to 7 days, I evaluated that large colonies with the diameter over 200 µm were formed in more than 50 % cases, indicating the device offers the suitability for long-term mES incubation. Thus, time-consuming differentiation processes can be monitored with this device.

Apart from that the chip is suitable for providing a micro-environment that allows mES to maintain pluripotency and to form large colonies, the application of gradients and counter-gradients on mES can now be used. That helps to define threshold concentrations of different molecules in various combinations and supplements common cell culture experiments regarding to niches of mES.

## 6.5 Practical considerations of a microfluidic chip for biological application

The new microfluidic chip has potential to recreate environments closer to *in vivo* environments with several considerations of operation, including effective culture time (ECT), critical perfusion rate (CPR), shear stress (Walker *et al.,* 2004). In this work, it was considered to limit the static incubation time in the chip to a maximum of 18 hours to prevent nutrient depletion and waste accumulation in the micro-chamber. Flow rates between 0.19 µl/min and 6.8 µl/min in the upper micro-chamber are suitable to feed the cells, to avoid waste accumulation and to give negligible shear stress. This holds true at least for HeLa cells which are 2-10 µm (R, Fig. 6.2A) height cells when spread in a 500 µm high micro-channel height ($H_c$). Thus, $R/H_c$ is much below the critical value of 0.3 introduced by Gaver and Kute (1998) that gives negligible increase of shear stress on cells compared to the channel wall. Thus, the above mentioned flow rates should be applicable for standard adherent cells including stem cells, as long as they do not form colonies.

For large colonies of ES this might be different. Spinning disc microscopic observation determined the height of Oct4-GFP mES colonies in the micro-chamber to approximately $153 \pm 12$ µm after 7 days culture, giving an $R/H_c$ ratio of 0.15. Based on the Gaver and Kute (1998) report, when the ratio of an adherent cell radius to channel height ($R/H_c$) is $\approx 0.1$, a cell in the micro-channel faces three times amplified shear stress than that in cell-free wall. For mES, 5 µl/min was applied in the channel, which gives spread cells shear stress as $\approx 0.0054$ dyne/cm². However, as mES colonies grow this value could be increased to 0.016 dyne/cm² to a single colony. The applied flow rate 5 µl/min in this microfluidic chip does not affect colony growth in agreement with the empirical data (Kim *et al.,* 2006). The density of colonies also can affect the shear stress on each cell since intercellular spacing plays an important role in deciding the fluid forces on each cell (Fig. 6.2B, Sugihara-Seki, 2000; Sugihara-Seki, 2001).

Walker *et al.* (2004) discussed that a small flow pulse in a microenvironment could differentiate the exposure of the larger molecules and the smaller molecules to cells, depending on their different diffusion coefficients (Fig. 6.2C). This is one of the considerations when stem cells are grown in micro-channels by

perfusion.
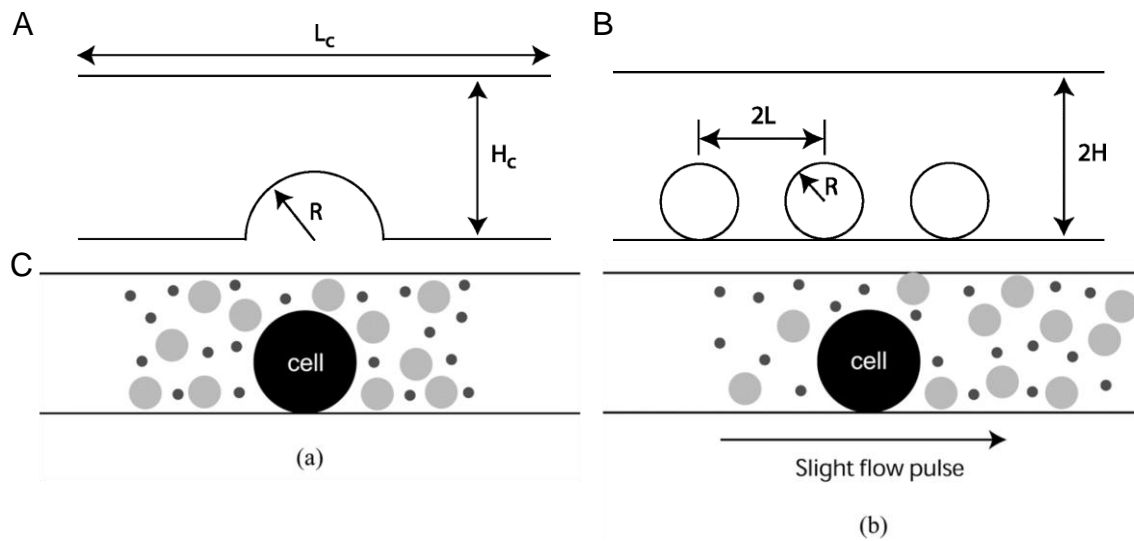


**Fig. 6.2 Schemes of adherent cells in a micro-channel. (A) Single cell with radius (R) adheres in a micro-channel with height ($H_c$) and length ($L_c$). (B) Multiple cells with radius (R) are placed with spacing (2L) to each other in a micro-channel with height (2H). (C) Schematical drawings of soluble factors transport by flow. Cells in a micro-channel are exposed to different size of molecules in static (a) culture. The molecules are differently transported by size, i.e. different diffusion coefficient by flow(b). Adapted from Walker *et al.*, 2004.**

The developed microfluidic chip, however, is two-stacked (Fig. 6.3). The set of soluble factors can be varied to control the soluble environment, which is transported by convective flow in the upper chamber and diffuses from the lower gradient channels. The latter way to transport soluble factors can minimize shear stress even for large mES colonies and can avoid the uneven exposure of soluble factors. The integrated cylindrical porous membrane minimizes convective flow by its fluidic resistance that depends on the membrane porosity and thickness (diffusion length) (VanDersarl *et al.*, 2011). The signaling molecules either small molecules or proteins of different size are supposed to pass through the porous membrane. Due to the smaller contact area (porosity: 5-20 % provided by Milllipore, ≈13 % measured by SEM), cells are exposed to smaller amounts of signaling molecules as shown for BIO resulting in a shift of the threshold to the higher channel number. Considering this point, I increased the concentration of molecules in the case of Wnt3a. Alternatively one can use the specific transport rates of molecules differing in size to regulate a gradient, for instance, a small

molecule as an activator and a larger one as an inhibitor.
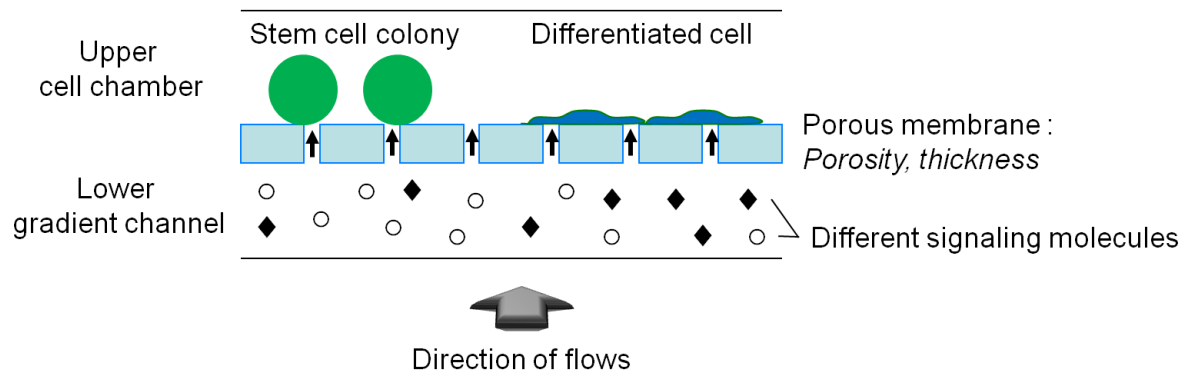


**Fig. 6.3** **Schematic drawing of the diffusive transport (small arrows) of different signaling molecules in the chip. That might lead stem cell self-renewal / differentiation controlled in the two-stacked microfluidic chip. Not to scale.**

## 6.6 The use of AFM for nanografting

To mimic the adhesive properties of a stem cell niche, functionalized micro-structured surfaces were developed and validated. Among a number of soft lithography-based techniques, micro-contact printing has widely been used for its convenience towards cell biological applications (Ruiz & Chen, 2007). However, because of its limitations there have been on-going achievements in developing other soft lithography methods (reviewed in Perl *et al.*, 2009; Kim *et al.*, 2010). For instance, the PDMS stamps loose its mechanical integrity and deform during stamp removal from the template, resulting in limitation of resolution especially in the sub-micrometer range (Delamarche *et al.*, 1997; Bietsch & Michel, 2000; Sharp *et al.*, 2004; Yoo *et al.*, 2004). Also, contamination of uncured fragments during the PDMS cross-linking process and swelling of PDMS caused by organic solvents (Favre, 1996; Lee *et al.*, 2003) can hinder the appropriate applicability. The SAM on the substrates is formed by ink diffusion from stamps to surfaces (Poirier *et al.*, 1994; Stranick *et al.*, 1994). The lateral spreading of the ink from the edge of pattern area to non-pattern area while stamping can cause smearing at the margin of the patterns especially in the sub-micrometer scale (Xia & Whitesides, 1995; Sharpe *et al.*, 2004; Delamarche *et al.*, 1998; Workman &

Manne, 2004).

The AFM-assisted lithography, so called nanografting, introduces some advantages. A minimal pattern of 5x5 µm² produced by nanografting was taken as proof-of-concept in this work. Nanografting allows systematic investigations of size-dependent mechanics at the nanometer scale (Liu *et al.*, 2008) as well as different geometry of pattern for instance lines, squares, circles etc (Ngunjiri *et al.*, 2008). This motivates the work of performing patterns with nano-sized lines to control resolution of cadherin-anchoring sites and to study how cells react in response to these adhesion molecules.

By *in situ* examination of the formed patterns, structural information was obtained. Two different length EG-thiols, $EG_4OH$ and $EG_6OH$ were grafted on pre-formed $EG_3OMe$ SAM. Based on the literature, the molecular length of $CH_2$ is $\approx 0.15$ nm (Bain *et al.*, 1989) and that of EG unit is $\approx 0.3$ nm (Harder *et al.*, 1998; Valiokas *et al.*, 1999). On Au(111) surface alkanethiol form close-packed domains with a tilt angle of $\approx 30$ ° from the surface, adopting an all-*trans* configuration (Porter *et al.*, 1987; Poirier & Pylant, 1996; Poirier 1997). It results in $\approx 2.47$ nm theoretical length of $EG_4OH$ and $\approx 2.99$ nm of $EG_6OH$. The topographical difference measured by profiling from AFM images after creating patterns was $\approx 0.4$ nm in agreement with theoretical values. That gives a hint that the newly replaced SAM in the patterns had the right orientation and conformation.

To validate that the benzyl guanine group is located in the grafted area, a ToF-SIMS analysis was performed at the Institute of Biological Interfaces, Karlsruhe Institute of Technology. ToF-SIMS generates very indicative and characteristic signals - fragmented ions and molecular ions, which allow the identification of SAM compounds. The assignment is based on the exact mass of the secondary ion (mass resolution as expressed by $m/\Delta m$ is usually better than 5000), and, if applicable, the isotope distribution of the fragment. The corresponding regions were selected to identify $EG_3$ and $EG_6$ at the 740-750 amu, $[C_{18}H_{38}O_4SAu_2]^-$ and 665-670 amu, $[C_{23}H_{47}O_7SAu]^-$, respectively. Unlike EG-SAMs, BGT hardly provides a molecular ion rather one can track the yielded guanine head group as a stable fragment $[C_5H_4N_5O^-]$ at 150 amu. In the ToF-SIMS results, there is also BGT-indicating region at 149 amu. One should be careful to interpret the peak

since a peak at 149.03 amu appears by [$C_5H_4N_5O^-$] however the fragment of [$(C_2H_4O)_3$-OH] at 149.08 shows as well. This fragment extracted from both ethylene glycol SAMs and the BGT spacer part (personal communication with Dr. Welle). For BGT some low molecular weight peaks containing nitrogen, like [CN]$^-$ at 26 amu and [CNO]$^-$ at 42 amu are found. However, they are not unambiguous indicators of BGT since they also represent frequent trace contaminations on gold surfaces. SIMS is also quite sensitive for [$SO_3$]$^-$ at 79.96 amu and [$SO_4H$]$^-$ at 96.96 amu (Kwok *et al.,* 2011) being fragments of oxidized thiols in the SAM. Thus, the guanine head group fragment at 150 amu is highly characteristic for BGT that is mostly used in this analysis.

## 6.7 Specificity of generated surfaces and cell recognition on the functionalized surfaces

The patterns generated by the grafting method consist of BGT:EG$_6$OH within the passivating background EG$_3$OMe. On BGT:EG$_6$OH sites, proteins of interest with SNAP tag specifically react to benzyl guanine as a substrate. Slight unspecific protein binding was found in the background in both cases of SNAP-GFP and SNAP-E-Cadherin EC1-5. In the case of E-Cadherin EC1-5 immobilization more unspecific binding (high background) was found than in the case of GFP immobilization. A possible explanation could rely on the different visualizing methods. For SNAP-GFP only 2 hours incubation was performed before the successful immobilization and it could be monitored directly by the GFP fluorescence. For SNAP-E-Cadherin EC1-5 instead, immunostaining was conducted including several incubation and washing steps, application of antibodies and non-specific proteins i.e. BSA or serum.

This unspecific background might be influenced by the different end groups between EG$_6$OH and EG$_3$OMe even though the ethylene glycol (EG) unit itself is known as protein repelling molecule (Lee *et al.*, 1989; Pale-Grosdemange *et al.*, 1991; Desai *et al.*, 1991). Schilp *et al.* (2009) described that there is no significant difference between three and six EG units of SAM with –OH end group, regarding to contact angle (hydration) and thickness of adsorbed fibrinogen. Therefore, the end groups, the hydroxyl group in case of EG$_6$OH and the methoxy

group in case of $EG_3OMe$ could make the slight difference of non-specific protein adsorption. Nevertheless, both $EG_3OMe$ (Engin *et al.*, 2010) and $EG_6OH$ can be used as a protein-resistant background. The fluorescent signal intensity of the grafted patterns where BG and SNAP are coupled is much higher than $EG_3OMe$ background, indicating the specific immobilization overcomes the unspecific binding in this work.

When a SNAP-E-Cadherin pattern is made, it is supposed to attract to E-Cadherin expressing cells to make cell-cell contact through homophilic cadherin interaction. The shape of the spreading cell adapting the E-Cadherin EC1-5 square pattern was found to support the principle. However, it was also observed that cell recognizes the non-functionalized areas of scanning ($90x90$ $\mu m^2$). It could be reasoned that the surface analysis by applying the non-contact mode would change conformation or orientation of SAM (personal communication with Dr. Welle).

## 6.8 Outlook

In this work, two different approaches were chosen to reconstruct the molecular environment of a stem cell niche: (1) the design and the testing of a microfluidic chip that mimics gradients of soluble signaling molecules and (2) the production of patterns of immobilized proteins on surfaces that serve in stem cell adhesion but also in regulating stem cell differentiation. In future, both techniques should be combined to optimize the recapitulation of a stem cell niche (Fig. 6.4). Morphogens, instructive extrinsic niche soluble signals, can be generated with a single morphogen and with activator/inhibitor combinations, for instance, Wnt/Dkk, Wnt/Cerberus or Wnt/Frzb. A crosstalk between Wnt and TGF-ß pathway was demonstrated by Besser (2004) for human embryonic stem cells. Thus, combining different morphogens such as Wnt/BMP, BMP/Shh could be another more specific application for stem cell development. Adding to this gradient-generating system, a modified membrane by chemical (Saha *et al.*, 2011), material (Mei *et al.*, 2010) or biofunctionl improvements (Fig. 6.4) might come closer to recreate the stem cell microenvironment, thereby to manipulate self renewal or differentiation if appropriately embedded, which is a potential of the developed microfluidic chip.
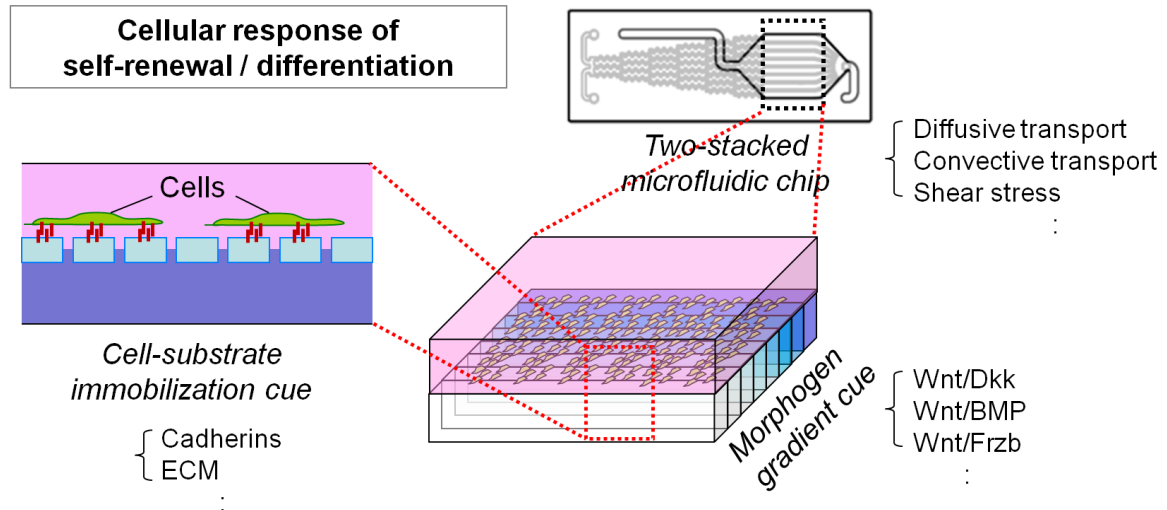
**Fig. 6.4 The overview of possibilities to use the developed microfluidic chip for self-renewal / differentiation of stem cells. The flexible operation of fluids enables diffusive/convective transport of morphogen gradients under shear stress-free or shear stress condition. The activator/inhibitor combinations or different morphogens can be applied together with adhesion or signaling molecules immobilized in suitable geometric patterns on the porous membrane that separates the morphogen reservoir (the lower channels) from the cell cultivator (the upper chamber).**

# 7. Literature

**Abhyankar, V.V., Toepke, M.W., Cortesio, C.L., Lokuta, M.A., Huttenlocher, A. & Beebe, D.J. (2008).** A platform for assessing chemotactic migration within a spatiotemporally defined 3D microenvironment. *Lab Chip* **8**, 1507-1515.

**Adams, G.B., Chabner, K.T., Alley, I.R., Olson, D.P., Szczepiorkowski, Z.M., Poznansky, M.C., Kos, C.H., Pollak, M.R., Brown, E.M. & Scadden, D.T. (2006).** Stem cell engraftment at the endosteal niche is specified by the calcium sensing receptor. *Nature* **439**, 599-603.

**Alonso, L. & Fuchs, E. (2003).** Stem cells in the skin: waste not, Wnt not. *Genes Dev* **17**, 1189-1200.

**Artavanis-Tsakonas, S., Rand, M.D. & Lake, R.J. (1999).** Notch signaling: cell fate control and signal integration in development. *Science* **284**, 770-776.

**Atencia, J., Morrow, J. & Locascio, L.E. (2009).** The microfluidic palette: a diffusive gradient generator with spatio-temporal control. *Lab Chip* **9**, 2707-2714.

**Auerbach, W., Dunmore, J.H., Fairchild-Huntress, V., Fang, Q., Auerbach, A.B., Huszar, D. & Joyner, A.L. (2000).** Establishment and chimera analysis of 129/SvEv- and C57BL/6-derived mouse embryonic stem cell lines. *Biotechniques* **29**, 1024-1028, 1030, 1032.

**Aulehla, A., Wehrle, C., Brand-Saberi, B., Kemler, R., Gossler, A., Kanzler, B & Herrmann, B.G. (2003).** Wnt3a plays a major role in the segmentation clock controlling somitogenesis. *Dev Cell* **4**, 395-406.

**Bain, C.D., Troughton, E.B., Tao, Y.-T., Evall, J., Whitesides, G.M. & Nuzzo, R.G. (1989).** Formation of monolayer films by the spontaneous assembly of organic thiols from solution onto gold. *J Am Chem Soc* **111**, 321-335.

**Bartscherer, K. & Boutros, M. (2008).** Regulation of Wnt protein secretion and its role in gradient formation. *EMBO Rep* **9**, 977-982.

**Becker, H. & Gaertner, C. (2008).** Polymer microfabrication technologies for microfluidic systems. *Anal Bioanal Chem* **390**, 89-111.

**Beebe, D.J., Mensing, G.A. & Walker, G.M. (2002).** Physics and applications of microfluidics in biology. *Annu Rev Biomed Eng* **4**, 261-286.

**Besser, D. (2004).** Expression of nodal, lefty-a, and lefty-B in undifferentiated human embryonic stem cells requires activation of Smad2/3. *J Biol Chem* **279**, 45076-45084.

**Bessoth, F., deMello, A. & Manz, A. (1999).** Microstructure for efficient continuous flow mixing. *Anal Commun* **36**, 213-215.

**Bhushan, B. & Marti, O. (2007).** Scanning probe microscopy – principle of operation, instrumentation, and probes. *Springer Handbook of Nanotechnology*, pp. 591-636.

**Bietsch, A & Michel, B. (2000).** Conformal contact and pattern stability of stamps used for soft lithography. *J Appl Phys* **88**, 4310-4318.

**Bixby, J.L. & Zhang, R. (1990).** Purified N-cadherin is a potent substrate for the rapid induction of neurite outgrowth. *J Cell Biol* **110**,1253-1260.

**Boyden, S. (1962).** The chemotactic effect of mixtures of antibody and antigen on polymorphonuclear leucocytes. *J Exp Med* **115**, 453-466.

**Brivanlou, A.H. & Darnell, J. (2002).** Signal Transduction and control of Gene Expression. *Science* **295**, 813-818.

**Burrus, L.W. & McMahon, A.P. (1995).** Biochemical analysis of murine Wnt proteins reveals both shared and distinct properties. *Exp. Cell Res* **220**, 363-373.

**Cano, A., Pérez-Moreno, M.A., Rodrigo, I., Locascio, A., Blanco, M.J., del Barrio, M.G., Portillo, F. & Nieto, M.A. (2000).** The transcription factor snail controls epithelial-mesenchymal transitions by repressing E-cadherin expression. *Nat Cell Biol* **2**, 76-83.

**Capretto, L., Cheng, W., Hill, M & Zhang, X. (2011).** Micromixing within microfluidic devices. *Top Curr Chem* **304**, 27-68.

**Carmona-Fontaine, C., Matthews, H.K., Kuriyama, S., Moreno, M., Dunn, G.A., Parsons, M., Stern, C.D. & Mayor, R. (2008).** Contact Inhibition of Locomotion *in vivo* controls neural crest directional migration. *Nature* **456**, 957-961.

**Cavallaro, U. & Christofori, G. (2004).** Cell adhesion and signaling by cadherins and Ig-CAMs in cancer. *Nat Rev Cancer* **4**, 118-132.

**Chapman, R.G., Ostuni, E., Yan, L. & Whitesides, G.M. (2000).** Preparation of mixed self-assembled monolayers (SAMs) that resist adsorption of proteins using the reaction of amines with a SAM that presents interchain carboxylic anhydride groups. *Langmuir* **16**, 6927-6936.

**Chen, D. & McKearin, D. (2003).** Dpp signaling silences *bam* transcription directly to establish asymmetric divisions of germline stem cells. *Curr Biol* **13**, 1786-1791.

**Chen, H., He, Z., Bagri, A & Tessier-Lavigne, M. (1998).** Semaphorin-neuropilin interactions underlying sympathetic axon responses to class III semaphorins. *Neuron* **21**, 1283-1290.

**Chou, Y.F., Chen, H.H., Eijpe, M., Yabuuchi, A., Chenoweth, J.G., Tesar, P., Lu, J., McKay, R.D. & Geijsen, N. (2008).** The growth factor environment defines distinct pluripotent ground states in novel blastocyst-derived stem cells. *Cell* **135**, 449-461.

**Chumley, M.J., Catchpole, T., Silvany, R.E., Kernie, S.G. & Henkemeyer, M. (2007).** EphB receptors regulate stem/progenitor cell proliferation, migration, and polarity during hippocampal neurogenesis. *J Neurosci* **27**, 13481-13490.

**Chung, B.G., Flanagan, L.A., Rhee, S.W., Schwartz, P.H., Lee, A.P., Monuki, E.S. & Jeon, N.L. (2005).** Human neural stem cell growth and differentiation in a gradient-generating microfluidic device. *Lab Chip* **5**, 401-406.

**Cimetta, E., Cannizzaro, C., James, R., Biechele, T., Moon, R.T., Elvassore, N. & Vuniak-Novakovic, G. (2010).** Microfluidic device generating stable concentration gradients for long term cell culture: application to Wnt3a regulation of ß-catenin signaling. *Lab Chip* **10**, 3277-3283.

**Comoglio, P.M., Boccaccioy, C. & Trusolino, L. (2003).** Interactions between growth factor receptors and adhesion molecules: breaking the rules. *Curr Opin Cell Biol* **15**, 565-571.

**Cooke, J. (1995).** Morphogens in vertebrate development: how do they work? *Bioessays* **17**, 93-96.

**Couso, J. P. & Arias, A. M. (1994).** Notch is required for wingless signaling in the epidermis of Drosophila. *Cell* **79**, 259–272.

**Crittenden, S.L., Bernstein, D.S., Bachorik, J.L., Thompson, B.E., Gallegos, M., Petcherski, A.G., Moulder, G., Barstead, R., Wickens, M. & Kimble, J. (2002).** A conserved RNA-binding protein controls germline stem cells in *Caenorhabditis elegans*. *Nature* **417**, 660-663.

**Cussler, E.L., Aris, R. & Bhown, A. (1989).** On the limits of facilitated diffusion. *J Membrane Sci* **43**, 149-164.

**Cussler, E.L. (2009).** *Diffusion: Mass Transfer in Fluid Systems,* 3rd edn. Cambridge University Press.

**Delamarche, E., Schmid, H., Michel, B., Biebuyck, H. (1997).** Stability of molded polydimethylsiloxane microstructures. *Adv Mater* **9**, 741-746.

**Delamarche, E., Schmid, H., Bietsch, A., Larsen, N.B., Rothuizen, H., Michel, B. & Biebuyck, H. (1998).** Transport Mechanisms of Alkanethiols during Microcontact Printing on Gold. *J Phys Chem B* **102***, 3324-3334.

**Dertinger, S.K.W., Chiu, D.T., Jeon, N.L. & Whitesides, G.M. (2001).** Generation of gradients having complex shapes using microfluidic networks. *Anal Chem* **73**, 1240-1246.

**Desai, N.P & Hubbell, J.A. (1991).** Solution technique to incorporate polyethylene oxide and other water-soluble polymers into surfaces of polymeric biomaterials. *Biomaterials* **12**, 144-153.

**Du, Y., Shim, J., Vidula, M., Hancock, M.J., Lo, E., Chung, B.G., Borenstein, J.T., Khabiry, M., Cropek, D.M., Khademhosseini, A. (2009).** Rapid generation of spatially and temporally controllable long-range concentration gradients in a microfluidic device. *Lab Chip* **9**, 761-767.

**Eastham, A., Spencer, H., Soncin, F., Ritson, S., Merry, C., Stern, P. & Ward, C. (2007).** Epithelial-mesenchymal transition events during human embryonic stem cell differentiation. *Cancer Res* **67**, 11254-11262.

**Engin, S., Trouillet, V., Franz, C.M., Welle, A., Bruns, M. & Wedlich, D. (2010).** Benzylguanine thiol self-assembled monolayers for the immobilization of SNAP-tag proteins on microcontact-printed surface structures. *Langmuir* **26**, 6097-6101.

**Engin, S. (2010).** *Funktionalisierung strukturierter Oberflächen mit E-Cadherin-Ektodomänen.* PhD dissertation, Karlsruhe Institute of Technology (KIT).

**Erbacher, C., Bessoth, F., Busch, M., Verpoorte, E. & Manz, A. (1999).** Towards integrated continuous-flow chemical reactors. *Microchim Acta* **131**, 19-24.

**Etienne-Manneville, S. & Hall, A. (2003).** Cell polarity: Par6, aPKC and cytoskeletal crosstalk. *Curr Opin Cell Biol* **15**, 67-72.

**Fang, W. & Yang, J. (2009).** A novel microreactor with 3D rotating flow to boost fluid reaction and mixing of viscous fluids. *Sens Actuators B Chem* **140**, 629-642.

**Favre, E. (1996).** Swelling of crosslinked polydimethylsiloxane networks by pure solvents: Influence of temperature. *Eur Polym J* **32**, 1183-1188.

**Fichtner, D. (2012).** *Zelluläres Adhäsionsverhalten auf strukturierten und bio-funktionalisierten Oberflächen.* PhD dissertation, Karlsruhe Institute of Technology (KIT).

**Flaim, C.J., Teng, D., Chien, S. & Bhatia, S.N. (2006).** Combinatorial signaling microenvironments for studying stem cell fate. *Stem Cells Dev* **17**, 29-39.

**Foxman, E.F., Campbell, J.J. & Butcher, E.C. (1997).** Multistep navigation and the combinatorial control of leukocyte chemotaxis. *J Cell Biol* **139**, 1349-1360.

**Frevert, C.W., Boggy, G., Keenan T.M. & Folch, A. (2006).** Measurement of cell migration in response to an evolving radial chemokine gradient triggered by a microvalve. *Lab Chip* **6**, 849-856.

**Fuchs, E., Tumbar, T. & Guasch, G. (2004).** Socializing with the neighbors: stem cells and their niche. *Cell* **116**, 769-778.

**Fujii, S., Uematsu, M., Yabuki, S., Abo, M., Yoshimura, E. & Sato, K. (2006).** Microbioassay system for an anti-cancer agent test using animal cells on a microfluidic gradient mixer. *Anal Sci* **22**, 87-90.

**Garcion, E., Halilagic, A., Faissner, A. & Ffrench-Constant, C. (2004).** Generation of an environmental niche for neural stem cell development by the extracellular matrix molecule tenascin C. *Development* **131**, 3423-3432.

**Gaver, D. & Kute, S. (1998).** A Theoretical model study of the influence of fluid stresses on a cell adhering to a microchannel wall. *Biophys. J* **75**, 721-733.

**Glinka, A., Wu, W., Delius, H., Monaghan, A.P., Blumenstock, C. & Niehrs, C. (1998).** Dickkopf-1 is a member of a new family of secreted proteins and functions in head induction. *Nature* **391**, 357-362.

**Gregorieff, A., Pinto, D., Begthel, H., Destree, O., Kielman, M. & Clevers, H. (2005).** Expression pattern of Wnt signaling components in the adult intestine. *Gastroenterology* **129**, 626-638.

**Grumolato, L., Liu, G., Mong, P., Mudbhary, R., Biswas, R., Arroyave, R., Vijayakumar, S., Economides, A.N. & Aaronson, S.A. (2010).** Canonical and noncanonical Wnts use a common mechanism to activate completely unrelated coreceptors. *Genes Dev* **24**, 2517-2530.

**Gunawan, R.C., Silvestre, J., Gaskins, H.R., Kenis, P.J. & Leckband, D.E. (2006).** Cell migration and polarity on microfabricated gradients of extracellular matrix proteins. *Langmuir* **22**, 4250-4258.

**Gupta, K., Kim, D.H., Ellison, D., Smith, C., Kundu, A., Tuan, J., Suh, K.Y. & Levchenko. (2010).** A. Lab-on-a-chip devices as an emerging platform for stem cell biology. *Lab Chip* **10**, 2019-2031.

**Gurdon, J.B., Harger, P., Mitchell, A. & Lemaire, P. (1994).** Activin signalling and response to a morphogen gradient. *Nature* **371**, 487-492.

**Gurdon, J.B. & Bourillot, P.-Y. (2001).** Morphogen gradient interpretation *Nature* **413**, 797-803.

**Habara-Ohkubo, A. (1996).** Differentiation of beating cardiac muscle cells from a derivative of P19 embryonal carcinoma cells. *Cell Struct Funct* **21**, 101-110.

**Hacker, C.A., Batteas, J.D., Garno, J.C., Marquez, M., Richter, C.A., Richter, L.J., van Zee, R.D. & Zangmeister, C.D. (2004).** Structural and chemical characterization of monofluoro-substituted oligo (phenylene−ethynylene) thiolate self-assembled mono-layers on gold. *Langmuir* **20,** 6195-6205.

**Haessler U, Pisano M, Wu M. & Swartz MA. (2011).** Dendritic cell chemotaxis in 3D under defined chemokine gradients reveals differential response to ligands CCL21 and CCL19. *Proc Natl Acad Sci USA* **108**, 5614-5619.

**Harder, P., Grunze, M., Dahint, R., Whiteseides, G.M. & Laibinis, P.F. (1998).** Molecular conformation in oligo(ethylene glycol-)terminated self-assembled monolayers on gold and silver surfaces deteminates their ability to resist protein adsorption. *J Phys Chem B* **102**, 426-436.

**Hay, E.D. & Zuk, A. (1995).** Transformations between epithelium and mesenchyme: normal, pathological, and experimentally induced. *Am J Kidney Dis* **26**, 678-690.

**Hoang, B., Moos, M., Jr., Vukicevic, S. & Luyten, F.P. (1996).** Primary structure and tissue distribution of FRZB, a novel protein related to Drosophila frizzled, suggest a role in skeletal morphogenesis. *J Biol Chem* **271**, 26131-26137.

**Holmberg, J., Genander, M., Halford, M.M., Annerén, C., Sondell, M., Chumley, M.J., Silvany, R.E., Henkemeyer, M. & Frisén, J. (2006).** EphB receptors coordinate migration and proliferation in the intestinal stem cell niche. *Cell* **125**, 1151-1163.

**Holzer, T., Liffers, K., Rahm, K., Trageser, B., Ozbek, S. & Gradl, D. (2012).** Live imaging of active fluorophore labelled Wnt proteins. *FEBS Lett* **586**, 1638-1644.

**Huelsken, J., Vogel, R., Erdmann, B., Cotsarelis, G. & Birchmeier, W. (2001).** Beta-catenin controls hair follicle morphogenesis and stem cell differentiation in the skin. *Cell* **105**, 533-545.

**Huh, D., Fujioka, H., Tung, Y.C., Futai, N., Paine, R. 3rd, Grotberg, J.B. & Takayama, S. (2007).** Acoustically detectable cellular-level lung injury induced by fluid mechanical stresses in microfluidic airway systems. *Proc Natl Acad Sci USA* **104**, 18886-18891.

**Ismagilov, R. F., Ng, J.M.K., Kenis, P.J.A. & Whitesides, G.M. (2001).** Microfluidic arrays of fluid-fluid diffusional contacts as detection elements and combinatorial tools. *Anal Chem* **73**, 5207-5213.

**Itasaki, N. & Hoppler, S. (2010).** Crosstalk between Wnt and bone morphogenic protein signaling: a turbulent relationship. *Dev Dyn* **239**, 16-33.

**Iversen, L., Cherouati, N., Berthing, T., Stamou, D. & Martinez, K.L. (2008).** Templated protein assembly on micro-contact-printed surface patterns. Use of the SNAP-tag protein functionality. *Langmuir* **24**, 6375-6381.

**Jan, Y.N. & Jan L.Y. (1998).** Asymmetric cell division. *Nature* **392**, 775-778.

**Janda, C.Y., Waghray, D., Levin, A.M., Thomas, C. & Garcia, K.C. (2012).** Structural basis of Wnt recognition by Frizzled. *Science* **337**, 59-64.

**Jensen, P.B., Pedersen, L., Krishna, S. & Jensen, M.H. (2010).** A Wnt oscillator model for somitogenesis. *Biophys J* **98**, 943-950.

**Jensen, U.B., Lowell, S. & Watt, F.M. (1999).** The spatial relationship between stem cells and their progeny in the basal layer of human epidermis: a new view based on whole-mount labelling and lineage analysis. *Development* **126**, 2409-2418.

**Jeon, N.L., Dertinger, S.K.W., Chiu, D.T., Choi, I.S., Stroock, A.D. & Whitesides, G.M. (2000).** Generation of Solution and Surface Gradients Using Microfluidic Systems. *Langmuir* **16**, 8311-8316.

**Jeon N.L., Baskaran, H., Dertinger, S.K.W., Whitesides, G.M., Van de Water, L. & Toner, M. (2002).** Neutrophil chemotaxis in linear and complex gradients of interleukin-8 formed in a microfabricated device. *Nat Biotechnol* **20**, 826-830.

**Jiang, F., Drese, K., Hardt, S., Kuepper, M. & Schoenfeld, F. (2004).** Helical flows and chaotic mixing in curved micro channels. *AIChE J* **50**, 2297-2305.

**Johnson, K.R., Lewis, J.E., Li, D., Wahl, J., Soler, A.P., Knudsen K.A., Wheelock, M.J. (1993).** P- and E-Cadherin are in separate complexes in cells expressing both cadherins. *Exp Cell Res* **207**, 252-260.

**Jones, P.H. & Watt, F.M. (1993).** Separation of human epidermal stem cells from transit amplifying cells on the basis of differences in integrin function and expression. *Cell* **73**, 713-724.

**Jubert, C. (2009).** *Mikrofluidikchip zur gezielten Stammzellendifferenzierung.* Diplom thesis, Karlsruhe Institute of Technology (KIT).

**Juillerat, A., Heinis, C., Sielaff, I., Barnikow, J., Jaccard, H., Kunz, B., Terskikh, A., Johnsson, K. (2005).** Engineering substrate specificity of $O^6$-Alkylguanine-DNA alkyltransferase for specific protein labeling in living cells. *ChemBioChem* **6**, 1263-1269.

**Kadowaki, T., Wilder, E., Klingensmith, J., Zachary, K., Perrimon, N. (1996).** The segment polarity gene *porcupine* encodes a putative multitransmembrane protein involved in wingless processing. *Genes Dev* **10**, 3116-3128.

**Kamholz, A., Weigl, B., Finlayson, B. & Yager, P. (1999).** Quantitative analysis of molecular interaction in a microfluidic channel: the T-sensor. *Anal Chem* **71**, 5340-5347.

**Keenan, T.M. & Folch, A. (2008).** Biomolecular gradients in cell culture systems. *Lab Chip* **8**, 34-57.

**Keller, R. (2002).** Shaping the vertebrate body plan by polarized embryonic cell movements. *Science* **298**, 1950-1954.

**Kenseth, J.R., Harnisch, J.A., Jones, V.W. & Porter, M.D. (2001).** Investigation of approaches for the fabrication of protein patterns by scanning probe lithography. *Langmuir* **17**, 4105-4112.

**Keppler, A., Gendreizig, S., Gronemeyer, T., Pick, H., Vogel, H. & Johnsson, K. *(2003).*** A general method for the covalent labeling of fusion proteins with small molecules *in vivo. Nat Biotechnol* **21***, 86-89.

**Kiecker, C. & Niehrs, C. (2001).** A morphogen gradient of Wnt/beta-catenin signalling regulates anteroposterior neural patterning in Xenopus. *Development* **128**, 4189-4201.

**Kiger, A. A., Jones, D. L., Schulz, C., Rogers, M. B. & Fuller, M. T. (2001).** Stem cell self-renewal specified by JAK–STAT activation in response to a support cell cue. *Science* **294**, 2542-2545.

**Kim, D., Lokuta, M.A., Huttenlocher, A. & Beebe, D.J. (2009).** Selective and tunable gradient device for cell culture and chemotaxis study. *Lab Chip* **9**, 1797-800.

**Kim, D.H., Lee, H., Lee, Y.K., Nam, J.M. & Levchenko, A. (2010).** Biomimetic nanopatterns as enabling tools for analysis and control of live cells. *Adv Mater* **22**, 4551-4566.

**Kim, H.J., Huh, D., Hamilton, G. & Ingber, D.E. (2012).** Human gut-on-a-chip inhabited by microbial flora that experiences intestinal peristalsis-like motions and flow. *Lab Chi*p **12**, 2165-2174.

**Kim, K.-A., Kakitani, M., Zhao, J., Oshima, T., Tang, T., Binnerts, M., Liu, Y., Boyle, B., Park, E., Emtage, P., Funk, W.D. & Tomizuka, K. (2005).** Mitogenic influence of human R-spondin1 on the intestinal epithelium. *Science* **309**, 1256-1259.

**Kim, L., Vahey, M.D., Lee, H.-Y. & Voldman, J. (2006).** Microfluidic arrays for logarithmically perfused embryonic stem cell culture. *Lab Chip* **6**, 394-406.

**Kimura, H., Yamamoto, T., Sakai, H., Sakai, Y. & Fujii, T. (2008).** An integrated microfluidic system for long-term perfusion culture and on-line monitoring of intestinal tissue models. *Lab Chip* **8**, 741-746.

**Kirchhof, N., Carnwath, J.W., Lemme, E., Anastassiadis, K., Schöler, H. & Niemann, H. (2000).** Expression pattern of Oct4 in preimplantation embryos of different species. *Biol Reprod* **63**, 1698-1705.

**Ko, K., Arora, P., Lee, W. & McCulloch, C. (2000).** Biochemical and functional characterization of intercellular adhesion and gap junctions in fibroblasts. *Am J Physiol Cell Physiol* **279**, C147-C157.

**Kobel, S. & Lutolf M.P. (2011).** Biomaterials meet microfluidics: building the next generation of artificial niches. *Curr Opin Biotech* **22**, 690-697.

**Korinek, V., Barker, N., Moerer, P., van Donselaar, E., Huls, G., Peters, P.J. & Clevers, H. (1998).** Depletion of epithelia stem-cell compartments in the small intestine of mice lacking Tcf-4. *Nat Genet* **19**, 1-5.

**Kreppenhofer, K. (2010).** *Weiterentwicklung eines mikrofluidischen Handhabungs-systems zur Stammzellforschung*. Diplom thesis, Karlsruhe Institute of Technology (KIT).

**Kreppenhofer, K. (2012).** PhD dissertation, Karlsruhe Institute of Technology (KIT).

**Kwok, C.-W., Strähle, U., Zhao, Y., Scharnweber, T., Weigel, S. & Welle, A. (2011).** Selective immobilization of Sonic hedgehog on benzylguanine terminated patterned self-assembled monolayers. *Biomaterials* **32**, 6719-6728.

**Lander, A.D., Nie, Q. & Wan, F.Y.M. (2002).** Do morphogen gradients arise by diffusion? *Dev Cell* **2**, 785-796.

**Larue, L., Ohsugi, M., Hirchenhain, J. & Kemler, R. (1994).** E-cadherin null mutant embryos fail to form a trophectoderm epithelium. *Proc Natl Acad Sci USA* **91**, 8263-8267.

**Larue, L., Antos, C., Butz, S., Huber, O., Delmas, V., Dominis, M. & Kemler, R. (1996).** A role for cadherins in tissue formation. *Development* **122**, 3185-3194.

**Lawrence, P. A. & Struhl, G. (1996).** Morphogens, compartments, and pattern: lessons from Drosophila? *Cell* **85**, 951-961.

**Leckband D & Prakasam A. (2006).** Mechanism and dynamics of cadherin adhesion. *Annu Rev Biomed Eng* **8**, 259-287.

**Lee, J.H., Kopecek, J. & Andrade, J.D. (1989).** Protein-resistant surfaces prepared by PEO-containing block copolymer surfactants. *J Biomed Mater Res* **23**, 351-368.

**Lee, J.N., Park, C & Whitesides, G.M. (2003).** Solvent compatibility of poly (dimethylsiloxane)-based microfluidic devices. *Anal Chem* **75,** 6544-6554.

**Lee, P.J., Hung, P.J., Rao, V.M. & Lee, L.P. (2006).** Nanoliter scale microbioreactor array for quantitative cell biology. *Biotechnol Bioeng* **94**, 5-14.

**Lee, S., Kim, D., Lee, S. and Kwon, T. (2006).** A split and recombination micromixer fabricated in a PDMS three-dimensional structure. *J Micromech Microeng* **16**, 1067.

**Levy, V., Lindon, C., Harfe, B. D. & Morgan, B. A. (2005).** Distinct stem cell populations regenerate the follicle and interfollicular epidermis. *Dev Cell* **9**, 855-861.

**Lewis, J. (1998).** Notch signalling and the control of cell fate choices in vertebrates. *Semin Cell Dev Biol* **9**, 583-589.

**Lin, H. (1998).** The self-renewing mechanism of stem cells in the germline. *Curr Opin Cell Biol* **10**, 687-693.

**Liu, G.Y. & Amro, N.A. (2002).** Positioning protein molecules on surfaces: a nanoengineering approach to supramolecular chemistry. *Proc Natl Acad Sci USA* **99**, 5165-5170.

**Liu, M., Amro, N.A. & Liu, G.-y. (2008).** Nanografting for surface physical chemistry. *Annu Rev Phys Chem* **59**, 367-386.

**Liu, M.Z., Amro, N.A., Chow, C.S. & Liu, G.-y. (2002).** Production of nanostructures of DNA on surfaces. *Nano Lett* **2**, 863-867.

**Logan, C.Y. & Nusse, R. (2004).** The Wnt signaling pathway in development and disease. *Annu Rev Cell Dev Biol* **20**, 781-810.

**Lowry, W.E., Blanpain, C., Nowak, J.A., Guasch, G., Lewis, L. & Fuchs, E. (2005).** Defining the impact of beta-catenin/Tcf transactivation on epithelial stem cells. *Genes Dev* **19**, 1596-1611.

**Lu, B., Jan, L.Y., Jan & Jan, Y.N. (1998).** Asymmetric cell division: lessons from flies and worms. *Curr Opin Genet Dev* **8**, 392-399.

**Luis, T.C., Naber, B.A.E., Roozen, P.P.C., Brugman, M.H., de Haas, E.F.E., Ghazvini, M., Fibbe, W.E., van Dongen, J.J.M., Fodde, R & Staal, F.J.T. (2011).** Canonical Wnt signaling regulates hematopoiesis in a dosage-dependent fashion. *Cell Stem Cell* **9**, 345-356.

**Lumsden, A. (1999).** Closing in on rhombomere boundaries. *Nat Cell Biol* **1**, E83-85.

**Lutolf, M.P. & Blau, H.M. (2009).** Artificial stem cell niches. *Adv Mater* **21**, 3255-3268.

**Lyashenko, N., Winter, M., Migliorini, D., Biechele, T., Moon, R.T. & Hartmann, C. (2011).** Differential requirement for the dual functions of ß-catenin in embryonic stem cell self-renewal and germ layer formation. *Nat Cell Biol* **13**, 753-761.

**Mao, J., Wang, J., Liu, B., Pan, W., Farr, G.H., Flynn, C., Yuan, H., Takada, S., Kimelman, D., Li, L.. & Wu, D. (2001).** Low-density lipoprotein receptor-related

protein-5 binds to Axin and regulates the canonical Wnt signaling pathway. *Mol Cell* **7**, 801–809.

**Matsunaga, M., Hatta, K., Nagafuchi, A. & Takeichi, M. (1988).** Guidance of optic nerve fibres by N-cadherin adhesion molecules. *Nature* **334**, 62-64

**Mei, Y., Saha, K., Bogatyrev, S.R., Yang, J., Hook, A.L., Kalcioglu, Z.I., Cho, S.W., Mitalipova, M., Pyzocha, N., Rojas, F., van Vliet, K.J., Davies, M.C., Alexander, M.R., Langer, R., Jaenisch, R. & Anderson, D.G. (2010).** Combinatorial Development of Biomaterials for Clonal Growth of Human Pluripotent Stem Cells. *Nat Mater* **9**, 768-778.

**Meijer, L., Skaltsounis, A.L., Magiatis, P., Polychronopoulos, P., Knockaert, M., Leost, M., Ryan, X.P., Vonica, C.A., Brivanlou, A., Dajani, R., Crovace, C., Tarricone, C., Musacchio, A., Roe, S.M., Pearl, L. & Greengard, P. (2003).** GSK-3-selective inhibitors derived from tyrian purple indirubins. *Chem Biol* **10**, 1255-1266.

**Mengeaud, V., Josserand, J., Girault, H. (2002).** Mixing processes in a zigzag microchannel: finite element simulations and optical study. *Anal Chem* **74**, 4279-4286.

**Merrill, B.J., Gat, U., DasGupta, R. & Fuchs, E. (2001).** Tcf3 and Lef1 regulate lineage differentiation of multipotent stem cells in skin. *Genes Dev* **15**, 1688-1705.

**Ming, G.-L., Wong, S.T., Henley, J., Yuan, X.-B., Song, H.-J., Spitzer, N.C. & Poo, M.-M. (2002).** Adaptation in the chemotactic guidance of nerve growth cones. *Nature* **417**, 411-418.

**Moledina, F., Clarke, G., Oskooei, A., Onishi, K., Günther, A., Zandstra, P.W. (2012).** Predictive microfluidic control of regulatory ligand trajectories in individual pluripotent cells. *Proc Natl Acad Sci USA* **109**, 3264-3269.

**Montague, M., Ducker, R.E., Chong, K.S.L., Manning, R.J., Rutten, F.J.M., Davies, M.C. & Leggett, G.J. (2007).** Fabrication of biomolecular nanostructures by scanning near-field photolithography of oligo(ethylene glycol)-terminated self-assembled monolayers. *Langmuir* **23,** 7328-7337.

**Montcouquiol, M., Crenshaw III, E.B. & Kelley, M.W. (2006).** Noncanonical Wnt signaling and neural polarity. *Annu Rev Neurosci* **29**, 363-386.

**Morel, M., Galas, J.-C., Dahan, M. & Studer, V. (2012).** Concentration landscape generators for shear free dynamic chemical stimulation. *Lab Chip* **12**, 1340-1346.

**Mosadegh, B., Huang, C., Park, J.W., Shin, H.S., Chung, B.G., Hwang, S.K., Lee, K.H., Kim, H.J., Brody, J. & Jeon, N.L. (2007).** Generation of stable complex gradients across two-dimensional surfaces and three-dimensional gels. *Langmuir* **23**, 10910-10912.

**Muramatsu, N. & Minton, A. P. (1988).** Tracer diffusion of globular proteins in concentrated protein solutions. *Proc. Natl. Acad. Sci USA* **85**, 2984-2988.

**Neeves, K.B. & Diamond, S.L. (2008).** A membrane-based microfluidic device for controlling the flux of platelet agonists into flowing blood. *Lab Chip* **8**, 701-709.

**Ngunjiri, J.N., Kelley, A.T., Lejeune, Z.M., Li, J.-R., Lewandowski, B.R., Serem, W.K., Daniels, S.L., Lusker, K.L. & Garno, J.C. (2008).** Achieving Precision and Reproducibility for Writing Patterns of *n*-alkanethiol Self-assembled Monolayers with Automated Nanografting. *Scanning* **30**, 123-136.

**Nguyen, N.T. & Wereley, S. (2006).** *Fundamentals and Applications of Microfluidics,* 2nd edn. Artech House, Boston, London.

**Nichols, J., Chambers, I., Taga, T., & Smith, A. (2001).** Physiological rationale for responsiveness of mouse embryonic stem cells to gp130 cytokines. *Development* **128**, 2333-2339.

**Niemann, C., Owens, D.M., Hulsken, J., Birchmeier, W. & Watt, F.M. (2002).** Expression of DeltaNLef1 in mouse epidermis results in differentiation of hair follicles into squamous epidermal cysts and formation of skin tumours. *Development* **129**, 95-109.

**Nilsson, S.K., Johnston, H.M., Whitty, G.A., Williams, B., Webb, R.J., Denhardt, D.T., Bertoncello, I., Bendall, L.J., Simmons, P.J. & Haylock, D.N. (2005).** Osteopontin, a key component of the hematopoietic stem cell niche and regulator of primitive hematopoietic progenitor cells. *Blood* **106**, 1232-1239.

**Niwa, H., Burdon, T., Chambers, I. & Smith, A. (1998).** Self-renewal of pluripotent embryonic stem cells is mediated via activation of STAT3. *Genes Dev* **12**, 2048-2060.

**Noggle, S. A., James, D., & Brivanlou, A. H. (2005).** A molecular basis for human embryonic stem cell pluripotency. *Stem Cell Rev* **1**, 111-118.

**Nusse, R. & Varmus, H. (2012).** Three decades of Wnts: a personal perspective on how a scientific field developed. *EMBO J* **31**, 2670-2684.

**Oh, K.W., Lee, K., Ahn, B. & Furlani, E.P. (2012).** Design of pressure-driven microfluidic networks using electric circuit analogy. *Lab Chip* **12**, 515-545.

**Okamura, R.M., Sigvardsson, M., Galceran, J., Verbeek, S., Clevers, H. & Grosschedl, R. (1998).** Redundant regulation of T cell differentiation and TCR alpha gene expression by the transcription factors LEF-1 and TCF-1. *Immunity* **8**, 11-20.

**Pale-Grosdemange, C., Simon, E.S., Prime, K.L. & Whitesides, G.M. (1991).** Formation of self-assembled monolayers by chemisorption of derivatives of oligo(ethylene glycol) of structure $HS(CH_2)_{11}(OCH_2CH_2)_mOH$ on gold. *J Am Chem Soc* **113**, 12-20.

**Papin, C. & Smith, J. C. (2000).** Gradual refinement of activin-induced thresholds requires protein synthesis. *Dev Biol* **217**, 166-172.

**Papkoff, J. (1989).** Inducible overexpression and secretion of int-1 protein. *Mol Cell Biol* **9**, 3377-3384.

**Park, J.Y., Hwang, C.M., Lee S.H. & Lee S.-H. (2007).** Gradient generation by an osmotic pump and the behavior of human mesenchymal stem cells under the fetal bovine serum concentration gradient. *Lab Chip* **7**, 1673-1680.

**Park, J.Y., Kim, S.-K., Woo, D.-H., Lee, E.-J., Kim, J.-H. & Lee, S.-H. (2009).** Differentiation of neural progenitor cells in a microfluidic chip-generated cytokine gradient. *Stem Cells* **27**, 2646-2654.

**Peerani, R., Rao, B.M., Bauwens, C., Yin, T., Wood, G.A., Nagy, A., Kumacheva, E. & Zandstra, P.W. (2007).** Niche-mediated control of human embryonic stem cell self-renewal and differentiation. *EMBO J* **26**, 4744-4755.

**Pegg, A.E. (2000).** Repair of $O^6$-alkylguanine by alkyltransferases. *Mutat Res* **462**, 83-100.

**Perez-Moreno, M., Jamora, C. & Fuchs, E. (2003).** Sticky business: orchestrating cellular signals at adherens junctions. *Cell* **112**, 535-548.

**Perl, A., Reinhoudt, D.N. & Huskens, J. (2009).** Microcontact printing: limitations and achievements. *Adv Mater* **21**, 2257–2268.

**Petritsch, C., Tavosanis, G., Turck, C.W., Jan, L.Y. & Jan, Y.N. (2003).** The Drosophila myosin VI Jaguar is required for basal protein targeting and correct spindle orientation inmitotic neuroblasts. *Dev Cell* **4**, 273-281.

**Poirier, G.E., Tarlov, M.J. & Rushmeier, H.E. (1994).** Two-dimensional liquid phase and the px.sqroot.3 phase of alkanethiol self-assembled monolayers on Au(111). *Langmuir* **10**, 3383-3386.

**Poirier, G.E. & Pylant, E.D. (1996).** The self-assembly mechanism of alkanethiols on Au (111). *Science* **272**, 1145-1148.

**Poirier, G.E. (1997).** Characterization of organosulfur molecular monolayers on Au(111) using scanning tunneling microscopy. *Chem Rev* **97**,1117-1127.

**Porter, M.D., Bright, T.B., Allara, D.L. & Chidsey, C.E.D. (1987).** Sponatenously organized molecular assemblies. 4. Structural characterization of *n*-alkyl thiol monolayers on gold by optical ellipsometry, infrared spectroscopy, and electrochemistry. *J Am Chem Soc* **109**, 3559-3568.

**Powers, M.J., Domansky, K., Kaazempur-Mofrad, M.R., Kalezi, A., Capitano, A., Upadhyaya, A., Kurzawski, P., Wack, K.E., Stolz, D.B., Kamm, R. & Griffith, L.G. (2001).** A microfabricated array bioreactor for perfused 3D liver culture. *Biotechnol Bioeng* **78**, 257-269.

**Quillin, M. L. & Matthews, B. W. (2000).** Accurate calculation of the density of proteins. *Acta Crystallogr. D Biol. Crystallogr* **56**, 791-794.

**Ranjan, V., Waterbury, R., Xiao, Z. & Diamond, S.L. (1996).** Fluid shear stress induction of the transcriptional activator c-fos in human and bovine endothelial cells, HeLa, and Chinese hamster ovary cells. *Biotechnol Bioeng* **49**, 383-390.

**Redmer, T., Diecke, S., Grigoryan, T., Quiroga-Negreira, A., Birchmeier, W. & Besser, D. (2011).** E-cadherin is crucial for embryonic stem cellpluripotency and can replace OCT4 duringsomatic cell reprogramming. *EMBO Rep* **12**, 720-726.

**Reya, T., Duncan, A.W., Ailles, L., Domen, J., Scherer, D.C., Willert, K., Hintz, L., Nusse, R. & Weissman, I.L. (2003).** A role for Wnt signaling in self-renewal of haematopoietic stem cells. *Nature* **423**, 409-414.

**Reya, T. & Clevers, H. (2005).** Wnt signaling in stem cells and cancer. *Nature* **434**, 843-850.

**Riet, J. t., Smit, T., Gerritsen, J.W., Cambi, A., Elemans, J.A.A.W., Figdor, C.G. & Speller, S. (2010).** Molecular friction as a tool to identify functionalized alkanethiols. *Langmuir* **26**, 6357-6366.

**Ruiz, S.A. & Chen, C.S. (2007).** Microcontact printing: A tool to pattern. *Soft Matter* **3**, 168-177.

**Saadi, W., Rhee, S.W., Lin, F., Vahidi, B., Chung B.G. & Jeon, N.L. (2007).** Generation of stable concentration gradients in 2D and 3D environments using a microfluidic ladder chamber. *Biomed Microdevices* **9**, 627-635.

**Saha, K., Mei, Y., Reisterer, C.M., Pyzocha, N.K., Yang, J., Muffat, J., Davies, M.C., Alexander, M.R., Langer, R., Anderson, D.G. & Jaenisch, R. (2011).** Surface-engineered substrates for improved human pluripotent stem cell culture under fully defined conditions. *Proc Natl Acad Sci USA* **15**, 18714-18719.

**Sato, N., Meijer, L., Skaltsounis, L., Greengard, P. & Brivanlou, A.H. (2004).** Maintenance of pluripotency in human and mouse embryonic stem cells through activation of Wnt signaling by a pharmacological GSK-3-specific inhibitor. *Nat Med* **10**, 55-63.

**Scadden, D.T. (2006).** The stem-cell niche as an entity of action. *Nature* **441**, 1075-1079.

**Schambony, A., Kunz, M. & Gradl, D. (2004).** Cross-regulation of Wnt signaling and cell adhesion. *Differentiation* **72**, 307-318.

**Schilp, S., Rosenhahn, A., Pettitt, M.E., Bowen, J., Callow, M.E., Callow, J.A. & Grunze, M. (2009).** Physicochemical properties of (ethylene glycol)-containing self-assembled monolayers relevant for protein and algal cell resistance. *Langmuir* **25**, 10077-10082.

**Schofield, R. (1978).** The relationship between the spleen colony-forming cell and the haemopoietic stem cell. *Blood Cells* **4**, 7-25.

**Schryver, B., Hinck, L. & Papkoff, J. (1996).** Properties of Wnt-1 protein that enable cell surface association. *Oncogene* **13**, 333-342.

**Schulte, G., Bryja, V., Rawal, N., Castelo-Branco, G., Sousa, K.M. & Arenas, E. (2005).** Purified Wnt-5a increases differentiation of midbrain dopaminergic cells and dishevelled phosphorylation. *J Neurochem* **92**, 1550-1553.

**Schwartz, P.V. (2001).** Meniscus force nanografting: nanoscopic patterning of DNA. *Langmuir* **17**, 5971-5977.

**Sharp, K.G., Blackman, G.S., Glassmaker, N.J., Jagota, A. & Hui, C.-Y. (2004).** Effect of stamp deformation on the quality of microcontact printing: Theory and experiment. *Langmuir* **20,** 6430–6438.

**Sharpe, R.B.A., Burdinski, D., Huskens, J., Zandvliet, H.J.W., Reinhoudt, D.N. & Poelsema, B. (2004).** Spreading of 16-mercaptohexadecanoic acid in microcontact printing. *Langmuir* **20,** 8646-8651.

**Sia, S.K. & Whitesides, G.M. (2003).** Microfluidic devices fabricated in poly (dimethylsiloxane) for biological studies. *Electrophoresis* **24,** 3563-3576.

**Sip, C.G., Bhattacharjee, N. & Folch, A. (2011).** A modular cell culture device for generating arrays of gradients using stacked microfluidic flows. *Biomicrofluidics* **5**, 22210.

**Smith, J.C.,Lee, K.-B., Wang, Q., Finn, M.G., Johnson, J.E., Mrksich, M. & Mirkin, C.A. (2003).** Nanopatterning the chemospecific immobilization of cowpea mosaic virus capsid. *Nano Letters* **3**, 883-886.

**Smolich, B.D., McMahon, J.A., McMahon, A.P. & Papkoff, J. (1993).** Wnt family proteins are secreted and associated with the cell surface. *Mol Biol Cell* **4**, 1267-1275.

**Solanki, A., Kim, J.D. & Lee, K.-B. (2008).** Nanotechnology for regenerative medicine: nanomaterials for stem cell imaging. *Nanomedicine* **3**, 567-578.

**Soncin, F., Mohamet, L., Eckardt, D., Ritson, S., Eastham, A.M., Bobola, N., Russell, A., Davies, S., Kemler, R., Merry, C.L.R. & Ward, C.M. (2009).** Abrogation of E-Cadherin-mediated cell–cell contact in mouse embryonic stem cells results in reversible LIF-independent self-renewal. *Stem Cells* **27**, 2069-2080.

**Song, J.W., Cavnar, S.P., Walker, A.C., Luker, K.E., Gupta, M., Tung, Y.C., Luker, G.D. & Takayama, S. (2009).** Microfluidic endothelium for studying the intravascular adhesion of metastatic breast cancer cells. *PLoS One* **4**, e5756.

**Song, X., Zhu, C.H., Doan, C. & Xie, T. (2002).** Germline stem cells anchored by adherens junctions in the Drosophila ovary niches. *Science* **296**, 1855-1857.

**Song, X., Wong, M.D., Kawase, E., Xi, R., Ding, B.C., McCarthy, J.J. & Xie, T. (2004).** Bmp signals from niche cells directly repress transcription of a differentiation-promoting gene, *bag of marbles*, in germline stem cells in the *Drosophila* ovary. *Development* **131**, 1353–1364.

**Sousa, K.M., Villaescusa, J.C., Cajanek, L., Ondr, J.K., Castelo-Branco, G., Hofstra, W., Bryja, V., Palmberg, C., Bergman, T., Wainwright, B., Lang, R.A. & Arenas, E. (2010).** Wnt2 regulates progenitor proliferation in the developing ventral midbrain. *J Biol Chem* **285**, 7246-7253.

**Spencer, H., Eastham, A., Merry, C., Southgate, T., Perez-Campo, F., Soncin, F., Ritson, S., Kemler, R., Stern, P. & Ward, C. (2007).** E-cadherin inhibits cell surface localization of the pro-migratory 5T4 oncofetal antigen in mouse embryonic stem cells. *Mol Biol Cell* **18**, 2838-2851.

**Stepniak, E., Radice, G.L. & Vasioukhin, V. (2009).** Adhesive and signaling functions of cadherins and catenins in vertebrate development. *Cold Spring Harb Perspect Biol* **1**, a002949.

**Stier, S., Ko, Y., Forkert, R., Lutz, C., Neuhaus, T., Grünewald, E., Cheng, T., Dombkowski, D., Calvi, L.M., Rittling, S.R. & Scadden, D.T. (2005).** Osteopontin is a hematopoietic stem cell niche component that negatively regulates stem cell pool size. *J Exp Med* **201**, 1781-1791.

**St-Jacques, B., Dassule, H.R., Karavanova, I., Botchkarev, V.A., Li, J., Danielian, P.S., McMahon, J.A., Lewis, P.M., Paus, R. & McMahon, A.P. (1998).** Sonic hedgehog signaling is essential for hair development. *Curr Biol* **8**, 1058-1068.

**Stranick, S.J., Parikh, A.N., Allara, D.L. & Weiss, P.S. (1994).** A New Mechanism for Surface Diffusion: Motion of a Substrate-Adsorbate Complex. *J Phys Chem* **98,** 11136-11142.

**Strigini, M. & Cohen, S.M. (1999).** Formation of morphogen gradients in the *Drosophila* wing. *Semin Cell Dev Biol* **10**, 335-344.

**Strigini, M. & Cohen, S.M. (2000).** Wingless gradient formation in the *Drosophila* wing. *Curr Biol* **10**, 293-300.

**Stroock, A.D., Dertinger, S.K.W., Ajdari, A., Mezic, I., Stone, H.A. & Whiteside, G.M. (2002).** Chaotic mixer for microchannels. *Science* **295**, 647-651.

**Stroock, A.D., Dertinger, S.K.W, Whitesides, G.M. & Ajdari, A. (2002).** Patterning flows using grooved surfaces. *Anal Chem* **74**, 5306-5312.

**Sugihara-Seki, M. (2000).** Flow around cells adhered to a microvessel wall. I. Fluid stresses and forces acting on the cells. *Biorheology* **37**, 341-359.

**Sugihara-Seki, M. (2001).** Flow around cells adhered to a microvessel wall. II. Comparison to flow around adherent cells in channel flow, *Biorheology* **38**, 3-13.

**Suyama, K., Shapiro, I., Guttman, M. & Hazan, R.B. (2002).** A signaling pathway leading to metastasis is controlled by N-cadherin and the FGF receptor. *Cancer Cell* **2**, 301-314.

**Takahashi, K. & Yamanaka, S. (2006).** Induction of pluripotent stem cells from mouse embryonic and adult fibroblast cultures by defined factors. *Cell* **126**, 663-676.

**Tinoco, I., Sauer, K., Wang, J.C. & Puglisi, (2002).** *Physical Chemistry: Principles and Applications in Biological Sciences*, 4th edn. Prentice Hall.

**Toh, Y.-C., Blagović, K. & Voldman, J. (2010).** Advancing stem cell research with microtechnologies: opportunities and challenges. *Integr Biol* **2**, 305-325.

**Tsao, C.-W. & DeVoe, D.L. (2009).** Bonding of thermoplastic polymer microfluidics. *Microfluid Nanofluid* **6**, 1-16.

**Tulina, N. & Matunis, E. (2001).** Control of stem cell self-renewal in *Drosophila* spermatogenesis by JAK–STAT signaling. *Science* **294**, 2546-2549.

**Valiokas, R., Svehem, S., Svensson, S.C.T. & Liedberg, B. (1999).** Self-assembled monolayers of oligo(ethylene glycol)-terminated and amide group containing alkanethiolates on gold. *Langmuir* **15**, 3390-3394.

**van den Heuvel, M., Harryman-Samos, C., Klingensmith, J., Perrimon, N. & Nusse, R. (1993).** Mutations in the segment polarity genes wingless and porcupine impair secretion of the wingless protein. *EMBO J* **12**, 5293-5302.

**VanDersarl, J.J., Xu, A.M. & Melosh, N.A. (2011).** Rapid spatial and temporal controlled signal delivery over large cell culture areas. *Lab Chip* **11**, 3057-3063.

**van de Wetering, M., Sancho, E., Verweij, C., de Lau, W., Oving, I., Hurlstone, A., van der Horn, K., Batlle, E., Coudreuse, D., Haramis, A.P., Tjon-Pon-Fong, M., Moerer, P., van den Born, M., Soete, G., Pals, S., Eilers, M., Medema, R. & Clevers, H. (2002).** The beta-catenin/TCF-4 complex imposes a crypt progenitor phenotype on colorectal cancer cells. *Cell* **111**, 241-250.

**van Es, J.H., van Gijn, M.E., Riccio, O., van den Born, M., Vooijs, M., Begthel, H., Cozijnsen, M., Robine, S., Winton, D.J., Radtke, F. & Clevers, H. (2005).** Notch pathway/g-secretase inhibition turns proliferative cells in intestinal crypts and neoplasia into Goblet cells. *Nature* **435**, 959-963.

**van Genderen, C., Okamura, R.M., Farinas, I., Quo, R.G., Parslow, T.G., Bruhn, L., and Grosschedl, R. (1994).** Development of several organs that require inductive epithelial-mesenchymal interactions is impaired in LEF-1-deficient mice. *Genes Dev* **8**, 2691-2703.

**Vijayendran, R., Motsegood, K., Beebe, D. & Leckband, D. (2003).** Evaluation of a threedimensional micromixer in a surface-based biosensor. *Langmuir* **19**, 1824-1828.

**Waaler, J., Machon, O., von Kries, J.P., Wilson, S.R., Lundenes, E., Wedlich, D., Gradl, D., Paulsen, J.E., Machonova, O., Dembinski, J.L., Dinh, H. & Krauss, S. (2011).** Novel synthetic antagonists of canonical Wnt signaling inhibit colorectal cancer cell growth. *Cancer Res* **71**, 197-205.

**Wadu-Mesthrige, K., Amro, N.A., Garno, J.C., Xu, S. & Liu, G.-y. (2001).** Fabrication of nanometer-sized protein patterns using atomic force microscopy and selective immobilization. *Biophys J* **80**, 1891-1899.

**Walker, G.M., Zeringue, H.C. & Beebe, D.J. (2004).** Microenvironment design considerations for cellular scale studies. *Lab Chip* **4**, 91–97.

**Walker, G.M., Sai, J., Richmond, A., Stremler, M., Chung, C.Y. & Wikswo, J.P. (2005).** Effects of flow and diffusion on chemotaxis studies in a microfabricated gradient generator. *Lab Chip* **5**, 611-618.

**Wang, S., Krinks, M., Lin, K., Luyten, F.P. & Moos, M., Jr. (1997).** Frzb a secreted protein expressed in the Spemann organizer, binds and inhibits Wnt-8. *Cell* **88**, 757-766.

**Wang, S.J., Saadi, W., Lin, F., Nguyen. C. M-C. & Jeon N.L. (2004).** Differential effects of EGF gradient profiles on MDA-MB-231 breast cancer cell chemotaxis. *Exp Cell Res* **300**, 180-189.

**Wartlick, O., Kicheva, A. & González-Gaitán, M. (2009).** Morphogen gradient formation. *Cold Spring Harb Perspect Biol* **1**, a001255.

**Welle, A. & Gottwald, E. (2002).** UV-based patterning of polymeric substrates for cell culture applications. *Biomed Microdevices* **4**, 33-41.

**Wheelock, M.J. & Johnson, K.R. (2003).** Cadherin-mediated cellular signaling. *Curr Opin Cell Biol* **15**, 509-514.

**Whitesides, G.M. (2006).** Overview The origins and the future of microfluidics. *Nature* **442**, 368-373.

**Willert, K., Brown, J.D., Danenberg, E., Duncan, A.W., Weissman, I.L., Reya, T., Yates, JR III. & Nusse, R. (2003).** Wnt proteins are lipid-modified and can act as stem cell growth factors. *Nature* **423**, 448-452.

**Wizenmann, A. & Lumsden, A. (1997).** Segregation of rhombomeres by differential chemoaffinity. *Mol Cell Neurosci* **9**, 448-459.

**Wolpert, L. (1989).** Positional information revisited. *Development* **107**, Suppl:3-12.

**Worgull, M. (2009).** *Hot Embossing Theory and Technology of Microreplication*, 1st edn. William Andrew.

**Workman, R.K. & Manne, S. (2004).** Molecular transfer and transport in noncovalent microcontact printing. *Langmuir* **20,** 805-815.

**Wray, J., Kalkan, T., Gomez-Lopez, S., Eckardt, D., Cook, A., Kemler, R. & Smith, A. (2011).** Inhibition of glycogen synthase kinase-3 alleviates Tcf3 repression of the pluripotency network and increases embryonic stem cell resistance to differentiation. *Nat Cell Biol* **13**, 838-845.

**Xi, R. (2009).** Anchoring stem cells in the niche by cell adhesion molecules. *Cell Adh Migr* **3**, 396-401.

**Xia, Y. & Whitesides, G.M. (1995).** Use of controlled reactive spreading of liquid alkanethiol on the surface of gold to modify the size of features produced by microcontact Printing. *J Am Chem Soc* **117**, 3274-3275.

**Xie, T. & Spradling, A. C. (1998).** *decapentaplegic* is essential for the maintenance and division of germline stem cells in the *Drosophila* ovary. *Cell* **94**, 251-260.

**Xu, S. & Liu, G.-y. (1997).** Nanometer-scale fabrication by simultaneous nanoshaving and molecular self-assembly. *Langmuir* **13**, 127-129.

**Xu, S., Laibinis, P.E. & Liu, G.-y. (1998).** Accelerating the kinetics of thiol self-assembly on gold − A spatial confinement effect. *J Am Chem Soc* **120**, 9356-9361.

**Yan, D. & Lin, X. (2009).** Shaping morphogen gradients by proteoglycans. *Cold Spring Harb Perspect Biol* **1**, a002493.

**Yang, J., Fang, W. & Tung, K. (2008).** Fluids mixing in devices with connected-groove channels. *Chem Eng Sci* **63**, 1871-1881.

**Yap, A.S. & Kovacs, E.M. (2003).** Direct cadherin-activated cell signaling: a view from the plasma membrane. *J Cell Biol* **160**, 11-16.

**Ying, Q.-L., Nichols, J., Chambers, I. & Smith, A. (2003).** BMP induction of Id proteins suppresses differentiation and sustains embryonic stem cell self-renewal in collaboration with STAT3. *Cell* **115**, 281-292.

**Ying, Q.-L., Wray, J., Nichols, J., Batlle-Morera, L., Doble, B., Woodgett, J., Cohen, P. & Smith, A. (2008).** The ground state of embryonic stem cell self-renewal. *Nature* **453**, 519-523.

**Yoo, P.J., Choi, S.-J., Kim, J.H., Suh, D., Baek, S.J., Kim, T.W. & Lee, H.H. (2004).** Unconventional patterning with a modulus-tunable mold: From imprinting to microcontact printing. *Chem Mater* **16**, 5000-5005.

**Young, E.W.K. & Beebe, D.J. (2010).** Fundamentals of microfluidic cell culture in controlled microenvironments. *Chem Soc Rev* **39**, 1036-1048.

**Yu, H., Meyvantsson, I., Shkel, I.A. & Beebe, D.J. (2005).** Diffusion dependent cell behavior in microenvironments. *Lab Chip* **5**, 1089-1095.

**Yu, J.-j., Nolting, B., Tan, Y.H., Li, X., Gervay-Hague, J. & Liu, G.-y. (2006).** Polyvalent interactions of HIV-gp120 protein and nanostructures of carbohydrate ligands. *Nanobiotechnology* **1**, 201-210.

**Yu, J.-j., Tan, Y.H., Li, X., Kuo, P.-K. & Liu, G.-y. (2006).** A Nanoengineering Approach to Regulate the Lateral Heterogeneity of Self-Assembled Monolayers. *J. Am. Chem. Soc* **128**, 11574-11581.

**Zecca, M., Basler, K. & Struhl, G. (1996).** Direct and long-range action of a wingless morphogen gradient. *Cell* **87**, 833-844.

**Zeng, Y., Lee, T.-S., Yu, P., Roy, P., & Low, H.-T. (2006).** Mass transport and shear stress in a microchannel bioreactor: Numerical simulation and dynamic similarity. *J Biomech Eng* **128**, 185-193.

**Zicha, D., Dunn, G. & Jones, G. (1997).** Analyzing chemotaxis using the Dunn direct-viewing chamber. *Methods Mol Biol* **75**, 449-457.

**Zigmond, S.H. (1988).** Orientation chamber in chemotaxis. *Methods Enzymol* **162**, 65-72.

# Curriculum Vitae

**Chorong Kim**

## Personal Information

Date of birth : 17. 2. 1983
Place of birth : Incheon, South Korea

## Education

| | |
|---|---|
| Since Oct. 2009 | Candidate of Ph.D., Zoological Institute, Cell and Developmental Biology, Karlsruhe Institute of Technology (KIT), Karlsruhe, Germany<br>Title : "Morphogen gradient creation and bio-modified surfaces for rebuilding a stem cell microenvironment"<br>Advisor: Prof. Dr. Doris Wedlich |
| Mar. 2006 – Feb. 2008 | Master of Science, Materials Science and Engineering, Gwangju Institute of Science and Technology (GIST), Gwangju, South Korea<br>Title : "Carbon nanotubes – protein hybrids : preparation and assessment of biological and selective redox activity"<br>Advisor : Prof. Dr. Kurt E. Geckeler |
| Mar. 2001 – Feb. 2006 | Bachelor of Engineering, Chemical Engineering (Biotechnology), Inha University, Incheon, South Korea |

## Work experience

| | |
|---|---|
| Jan. 2008 – Dec. 2008 | Formula researcher, Research and Development, Unilever Korea, Daejeon, South Korea |

## Conference

**Chorong Kim**, Kristina Kreppenhofer, Jubin Kashef, Marc Schneider, Dietmar Gradl, Dirk Herrmann, Ralf Ahrens, Andreas Guber, Doris Wedlich. Diffusion- and convection-based activation of Wnt/ß-catenin signaling in a gradient generating microfluidic chip. Poster presentation at European Molecular Biology Laboratory (EMBL) Conference : Microfluidics 2012, Heidelberg, Germany. 25.- 27. July 2012

**Chorong Kim**, Kristina Kreppenhofer, Jubin Kashef, Marc Schneider, Dietmar Gradl, Dirk Herrmann, Ralf Ahrens, Andreas Guber, Doris Wedlich. Simultaneous selective activation of Wnt/ ß-catenin signaling transduction in a gradient generating microfluidic chip. Poster presentation at European Lab on a chip Congress of European Lab Automation, Hamburg, Germany. 30. June-1. July 2011

Kristina Kreppenhofer, **Chorong Kim**, Marc Schneider, Dirk Herrmann, Ralf Ahrens, Jubin Kashef, Dietmar Gradl, Doris Wedlich, Andreas Guber. Microfluidic polycarbonate chip for long-term cell analyses. Talk at BMT 2012 - 46. Deutsche Gesellschaft für Biomedizinische Technik (DGBMT) Jahrestagung, Jena, Germany. 16.-19. Sep. 2012

Kristina Kreppenhofer, **Chorong Kim**, Marc Schneider, Dirk Herrmann, Ralf Ahrens, Jubin Kashef, Dietmar Gradl, Doris Wedlich, Andreas Guber. Polycarbonate microfluidic chip for long-term cell investigations. Talk at World Congress on Medical Physics and Biomedical Engineering, Beijing, China. 26.-31. May 2012

# List of publication

## Journal

**Chorong Kim**, Kristina Kreppenhofer, Jubin Kashef, Dietmar Gradl, Dirk Herrmann, Marc Schneider, Ralf Ahrens, Andreas Guber & Doris Wedlich (2012). Diffusion- and convection-based activation of Wnt/β-catenin signaling in a gradient generating microfluidic chip. *Lab Chip* **12**, 5186-5194.

Dipen Debnath, **Chorong Kim**, Sung H. Kim & Kurt E. Geckeler (2010). Solid-state synthesis of silver nanoparticles at room temperature: poly(vinyl pyrrolidone) as a tool. *Macromol Rapid Comm* **31**, 549-553.

Jiyong Shin, **Chorong Kim** & Kurt E. Geckeler (2009). Single-walled carbon nanotube–polystyrene nanocomposites: dispersing nanotubes in organic media. *Polym Int* **58**, 579-583.

## Patent

"Vorrichtung und Verfahren zur Untersuchung oder Differenzierung von Zellen bei Kontakt mit einem Gradienten aus mindestens einer biologisch wirksamen Spezies." Dirk Herrmann, Jubin Kashef, **Chorong Kim**, Andreas Guber, Ralf Ahrens, Kristina Kreppenhofer, Doris Wedlich, Dietmar Gradl, Marc Schneider. German Patent Application, 102011102071.7 (May. 19. 2011)

"Solid-state synthesis method of silver nanoparticles, and silver nanoparticles synthesized thereby" Dipen Debnath, **Chorong Kim**, Sung H. Kim, Kurt E. Geckeler. US Patent Application, US201013509463 (Nov. 9, 2010)